

https://dspace.org/

High temperature oxidation and corrosion behaviour of titanium aluminide alloy Ti-52.5Al-10.0Ni-0.2Ru (at.%)

Mantyi, Hadio Caprice

2016

http://hdl.handle.net/10539/22671

Mantyi, Hadio Caprice (2016) High temperature oxidation and corrosion behaviour of Titanium Aluminide alloy Ti-52.5Al-10.0Ni-0.2Ru (at.%), University of the Witwatersrand, Johannesburg, <http://hdl.handle.net/10539/22671>

Downloaded from a DSpace repository. https://dspace.org/

High Temperature Oxidation and Corrosion Behaviour of Titanium Aluminide Alloy Ti-52.5Al-10.0Ni-0.2Ru (at.%)

by

Hadio Caprice Mantyi

(9902708W)

A dissertation submitted to the Faculty of Engineering and the Built Environment, University of the Witwatersrand, in fulfilment of the requirements for the degree of Master of Science in Engineering

15 October 2016

DECLARATION

I declare that this dissertation is my own unaided work. It is being submitted for the degree of Master of Science in Engineering to the University of the Witwatersrand, Johannesburg. It has not been submitted before for any degree or examination in any other University.

Signature: H.C. Mantyi

……..

October 2016

ABSTRACT

The alloys Ti-52.5Al-10.0Ni (at.%) and Ti-52.5Al-10.0Ni-0.2Ru (at.%) were made by mixing, and melting their powders in a button arc furnace under an argon atmosphere. The high temperature oxidation and room temperature corrosion of behaviour of the alloys was investigated. Isothermal oxidation in air at 950°C for 120 hours and 720 hours was done. Cyclic oxidation behaviour of the alloys was also investigated in air and in a hot salt (Na_2SO_4) environment. The corrosion tests were conducted in 5 wt% and 25 wt% HCl. All the samples were characterised using scanning electron microscopy with energy dispersive X-ray spectroscopy, X-ray diffraction and hardness measurements.

On solidification, the Ti-52.5Al-10.0Ni (at.%) alloy formed dendrites of γ-TiAl (~55 at.% Al) surrounded by a eutectic of γ-TiAl + Ti_2NiAl_3 (τ_3) phases. Most of the nickel was found in the Ti_2NiAl_3 (τ_3) phase (~12 at.%) with trace amounts in the dendrites (~0.5 at.%).

The Ti-52.5Al-10.0Ni-0.2Ru (at.%) alloy formed dendrites of γ-TiAl (~53 at.% Al) surrounded by a eutectic of γ-TiAl + Ti_2NiAl_3 (τ_3). Most of the nickel (~15 at.%) and ruthenium (~0.3 at.%) were in solid solution in the Ti_2NiAl_3 (τ_3) phase, although small amounts of both metals were present in the dendrites (~1 at.% Ni and 0.1 at.% Ru).

Under isothermal oxidation conditions, both alloys showed good oxidation resistance with a low mass gain (< 2%). The alloys formed a continuous scale of TiO_2 and Al_2O_3 with good adherence to the substrate, but as exposure time increased, the scale was severely degraded and exfoliated from the surface. Cyclic oxidation conditions were more aggressive for both alloys. The Ti-52.5Al-10.0Ni-0.2Ru (at.%) alloy was more resistant and formed a nickel-rich sub-surface zone between the substrate and intermixed oxide layer.

Both alloys had a fairly good corrosion resistance in HCl due to the presence of nickel. They formed a thin and non-continuous Al_2O_3 oxide scale on the surface of the γ-TiAl dendrites, with Ti_3NiAl_2O on the γ-TiAl + Ti_2NiAl_3 (τ_3) eutectic regions. The acid mainly corroded the τ_3 phase, thus attacking the eutectic and leaving the γ-TiAl dendrites exposed.

DEDICATION

To my husband Simbulele Mantyi. Thank you so much for all your love, support and encouragement. Ndiyabulela Qhinebe, Gqugqugqu, Zithonga Zithathu, Mkhomazi, Dukanamahlathi, Haha!

ACKNOWLEDGEMENTS

The Lord

Thank you God Almighty for all the opportunities that You have afforded me. Without You none of this would be possible.

My supervisors

I wish to express my gratitude and deep appreciation to my supervisor, Professor Lesley Cornish, for nurturing me until the end of this research work. I will remain grateful to you, for your effective mentorship, dedication, and supervision. Thank you Prof! I also wish to thank my co-supervisors, Mr Alain Mwamba and Dr Lesley Chown. Thank you for your mentorship and invaluable advice.

Technical assistance

Thanks to Edson Muhuma for sharing his technical knowledge on melting, preparing and examining samples. Thanks to Richard Couperthwaite for assistance with XRD analysis. Thanks to Ndivhuwo Brayner Nelwelani for assistance with all SEM work.

Institutions

I would like to thank the DST, NRF, Mintek, AMI and DST-NRF CoE in Strong Materials for sponsoring my postgraduate studies. I would like to thank Mintek (Advanced Materials Division) for their support in allowing me to use their world class equipment.

My family

Thank to my parents, Dulcie Tsotetsi and Michael Tsotetsi, for supporting me and encouraging me to study engineering in the first place. Thanks Refiloe and Karabo, for being such wonderful sisters. Thanks to my husband, Simbulele Mantyi, I love you so much. Thanks to my children, Lulo and Qhamani, you two are the joy in my life.

TABLE OF CONTENTS

CHAPTER 1: INTRODUCTION 1
1.1 Background and motivation 1
1.2 Rationale and objective of the study 2
1.3 General layout 4
CHAPTER 2: LITERATURE REVIEW 6
2.1 Introduction 6
2.2 Titanium aluminides 7
2.2.1 Microstructure and phase transformations 7
2.2.2 Binary phase diagrams 12
2.2.3 Mechanical properties of titanium aluminides 16
2.2.4 Alloy development 20
2.2.5 Effect of aluminium content 22
2.2.6 Effect of noble metal additions 22
2.3 The Ti-Al-Ni and Ti-Al-Ru ternary systems 24
2.4 Manufacturing of titanium aluminides 25
2.5 Uses and applications of titanium aluminides 26
2.6 High temperature oxidation of titanium aluminides 28
2.6.1 Mechanisms of oxidation 30
2.6.2 Thermodynamics of oxidation 33
2.6.3 Kinetics of oxidation 34
2.6.4 Oxide scales 36
2.6.5 Hot salt oxidation 37
2.7 Aqueous corrosion of titanium aluminides 38
2.7.1 Corrosion mechanisms 39
2.7.2 Kinetics of electrochemical reactions 43
2.7.3 Cathodic modification 46
2.8 Rationale of the study 49
CHAPTER 3: EXPERIMENTAL PROCEDURE 50
3.1 Alloy synthesis 50
3.2 Metallography 50
3.3 Characterisation of alloys 50
3.4 Oxidation testing 51

3.4.1 Thermogravimetric analysis 51
3.4.2 Isothermal oxidation tests in air 51
3.4.3 Cyclic oxidation tests 51
3.4.4 Hot salt oxidation tests 52
3.5 Aqueous corrosion testing 52
CHAPTER 4: RESULTS 53
4.1 Microstructure and morphology of TAN alloy 53
4.2 Microstructure and morphology of TAN+Ru alloy 55
4.3 Hardness 58
4.4 High temperature oxidation results 59
4.4.1 Thermogravimetric analysis (TGA) 59
4.4.2 Isothermal oxidation of TAN 61
4.4.3 Isothermal oxidation of TAN+Ru 66
4.4.4 Cyclic oxidation of TAN and TAN+Ru 71
4.5 Corrosion behaviour in hydrochloric acid 78
4.5.1 Corrosion behaviour of TAN 79
4.5.2 Corrosion behaviour of TAN+Ru 81
4.5.3 Electrochemical results 85
CHAPTER 5: DISCUSSION 88
5.1 Microstructure and morphology 88
5.3 Hardness evaluation 89
5.3 Oxidation behaviour at 950°C 92
5.5 Corrosion behaviour in HCl 96
CHAPTER 6: CONCLUSIONS 98
CHAPTER 7: RECOMMENDATIONS 100
REFERENCES 101
APPENDIX 109

LIST OF FIGURES

Figure 1.1: Jet engine illustration [2015Pix]. 2

Figure 2.1: Assessed titanium-aluminium binary phase diagram [1993Oka]. 8

Figure 2.2: Crystal structure for α_2-Ti_3Al [2012Kot]. 9

Figure 2.3: Crystal structure for γ-TiAl [2012Kot]. 10

Figure 2.4: Central portion of Ti-Al phase diagram [2003Chr]. 11

Figure 2.5: Microstructure types in dual phase titanium aluminides [1989Kim].
(a) fully lamellar, (b) nearly lamellar, (c) duplex, and d) near-gamma. 12

Figure 2.6: Assessed titanium-aluminium phase diagram [1986Mur]. 13

Figure 2.7: Assessed titanium-aluminium phase diagram [1992Kat]. 14

Figure 2.8: Experimental titanium-aluminium phase diagram [1995Hay]..... 14

Figure 2.9: Experimental titanium-aluminium phase diagram [2006Sch]. 15

Figure 2.10: Assessed titanium-aluminium phase diagram [2008Wit]. 16

Figure 2.11: Dependence of mechanical properties on the microstructure type, where
NG = near-gamma, NL = nearly lamellar, and FL = fully-lamellar, CR = creep strength,
IR = impact resistance and GS = grain size [2009Has]. 18

Figure 2.12: Ordered face-centred tetragonal ($L1_0$) TiAl structure, tetragonality ratio
c/a = 1.02 with the (111) plane shaded [1989Kim]. 19

Figure 2.13: Effect of Al content on the room temperature ductility of wrought Ti-Al
metals [2011App]. 22

Figure 2.14: Schematic diagram showing how alloying with a noble metal produces a
passive mixed potential and a marked reduction in corrosion rate [1959Ste]. 23

Figure 2.15: Isothermal section of Ti-Al-Ni at 1000°C [2007Sch]. 24

Figure 2.16: Isothermal section of Ti-Al-Ru at 950°C [1989Kha]..... 25

Figure 2.17: General Electric GEnX engine [2014Gea]..... 27

Figure 2.18: TiAl turbocharger wheels made by Howmet Corporation [2003Dim]. 27

Figure 2.19: Ellingham diagram showing the standard free energy of formation of
selected oxides at a function of temperature [2011App]. 30

Figure 2.20: Mechanism of oxidation in γ-based titanium aluminides [1996Bey]. 32

Figure 2.21: Model for the structure of the scale and the substrate near the scale/substrate
interface [1996Tan]. 33

Figure 2.22: Oxygen equilibrium pressures of selected metal/oxide system [2011App]... 34

Figure 2.23: Schematic diagram showing the kinetics of oxidation for TiAl alloys [2011App]..... 35

Figure 2.24: Schematic of the four sub-reaction which occur when a metal (iron) corrodes in contact in with an electrolyte (water) [2004McE]..... 40

Figure 2.25: Schematic anodic and cathodic polarisation curves for a metal corroding in an acid solution [1971Den]. 42

Figure 2.26: Corrosion characteristics of an active-passive metal as a function of solution oxidizing power (electrode potential) [1996Hin]. 45

Figure 2.27: Schematic diagram of the effect of cathodic modification [1990Pot]. 47

Figure 4.1: XRD pattern of as-cast TAN, showing dendrites (dark) in a TiAl + Ti_2NiAl_3 (τ_3) (light) eutectic. 53

Figure 4.2: SEM-BSE image of as-cast TAN showing γ-TiAl dendrites (dark) in a TiAl + Ti_2NiAl_3 (τ_3)(light) eutectic. 54

Figure 4.3: SEM-BSE image of annealed TAN showing γ-TiAl dendrites (dark) in a TiAl + Ti_2NiAl_3 (τ_3) (light) eutectic. 54

Figure 4.4: XRD pattern of as-cast TAN+Ru. 56

Figure 4.5: SEM-BSE image of as-cast TAN+Ru showing γ-TiAl dendrites (dark) in a TiAl+ Ti_2NiAl_3 (τ_3) (light) eutectic. 56

Figure 4.6: SEM-BSE image of annealed TAN+Ru showing γ-TiAl dendrites (dark) in a TiAl + Ti_2NiAl_3 (τ_3) (light) eutectic. 57

Figure 4.8: DSC/TGA curves for the TAN alloy. 60

Figure 4.9: DSC/TGA curves for the TAN+Ru alloy. 60

Figure 4.10: Thermogravimetric analysis curves for TAN and TAN+Ru. 61

Figure 4.11: SEM-SE image of TAN surface after 120 hours oxidation in air at 950°C, showing TiO_2 and Al_2O_3 scales. 62

Figure 4.12: SEM-SE image of TAN after 720 hours oxidation in air at 950°C, showing degraded TiO_2 and Al_2O_3 scales. 63

Figure 4.13: SEM-BSE image of a cross-section of TAN after 120 hours oxidation in air at 950°C, showing TiO_2 and Al_2O_3 scales. 63

Figure 4.14: SEM-BSE image of a cross-section of TAN after 720 hours oxidation in air at 950°C, showing extensive cracks and pores in the alloy with a TiO_2/Al_2O_3 scale..... 64

Figure 4.15: XRD pattern of TAN after oxidation in air for 120 hours at 950°C. 65

Figure 4.16: XRD pattern of TAN after oxidation in air for 720 hours at 950°C. 65

Figure 4.17: SEM-SE image of TAN+Ru surface after 120 hours oxidation in air at 950°C, showingTiO_2scale on the eutectic and Al_2O_3scale on the dendrites. 67

Figure 4.18: SEM-SE image of TAN+Ru surface after 720 hours oxidation in air at 950°C, showing severely degraded TiO_2 and Al_2O_3 scales. 68

Figure 4.19: SEM-BSE image of a cross-section of TAN+Ru after 120 hours oxidation in air at 950°C, showing a substrate with extensive cracks and an oxide scale with an outer Ti-rich layer and an inner Al-rich layer. 68

Figure 4.20: SEM-BSE image of a cross-section of TAN+Ru after 720 hours oxidation in air at 950°C, showing the oxide scale consuming a dendrite in the substrate. 69

Figure 4.21: XRD pattern of TAN+Ru after oxidation in air for 120 hours at 950°C. 70

Figure 4.22: XRD pattern of TAN+Ru after oxidation in air for 720 hours at 950°C. 70

Figure 4.24: SEM-BSE images a) 200x and b) 1000x of TAN after cyclic oxidation in air, showing γ-TiAl dendrites in a eutectic of γ-TiAl + Ti_2NiAl_3 (τ_3). 72

Figure 4.25: SEM-BSE image of the cross-section of TAN after cyclic oxidation in air, showing the substrate with cracks and without an oxide layer. 72

Figure 4.26: SEM-BSE image of TAN+Ru after 120 hours cyclic oxidation in air, showing γ-TiAl dendrites in a eutectic of γ-TiAl + Ti_2NiAl_3 (τ_3). 73

Figure 4.27: SEM-BSE image of a cross-section of TAN+Ru after 120 hours cyclic oxidation in air, showing an intermixed TiO_2/Al_2O_3 scale with a nickel-rich sub-surface zone between the substrate and oxide layer and an outer TiO_2 scale. 74

Figure 4.28: Mass gain data of TAN and TAN+Ru obtained during cyclic oxidation in air and salt (Na_2SO_4) 75

Figure 4.29: SEM-SE images a) 2000x and b) 10000x of the surface of TAN after hot salt corrosion in Na_2SO_4 at 950°C, showing long, prismatic crystals on the surface. 76

Figure 4.30: SEM-SE images a) 500x and b) 3000x of the surface of TAN+Ru after 120 hours hot salt corrosion in Na_2SO_4 at 950°C, showing $TiO_2$and Al_2O_3 scales, and crystals partially covering the surface. 77

Figure 4.31 Comparison of mass gains for γ-TiAl alloys TAN and TAN+Ru in different oxidation environments. 78

Figure 4.32: SEM-SE image of the corroded surface of TAN in 5 wt% HCl, showing a thin and non-continuous Al_2O_3 oxide scale on the surface of the γ-TiAl dendrites, with Ti_3NiAl_2O in the γ-TiAl + Ti_2NiAl_3 (τ3) eutectic 79

Figure 4.33: SEM-BSE image of a cross-section of corroded TAN in 5 wt% HCl, showing the corroded surface with exposed γ-TiAl dendrites. 80

Figure 4.34: XRD pattern for TAN surface corroded in 5 wt% HCl. 80

Figure 4.35: XRD pattern for TAN surface corroded in 25 wt% HCl. 81

Figure 4.36: SEM-SE image of the corroded surface of alloy TAN+Ru in 5 wt% HCl, showing the Al_2O_3 and Ti_3NiAl_2O scales. 82

Figure 4.37: SEM-BSE image of a cross-section of corroded TAN+Ru alloy in 5 wt% HCl, showing a substrate with extensive cracks, a dendrite falling out and an unstable oxide layer. 82

Figure 4.38: SEM-SE images a) 530x and b) 2710x of the corroded surface of alloyTAN+Ru in 25 wt% HCl, showing a discontinuous and unstable oxide layer. 83

Figure 4.39: XRD pattern for TAN+Ru surface corroded in 5 wt% HCl. 84

Figure 4.40: XRD pattern for TAN+Ru surface corroded in 25 wt% HCl. 84

Figure 4.41: Electrochemical behavior of TAN in 5 wt% HCl. 85

Figure 4.42: Electrochemical behaviour of TAN+Ru in 5 wt% HCl. 86

Figure 4.43: Potentiodynamic scans for plain Ti-52.5Al (at.%) [2013Mwa], TAN and TAN+Ru in 5 wt% HCl. 87

Figure 4.44: Potentiodynamic scans for plain Ti-52.5Al (at.%) [2013Mwa], TAN and TAN+Ru in 25 wt% HCl. 87

Figure 5.1: Isothermal section of Ti-Al-Ni at 1000°C [2007Sch], showing the composition of the TAN alloy. 88

Figure 5.2: Isothermal section of Ti-Al-Ru at 950°C [1989Kha], showing the composition of Ti-52.5Al-0.2Ru (at.%). 89

Figure 5.3: Elongation (EL) and Vickers hardness of Ti-Al dual phase ($\alpha_2 + \gamma$) and single phase (γ) alloys at room temperature (RT) and 1000°C [1989Kim]..... 90

Figure 5.4: Effect of heat treatment on the hardness of alloys Ti-47.5Al (at.%) [2012Mwa], plain Ti-52.5Al (at.%) [1989Kim], TAN and TAN+Ru..... 91

Figure 5.5: Isothermal section at 945°C of Ti-Al-O system at ~3.98 x 10^{-37} oxygen partial pressure [1995Kel]. 93

Figure 5.6: Proposed mechanism of oxidation for TAN+Ru in air. 95

LIST OF TABLES

Table 2.1: Mechanical properties of TiAl alloys compared to Ti alloys and superalloys [1989Kim, 1994Boy]. 17

Table 2.2: Effect of selected alloying elements on mechanical propertiesofTiAl[1994Has, 2011App, 2012Kot]. 21

Table 2.3: Commercial titanium aluminide alloys [2012Kot]. 21

Table 2.4: Potential applications for titanium aluminides [2003Das]. 28

Table 2.6: Effect of various alloying additions on corrosion resistance of titanium [1959Ste]. 48

Table 4.1: EDX analyses for *as-cast* alloy TAN. 55

Table 4.2: EDX analyses for *heat treated* alloy TAN. 55

Table 4.3: EDX analyses for *as-cast* alloy TAN+Ru. 57

Table 4.4: EDX analyses for *heat treated* alloy TAN+Ru. 57

Table 4.5:Vickers hardness (HV_{10}) ofTAN and TAN+Ru, in at.%. 58

Table 4.6: EDX analyses for TAN after 120 hours oxidation in air at 950°C. 64

Table 4.7: EDX analyses for TAN after 720 hours oxidation in air at 950°C. 64

Table 4.8: EDX analyses for alloy TAN+Ru after 120 hours oxidation in air at 950°C. 67

Table 4.9: EDX analyses for alloy TAN+Ru after 720 hours oxidation in air at 950°C. 69

a) SEM-BSE image of TAN (200x) after cyclic oxidation in air. 71

b) SEM-BSE image of TAN (1000x) after cyclic oxidation in air. 72

Table 4.10: EDX analyses for alloy TAN after 120 hours cyclic oxidation in air between room temperature and 950°C. 73

Table 4.11: EDX analyses for alloy TAN+Ru after 120 hours cyclic oxidation in air between room temperature and 950°C. 73

Table 4.12: EDX analyses for alloy TAN after 120 hours cyclic oxidation in Na_2SO_4. 75

a) SEM-SE image of TAN (2000x). 76

b) SEM-SE image of TAN (10000x). 76

a) SEM-SE images (500x) of TAN+Ru after hot salt corrosion in Na_2SO_4 at 950°C. 77

b) SEM-SE image (3000x) of TAN+Ru after hot salt corrosion in Na_2SO_4 at 950°C. 77

Table 4.13: EDX analyses for alloy TAN+Ru after 120 hours cyclic oxidation in Na_2SO_4. 78

a) SEM-SE image of TAN+Ru (530x) after exposure to 25 wt% HCl. 83

b) SEM-SE image of TAN+Ru (2710x) after exposure to 25 wt% HCl. 83

Table 4.14: Electrochemical characteristics of Ti-52.5Al (at.%) alloys in HCl..... 85

CHAPTER 1: INTRODUCTION

1.1 Background and motivation

The South African government is driving a beneficiation strategy which aims to encourage local industry to process and beneficiate raw materials, such as metals and minerals, prior to export [2011Ano]. This will create a value adding, downstream use for materials, create jobs and grow the economy. Metals such as titanium, aluminium and nickel are being explored as they are strategic for further beneficiation. South Africa has an abundance of these mineral resources, which are readily mined and processed [2011Ano]. However, these metals are either exported as unprocessed minerals, or only the primary processing of their ores are done locally [2008Mot, 2009Ika, 2011Ano]. Since South Africa then has to import expensive finished products, it would be better to locally process and manufacture these products. There is thus an opportunity for South African companies to be involved in the manufacture of finished products from these metals, to increase local job and wealth creation.

The Titanium Centre of Competence (TiCoC), hosted by the Council for Scientific and Industrial Research (CSIR) has developed process for producing titanium powder at a much lower cost than current imported powders [2013Ano]. Scaling-up of the process towards commercialisation is underway. Therefore, relatively large quantities of lower cost titanium powder may soon be available in South Africa. This development further increases the potential for a downstream industry for titanium metal components and products. The manufacturing of titanium aluminides to make aeroplane and automobile engine components is one such industry which can be developed to improve the economy [2008Mot, 2009Ika]. This industry is highly specialised and South Africa is still a small player. South Africa thus has the potential to grow in this sector which is labour intensive and value adding [2008Mot, 2009Ika].

Titanium aluminides are possible substitute materials for aeroplane and automobile components because they are lighter (~3.8 $g.cm^{-3}$) than nickel-based alloys (~8 $g.cm^{-3}$) and titanium alloys (~4.5$g.cm^{-3}$) currently used [1989Nis, 1997Kel, 2000Cha]. Consequently, most of the research on titanium aluminides is focused on high

temperature applications [1976Cho, 2011App, 2012Kot] and there is limited research on their room temperature aqueous corrosion. Titanium and titanium alloys have excellent corrosion resistance [1959Ste, 1996Sch, 2000Van]. However, in low pH chloride solutions, titanium alloys are susceptible to crevice and pitting corrosion, and it is possible that small additions of ruthenium could alleviate this, especially since they have improved the corrosion resistance of other Ti-containing alloys [2000Van, 2013Mwa]. The ruthenium additions would be small, and so would not affect the density too adversely, and if there was significant improvement in the properties, the increased price.(due to addition of expensive ruthenium) would be worth it.

In this study, two titanium aluminide alloys were made using elements available in South Africa. The behaviour of the alloy under high temperature oxidation and room temperature aqueous corrosion conditions were investigated.

1.2 Rationale and objective of the study

Conditions in jet engines (Figure 1.1) are highly corrosive, have high pressures and can reach temperatures of ~1300°C in the combustion section [1992Fro, 2012Kot]. Therefore, jet engines need to be made from strong, light-weight, corrosion-resistant and thermally stable components to make aircraft viable and safe for commercial use. Currently, jet engine components are mostly made from titanium, nickel and aluminium-based alloys as these alloys have high strength to-weight-ratios and high melting points [1992Fro, 2012Kot].

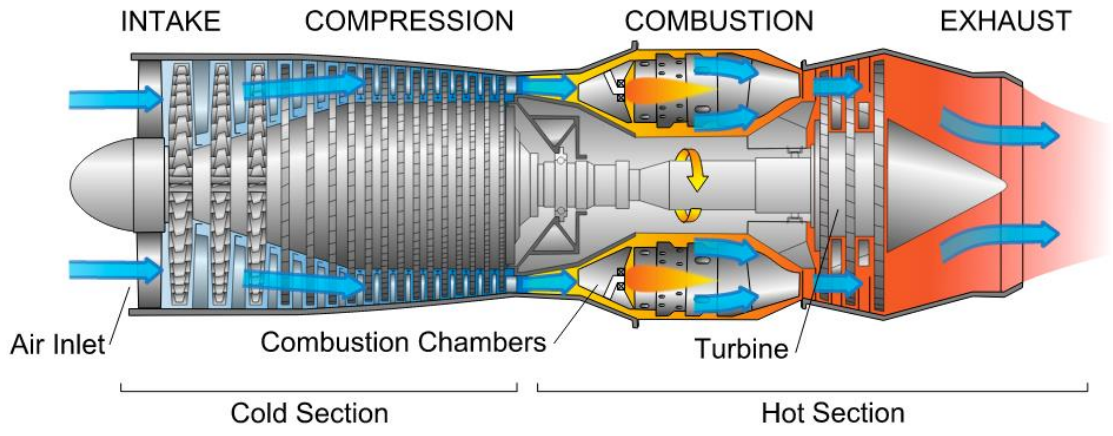

Figure 1.1: Jet engine illustration [2015Pix].

A typical jet engine consists of a cold section, with a maximum temperature of ~600-~750°C and a hot section, where temperatures can reach ~1400°C. The inlet fans and intermediate compressor in the cold section are primarily made from titanium-based alloys which have a low density (~4.5 $g.cm^{-3}$), high hardness and good corrosion resistance [1995Imm, 1999Voi].

However, titanium-based alloys do not have a good burn resistance (they are capable of igniting and burning when subjected to high temperatures) at temperatures above 800°C.This can cause titanium fires in the hot section of jet engines [1992Fro, 2012Kot]. Therefore, the combustion chambers and turbine blades are made from denser (~8 $g.cm^{-3}$) nickel-based superalloys (NBSAs) which are more burn resistant [1995Imm, 1999Voi]. The use of NBSAs is limited though, as jet engines already operate above their melting point (1360°C). NBSAs are kept from melting by air diverted from the compressor, which is used to cool the combustion chamber and turbine blades.

To improve the efficiency of jet engines, gamma titanium aluminides (γ-TiAls) are being used to replace NBSAs to make turbine blades in the hot section of jet engines [1989Nis, 1997Kel, 2000Cha]. They are more burn-resistant than titanium-based alloys and are lighter than both NBSAs and titanium-based alloys (~3.8 $g.cm^{-3}$). The mass savings through the use of γ-TiAl alloys could result in jet engines which use less fuel, are more environmentally friendly and cost less to operate.

Titanium aluminides are intermetallic compounds which retain their good thermo-physical properties at elevated temperatures [2000App]. They are thus used extensively in the aerospace and automotive industries due to their low density, high strength, creep resistance and good burn resistance [1989Nis, 1997Kel, 2000Cha].

In this study, Ti-52.5Al-10.0Ni (at.%) and Ti-52.5Al-10.0Ni-0.2Ru (at.%) alloys were made and subjected to typical conditions found in aerospace and automotive engines. The aim was to investigate if these alloy compositions could produce an alloy suitable to make lighter hot components for aerospace and automotive applications.

Since there is limited research on the room temperature aqueous corrosion of titanium aluminides, the corrosion of the alloys in low pH chloride solutions was investigated to

determine if they were susceptible to pitting corrosion. Titanium aluminides could be used to make lighter components (given that small amounts of ruthenium will not affect their density very much) in low pH chloride environments, such as petrochemical processing, offshore oil, gas and marine environments. In these environments, the pH is similar to that of 5 wt% and 25 wt% HCl [1996Saf].

The high aluminium content was selected to ascertain whether the alloy would form the protective Al_2O_3 oxide instead of TiO_2 oxide. At high temperatures, titanium alloys tend to form the less protective TiO_2 oxide, and thus become susceptible to excessive oxidation [1976Cho, 1988Sub, 1989Kim].

Nickel was added to improve the corrosion resistance of the alloy, as the corrosion resistance of nickel aluminides is high [1996Bra, 1996Sch].

Ruthenium was added to improve the corrosion and oxidation resistance of the alloy because additions of ruthenium to ferritic steels [1977Str, 1990Pot] and some titanium alloys [1959Ste, 1990Pot, 2000Van] have improved corrosion and oxidation resistance.

Therefore, the objectives of the study were to:

- Characterise the microstructure, morphology and phase compositions of the ternary Ti-52.5Al-10.0Ni (at.%) and quaternary Ti-52.5Al-10.0Ni-0.2Ru (at.%) alloys.
- Investigate the high temperature behaviour of the alloys in typical conditions found in aerospace engines.
- Investigate the room temperature aqueous corrosion behaviour of the alloys in two reducing environments (5 wt% and 25 wt% hydrochloric acid). This was done to investigate the effect of pH on the corrosion behavior of the alloys.

1.3 General layout

This dissertation comprises six chapters. Chapter 1 gives the motivation and objectives of the study. Chapter 2 gives the literature review, a background description of gamma titanium aluminides and their oxidation and corrosion behaviour. The experimental procedure is presented in Chapter 3. Chapter 4 presents the results which are discussed in Chapter 5. Chapter 6 provides the conclusions of the study and Chapter 7 gives the

recommendations for future research. Published peer-reviewed papers based on this research are included in the Appendix.

CHAPTER 2: LITERATURE REVIEW

2.1 Introduction

Titanium aluminides (Ti-Al) are classified as intermetallic compounds, together with nickel aluminides (Ni-Al) and iron aluminides (Fe-Al). They are compounds formed from two metals, with properties and crystal structures completely different from their parent metals [1984Yam, 1994Has, 1995Sau], and their properties are intermediate between ceramics and metals. Intermetallic compounds have long range ordered lattice structures which determine their deformation modes, resulting in high strengths at elevated temperatures, but with fast crack growth rates and very low ductility and fracture toughness at room temperature [1984Yam, 1994Has, 1995Sau, 1997Sob, 2004Sob].

Titanium aluminides (γ-TiAl) are lightweight (~3.8 $g.cm^{-3}$) compounds which retain their properties at elevated temperatures [1976Cho, 1995Sau, 2004Lut, 2007Lut, 2011App]. They are therefore considered good candidate materials for structural materials for high temperature applications as they have a high specific density, good oxidation resistance below ~800°C, good corrosion resistance, and excellent strength retention and creep resistance at elevated temperatures [1985Lip, 1995Kim, 1995Sau, 2000App]. Their widespread application has been limited by poor formability at room temperature and challenges in processing and manufacturing [1985Lip, 1995Kim, 1995Sau, 2000App].

Over the past ~40 years, extensive research on titanium aluminides has resulted in more knowledge on their microstructures and deformation mechanisms, discoveries in their microalloying and advances in manufacturing technologies [1985Lip, 1990Yam, 1995Kim, 1997Yam, 1998App, 2000App, 2003Nas]. This has led to an increasing use of titanium aluminides in commercial applications. In 2000, General Electric (GE) designed the GenEx gas turbine engine for the Boeing 787 Dreamliner which has titanium aluminide turbine blades, making the engine lighter and more fuel efficient [2000App, 2003Nas]. More burn-resistant TiAl exhaust valves have been used to replace alloys Ti-6242, Ti-1100 and IMI 834 in gas turbines.

In the future, TiAl turbocharger wheels could be used to replace denser nickel-based superalloys (NBSAs). There is a proposal to use TiAl for the divergent flap in high speed civil transport aircraft to meet the strict environmental requirements of reduced exhaust gas and noise pollution [2003Das, 2011App].

The majority of current TiAl commercial applications are in the aerospace industry with some applications in the automobile industry [1992Liu, 1997Yam, 2003Nas]. This is because most of the research on titanium aluminides has focused on improving their high temperature performance and therefore there is very little research on the room temperature corrosion behaviour of these materials [1996Sch, 2000Van, 2012Mwa]. Due to their low density and good corrosion resistance, titanium aluminides could potentially be used to make components for medical implants, petrochemical processing equipment, downhole oil and geothermal sour wells and chlor-alkali and chlorate cell anodes and liners [1996Sch, 2000Van, 2008Riv].

The challenge with titanium aluminides is that, although they can introduce weight savings in aircrafts and automobiles, they are more costly to manufacture than traditional titanium alloys and NBSAs [2012Kot]. However, the cost is expected to fall as they gain widespread use. Another challenge with titanium aluminides is that they still have inferior mechanical properties (low ductility and fracture toughness) than NBSAs.

2.2 Titanium aluminides

2.2.1 Microstructure and phase transformations

The Ti-Al system has a range of titanium aluminide compounds with three major phases: α_2-Ti_3Al, γ-TiAl and $TiAl_3$, as shown in Figure 2.1 [1993Oka]. The most important phases of the Ti-Al system are α_2-Ti_3Al and γ-TiAl as they have good properties to make lighter, structural components for high temperature aerospace and automobile applications [1989McC, 1993Oka, 2003Ber, 2006Bat, 2009Sar, 2012Kot].

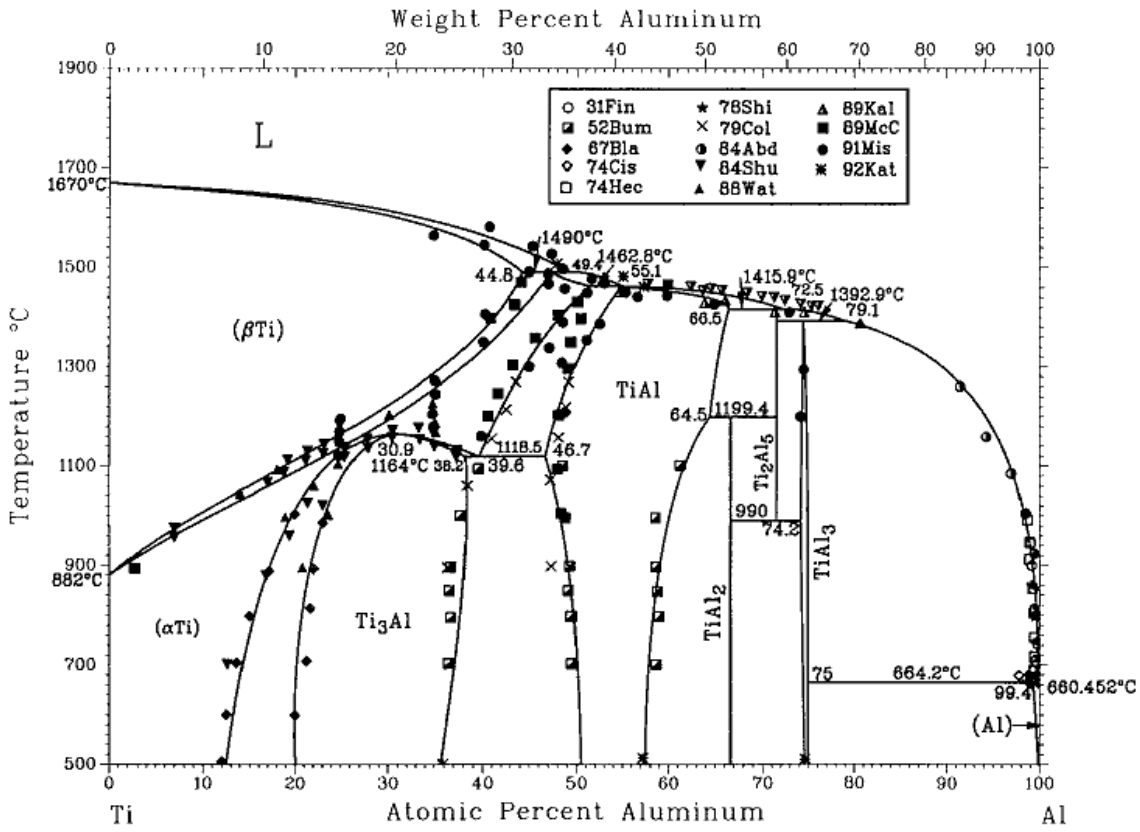

Figure 2.1: Assessed titanium-aluminium binary phase diagram [1993Oka].

The α_2-Ti_3Al phase (Figure 2.2 [2012Kot]) has a hexagonal DO_{19} structure with a homogeneity range from 20 - 38.2 at.% Al. The γ-TiAl phase (Figure 2.3 [2012Kot]) is an ordered face-centred tetragonal phase with an $L1_0$ structure, whose homogeneity ranges from 48.5-66.0 at.% Al. The γ-TiAl phase tetragonality is due to the different atomic radii of titanium and aluminium. For the equiatomic Ti-Al composition, the tetragonality ratio (c/a) is 1.02. The ratio increases to 1.03, with increasing aluminium content [1989Kim]. Alloys in the 37 - 49 at.% Al region have a dual microstructure consisting of γ grains and duplex lamellar grains of alternating layers of γ-TiAl and α_2-Ti_3Al [1989McC, 1993Oka, 2003Ber, 2006Bat, 2009Sar, 2012Kot]. The dual microstructure forms by the eutectoid transformation at 1118.5°C where the pro-eutectoid (αTi) transforms to the eutectoid α_2-Ti_3Al and γ-TiAl. There is consensus that between 50 and 66.0 at.% Al, TiAl exists as a single pure gamma (γ) phase with equiaxed gamma grains.

Pure titanium is a hexagonal close-packed α-phase at room temperature. At ~882°C, titanium transforms into the body-centred cubic β-phase (Figure 2.1). The dual phase α_2-Ti_3Al alloys are generally composed of α_2-Ti_3Al and β-Ti. The β-phase occurs as either ordered (B2) or disordered (bcc) phase depending upon the alloying content [1992Chi].

The gamma (γ) phase has excellent oxidation resistance at temperatures up to 800-950°C, and low hydrogen absorption, but it has no ductility at room temperature. The layered arrangement of titanium and aluminium atoms within the face-centred cubic structure, and the tetragonality ratio result in two types of deformation (twinning and slipping) along the {111} planes (shaded plane in Figure 2.3) [1986Hug, 1987Kaw]. On its own, γ-TiAl is therefore considered to be of little engineering significance [1991Kim1, 2003Ber, 2009Sar, 2012Kot]. The alpha 2 (α_2) phase has good high temperature strength, but this is offset by the high rate of oxygen and hydrogen absorption which leads to embrittlement at high temperatures. The α_2 phase has a very low density at room temperature. On its own, α_2-Ti_3Al also has no engineering significance [1991Kim1, 2003Ber, 2009Sar, 2012Kot].

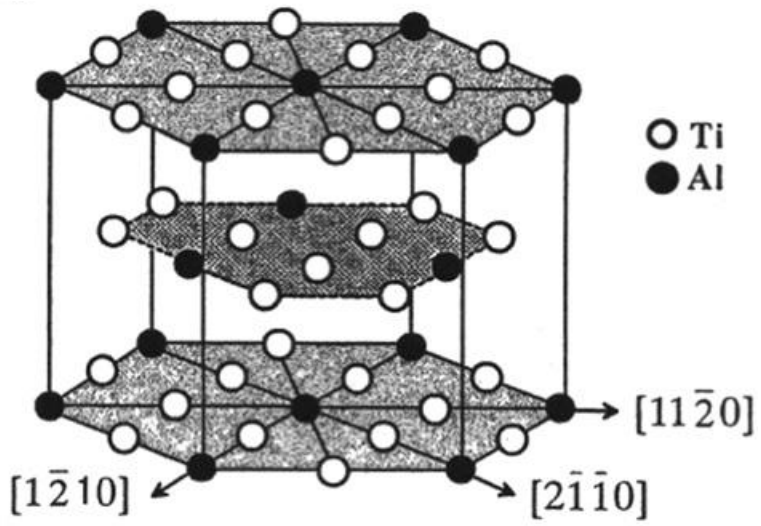

Figure 2.2: Crystal structure for α_2-Ti_3Al [2012Kot].

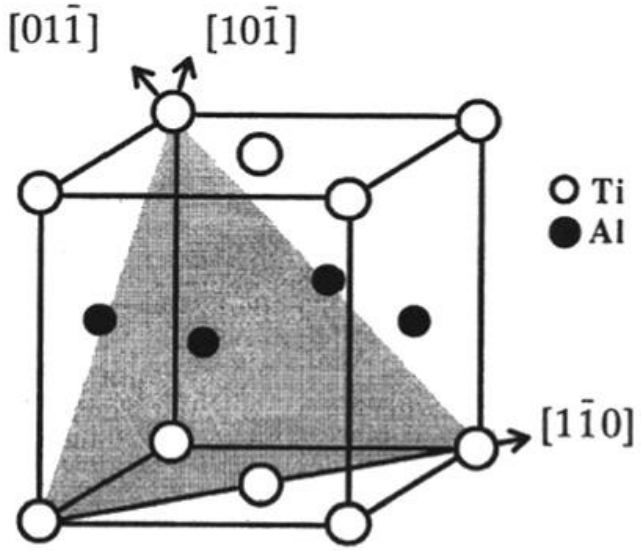

Figure 2.3: Crystal structure for γ-TiAl [2012Kot].

In most engineering applications, dual phase alloys containing $\gamma + \alpha_2$ are used to maximise thermo-physical properties [2011App, 2012Kot]. The most commonly used dual phase Ti-Al alloys are the duplex alloys with the composition Ti-(46-49) Al (at.%) as they have the best ductility [2011App, 2012Kot]. These alloys have fine lamellar colonies which aid the deformation of the gamma phase, thus improving ductility [2000Yam, 2011App, 2012Kot].

Depending on their processing, Al composition and subsequent heat treatment, the dual phase titanium aluminide alloys can form various microstructures with unique mechanical properties. The microstructures are grouped into four main categories: near-gamma, duplex, nearly lamellar and fully lamellar [1989Kim, 1991Kim2, 2006Sha]. The duplex and fully lamellar microstructures are the main alloys which have been used for commercial engineering applications [2000Yam, 2012Kot].

There are various phase diagrams for the Ti-Al system; however the phase diagram shown in Figure 2.4 is largely accepted for the central region of the Ti-Al system [1989Kim]. For an alloy with the composition C_0, the four main categories of microstructures can be obtained by heating it to T_1 and then subsequently cooling to T_2, T_3 and T_4 (Figure 2.4).

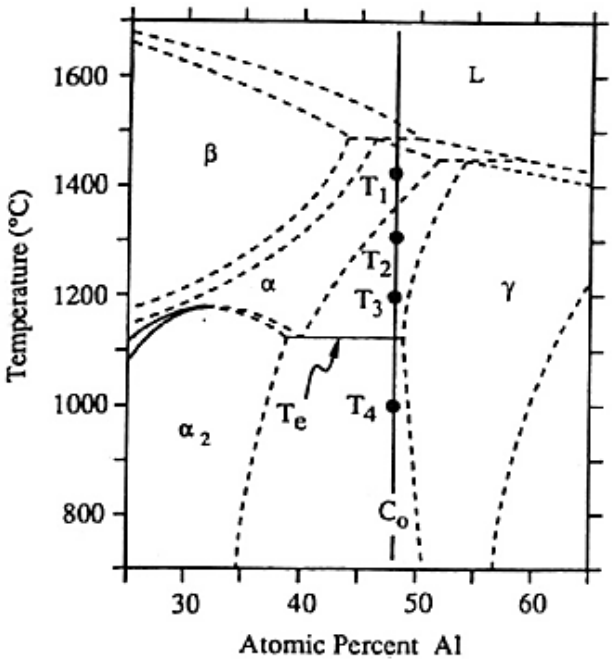

Figure 2.4: Central portion of Ti-Al phase diagram [2003Chr].

Cooling the alloy from T_1 (in the α-phase field) yields a fully lamellar microstructure with coarse grains in the range of 200 - 1000 µm. The phase transformation that occurs is: $\alpha \leftrightarrow \gamma + \alpha_2$, where the α phase transforms into alternating plates of $\gamma + \alpha_2$ (Figure 2.5a). The coarse grain size causes low ductility and strength, although the alloy has excellent creep and fatigue resistance.

Further heat treatment of the fully lamellar microstructure at T_3 (Figure 2.4) in the $\alpha + \gamma$ phase field, yields a duplex microstructure with fine (~10 µm) fully lamellar colonies and equiaxed γ grains [1989Kim]. The phase transformation that occurs is: $\alpha \leftrightarrow \alpha_{2s} \leftrightarrow \alpha_2 + \gamma$ where α_{2s} (α_2 supersaturated with aluminium) nucleates the γ phase. The resulting fine grain size (Figure 2.5c) is the reason this microstructure has the best ductility and strength at room temperature. The duplex microstructure has an α/γ phase volume ratio of 1.

Further heat treatment at T_2, in the $\gamma + \alpha$ phase field, produces nearly-lamellar microstructures which are between fully lamellar and duplex [1989Kim]. The α/γ phase volume ratio is greater than 1, with mostly coarse lamellar colonies and some fine γ grains (Figure 2.5b). The grain size is in the range of 150 - 200 µm.

Heat treatment at T_4 (Figure 2.4), in the $\alpha_2 + \gamma$ phase field, yields a near-gamma microstructure (Figure 2.5d) with coarse γ grains (30 - 50 µm), fine γ grain regions and dispersed α_2 precipitates at grain boundaries [1989Kim, 2012Kot].

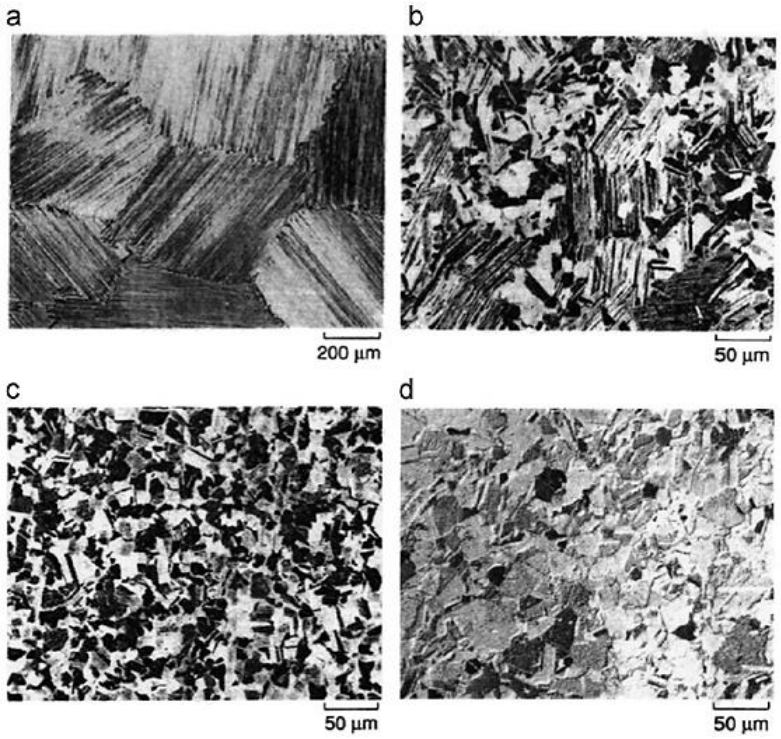

Figure 2.5: Microstructure types in dual phase titanium aluminides [1989Kim]. (a) fully lamellar, (b) nearly lamellar, (c) duplex, and d) near-gamma.

Due to their good properties, much research [1998Dim, 2002Cho, 2009Has] has been done on titanium aluminides to develop alloys with the best features of duplex and fully lamellar microstructures, i.e. alloys with a fine grain size, with good ductility and strength at room temperature and excellent creep and fatigue resistance.

2.2.2 Binary phase diagrams

Another challenge with the fabrication of titanium aluminides is that there are currently different versions of the phase diagrams with some dispute in the 55 - 77 at.% Al (single phase gamma) range at 900-1450°C [2006Bat]. Materials Science International (MSI) currently accepts the Ti-Al system in Figure 2.10 [2008Wit] which is based on experimental data. The phase diagram by Murray [1986Mur] in Figure 2.6 was the generally accepted phase diagram until the 1980s [1992Chi]. The dashed lines indicate

the estimated phase boundaries. Figure 2.6 shows the intermetallic compounds Ti_3Al (α_2), TiAl (γ), $TiAl_2$ and δ with variable compositions. It also shows the intermetallic compound $TiAl_3$ with constant composition, and no homogeneity range. The diagram shows three peritectic reactions, including the $L + \beta \rightarrow \gamma$ reaction.

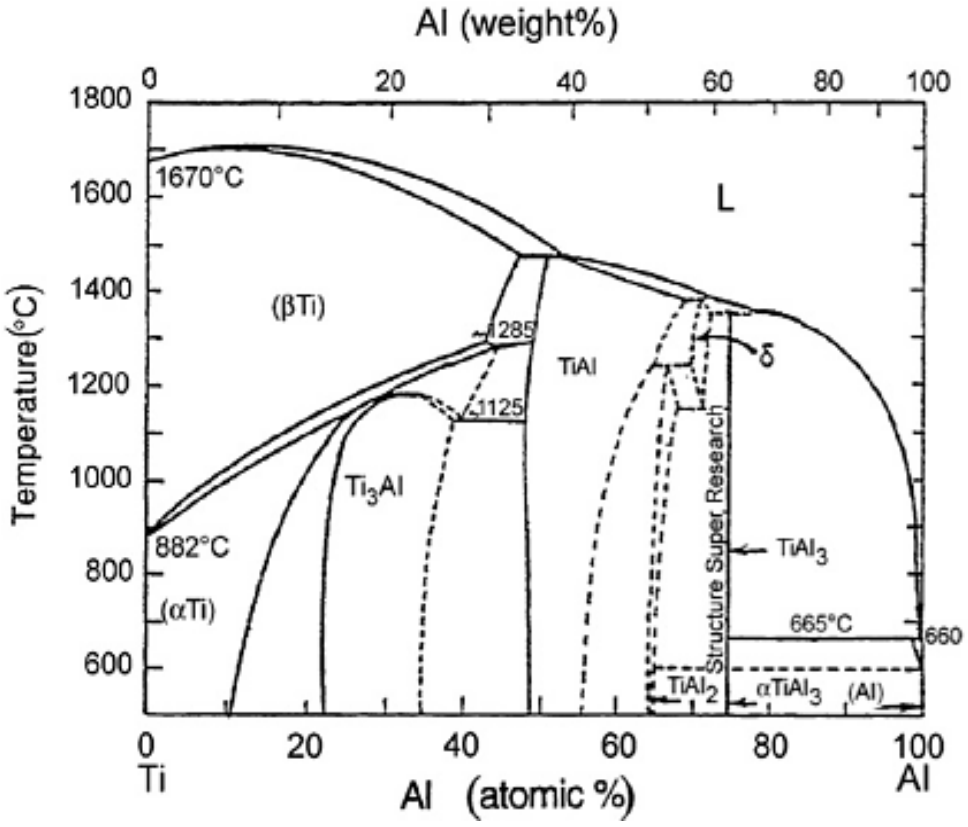

Figure 2.6: Assessed titanium-aluminium phase diagram [1986Mur].

Kattner et al. [1992Kat] proposed another phase diagram (Figure 2.7) showing two high temperature peritectic reactions $\beta + L \rightarrow \alpha$ and $\alpha + L \rightarrow \gamma$ [1992Chi]. Figure 2.7 shows the intermetallic compounds Ti_3Al (α_2), TiAl (γ) and $TiAl_3$ with variable compositions. The $TiAl_2$ and Ti_2Al_5 phases have a constant composition. In the 1990s, Figure 2.7 was the generally accepted phase diagram.

Figure 2.8 [1995Hay] presents a third version of the experimental Ti-Al binary phase diagram. The diagram shows the controversial ξ phase with dashed lines representing the likely phase boundaries because there have been many differences in showing them. The intermetallic compounds Ti_3Al (α_2) and TiAl (γ) have variable compositions and $TiAl_2$ and $TiAl_3$ have constant compositions. $TiAl_2$ is considered stable up to 1216°C compared with 1199.4°C in Figure 2.6 [1986Mur] and Figure 2.7 [1993Oka].

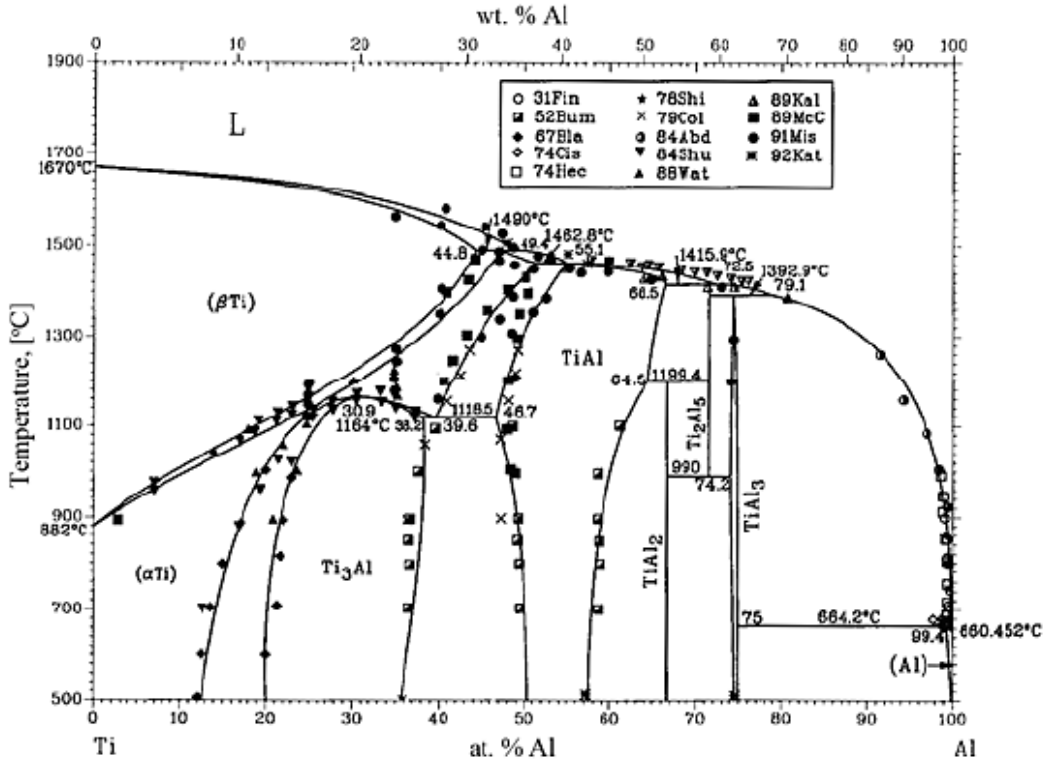

Figure 2.7: Assessed titanium-aluminium phase diagram [1992Kat].

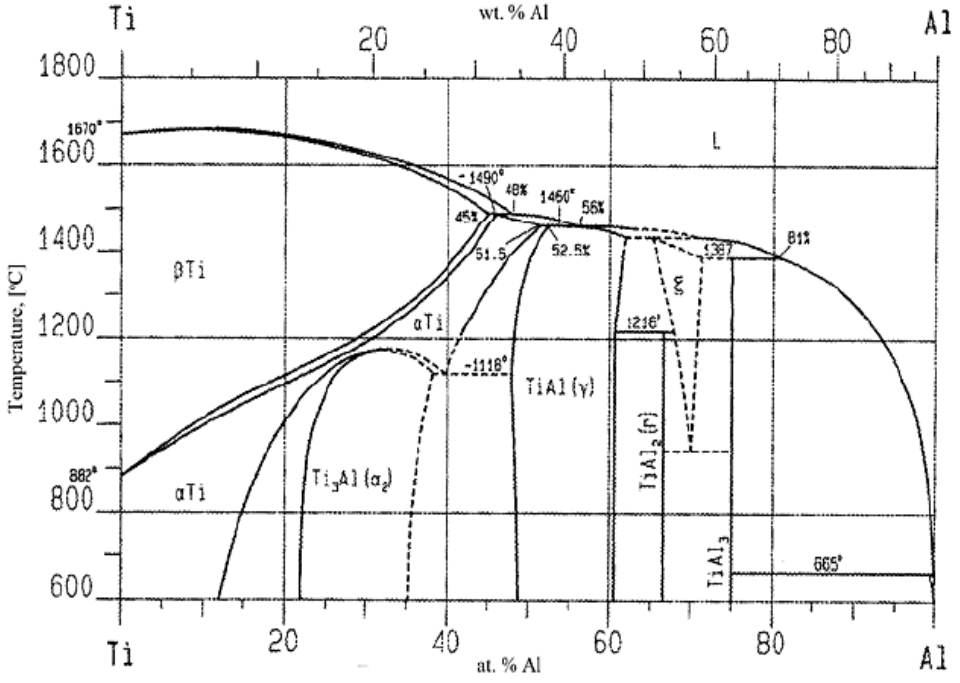

Figure 2.8: Experimental titanium-aluminium phase diagram [1995Hay].

Schuster and Palm [2006Sch] also produced a Ti-Al phase diagram shown in Figure 2.9 [2006Sch] using experimental data. It differs from the Murray [1986Mur] phase diagram (Figure 2.6) because it contains the peritectic reaction $L + \beta \rightarrow \alpha$.

Further evaluation of the Ti-Al system by Witusiewicz *et al.* [2008Wit] produced the diagram shown in Figure 2.10 [2008Wit], which is very similar to that of Schuster and Palm [2006Sch]. Figure 2.10 shows the occurrence of Ti_5Al_3 and the peritectoid reaction $\alpha + \beta \rightarrow \alpha_2$. In Figures 2.6 - 2.8, the α_2 phase is formed congruently from α. Figure 2.10 [2008Wit] is currently the generally accepted phase diagram for the Ti-Al system.

There is therefore contention on the Ti-Al phase diagram and the discrepancies in the experimental data are because of the high sensitivity of phase equilibria to non-metallic impurities such as oxygen [2006Sch]. Thus, as well as choosing the best phase diagram, researchers must be aware that the conditions of their alloys might not be in equilibrium and should take care and interpret phase diagrams carefully.

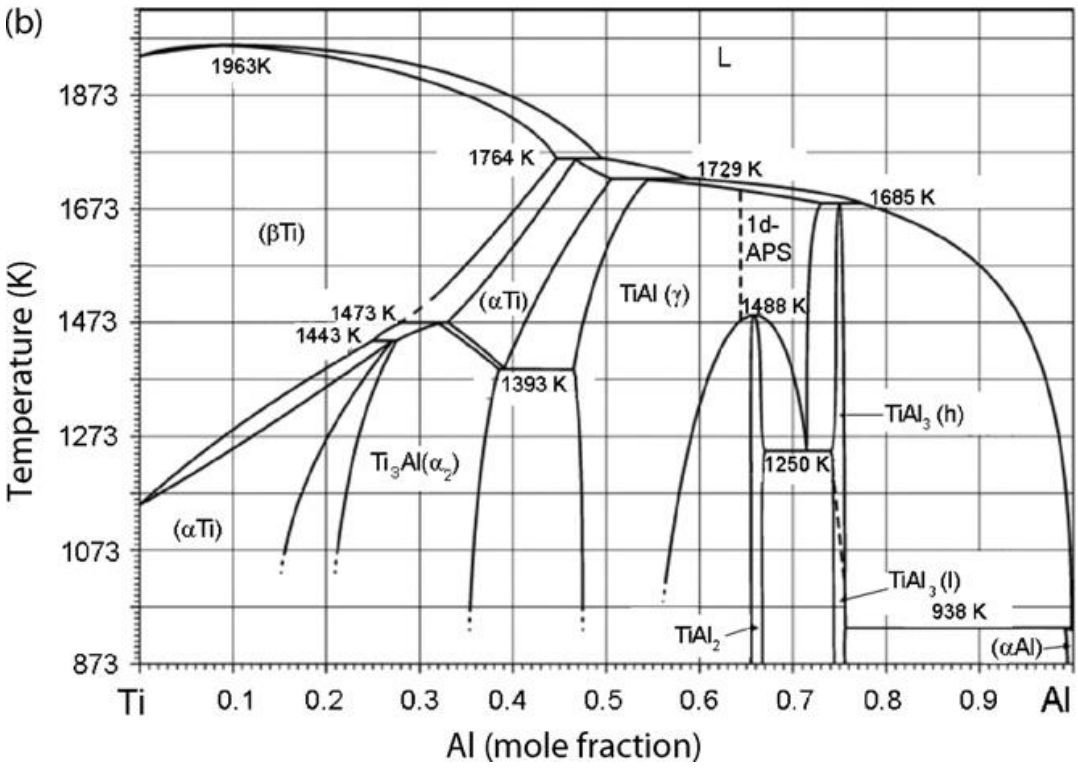

Figure 2.9: Experimental titanium-aluminium phase diagram [2006Sch].

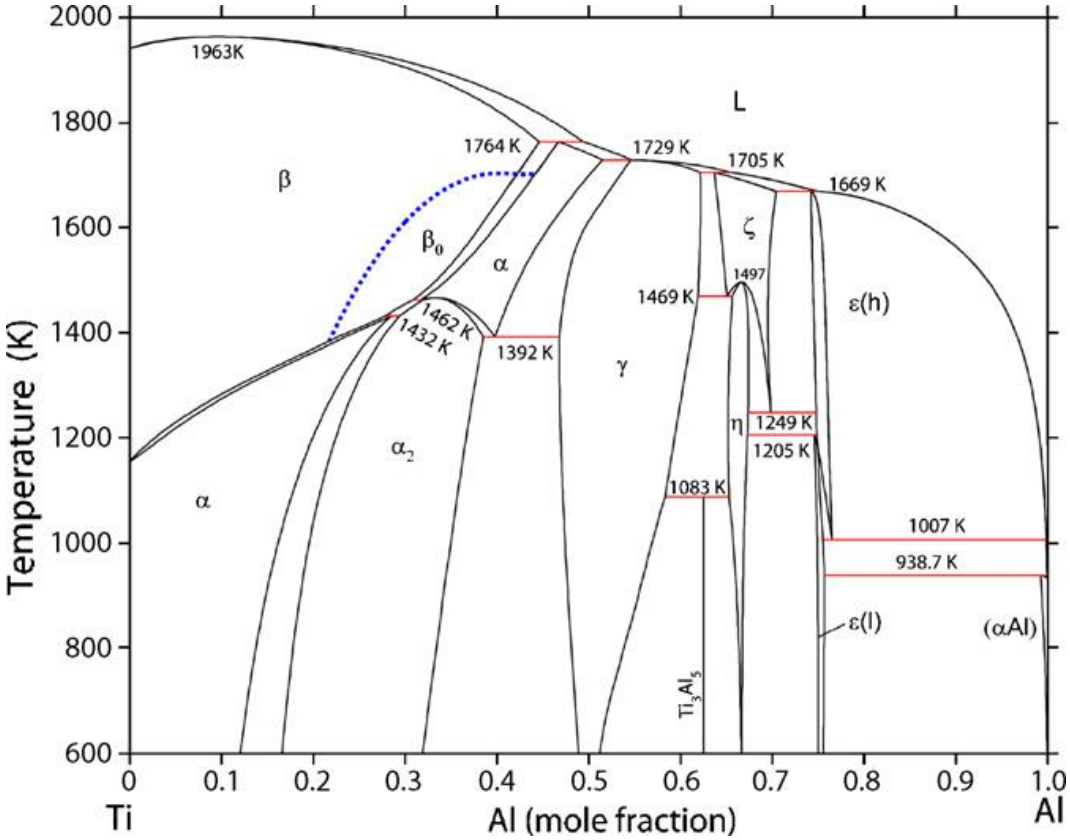

Figure 2.10: Assessed titanium-aluminium phase diagram [2008Wit].

2.2.3 Mechanical properties of titanium aluminides

As mentioned earlier, titanium aluminides have good properties at elevated temperatures [1985Lip, 1994Boy, 2011App]. They are considerably lighter (Table 2.1) than NBSAs and titanium alloys, have good oxidation resistance and creep limits and have good burn resistances. However, their ductility and fracture toughness at room temperature are inadequate compared to NBSAs and titanium alloys [1985Lip, 1994Boy, 2011App]. They have a lower elastic modulus than NBSAs, but they retain their properties at high temperatures because they have strong A-B bonding of their ordered structure and therefore require much higher energy for diffusion to occur. Consequently, titanium aluminides have better high temperature creep and fatigue strength [1989Kim].

Table 2.1: Mechanical properties of TiAl alloys compared to Ti alloys and superalloys [1989Kim, 1994Boy].

Property	Unit	Ti Alloys	α_2-Ti_3Al	γ-TiAl	Superalloys
Structure		Hcp/bcc	DO_{19}	$L1_0$	Fcc/$L1_2$
Density	$g.cm^{-3}$	4.5	4.1 - 4.7	3.7 - 3.9	7.9 - 8.5
Modulus	GPa	96 - 115	100 - 145	160 - 176	206
Yield stress σ_y	MPa	380 - 1150	700 - 790	400 - 630	800 - 1200
U.T.S.	MPa	480 - 200	800 - 1100	450 - 700	1250 - 1450
Toughness	$MPa.m^{1/2}$	12 - 120	12 - 35	12 - 25	30 - 100
Ductility R.T.	%	10 - 20	2 - 10	1 - 4	3 - 5
Ductility H.T.	%	12 - 50	10 - 20	10 - 90	10 - 20
Oxidation limit	(°C)	600	650	800 - 950	870 - 1090
Creep limit	(°C)	600	760	1000	1090
Burn resistance		Poor	good	good	excellent

The mechanical properties of γ-TiAl alloys, shown in Figure 2.11 [2009Has], are heavily dependent on composition, phases and microstructure morphology [2012Kot]. Duplex microstructures exhibit good room temperature ductility and strength due to their fine grain size. Fully lamellar microstructures have good high temperature properties such as creep and fatigue resistance; however, they have a low room temperature ductility and strength due to their coarse grain size. There are therefore many thermo-mechanical routes [1997Che, 2003Sun, 2009Che, 2010Cha] being explored to produce fine-grained fully lamellar microstructures with good ductility, creep resistance, fatigue life, fracture toughness and tensile strength.

Ductility

Ductility is dependent on four factors [2012Kot]:

- Grain size
- Lamellar/gamma ratio (L/γ)
- Changes in lattice dimensions (c/a)
- Presence of impurities

A smaller or finer grain size leads to an improvement in ductility because volume defects such as grain boundaries increase in size. Grain boundaries prevent further dislocation propagation and therefore increased grain boundary area improves ductility and yield strength [1996Mer]. For optimum ductility in TiAl alloys, the L/γ ratio should be 0.3 – 0.4 and the α_2/γ ratio should be 3 – 15%. Both ratios are dependent on Al concentration and are in their optimal range at 48.0 at.% Al. Ductility is also greatly affected by the tetragonality ratio (*c/a*) and unit cell volume, as shown in Figure 2.12 [1989Kim, 2012Kot]. A decrease in *c/a*, achieved by reducing the Al content, improves ductility. A decrease in unit cell volume, which can be achieved by adding ternary and quaternary alloying elements, also improves ductility in the γ phase. The presence of impurities such as oxygen and nitrogen also reduces ductility, and a reduction in impurities improves ductility.

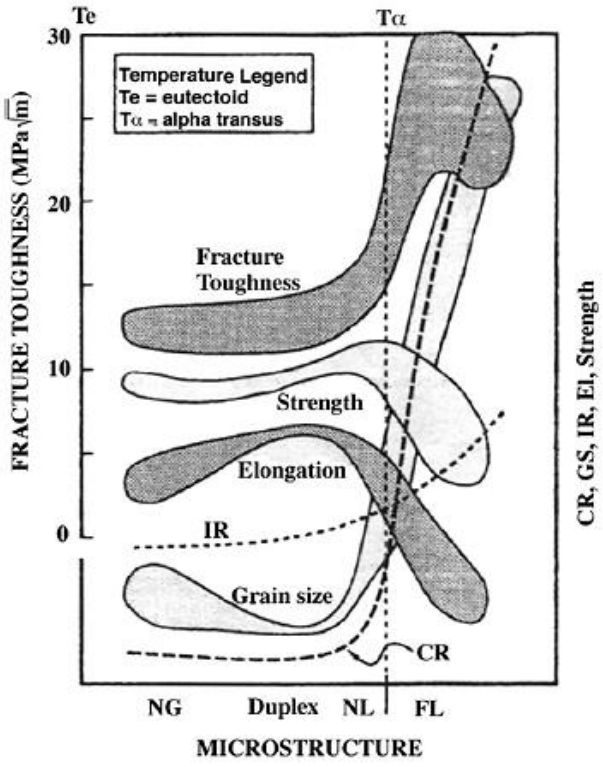

Figure 2.11: Dependence of mechanical properties on the microstructure type, where NG = near-gamma, NL = nearly lamellar, and FL = fully-lamellar, CR = creep strength, IR = impact resistance and GS = grain size [2009Has].

Creep resistance and fatigue life

Microstructure and the Al content control creep resistance in dual phase titanium aluminides [2012Kot]. Increasing the Al content improves creep resistance and fully

lamellar (coarse-grained) microstructures have a better creep resistance than fine-grained duplex microstructures, because the $\alpha_2$laths in fully lamellar structures act as reinforcements [1991Kim1]. For the same reasons, the fully lamellar microstructures have lower fatigue crack growth rates, whereas duplex microstructures have high fatigue crack growth rates.

Fracture toughness

Fully lamellar microstructures have the highest fracture toughness in dual phase alloys [2012Kot]. They experience large plastic strains near the crack tip and good crack propagation resistance.

Tensile strength

Tensile strength is inversely proportional to grain size [1996Mer, 2012Kot], as given by the Hall-Petch relationship [1951Hal]:

$$\sigma_y = \sigma_o + \frac{k_y}{\sqrt{d}} \qquad \text{(Equation 2.1)}$$

Where σ_y is the yield stress, σ_o is the resistance of the lattice to dislocation motion, k_y is the strengthening coefficient (a constant specific to each material), and d is the average grain diameter. Therefore, the fully lamellar microstructures with coarser grain sizes have the lowest tensile strengths in dual phase alloys.

Besides thermo-mechanical treatment, alloying of titanium aluminides is being used to improve the mechanical properties [2011App, 2012Kot].

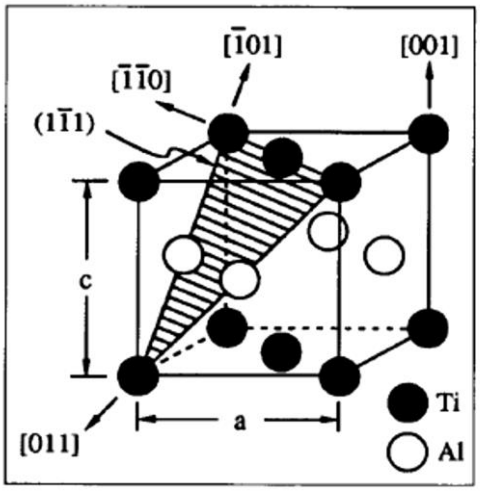

Figure 2.12: Ordered face-centred tetragonal ($L1_0$) TiAl structure, tetragonality ratio *c/a* = 1.02 with the (111) plane shaded [1989Kim].

2.2.4 Alloy development

Most of the microalloying research has been focused on enhancing the properties of duplex, dual phase microstructures and fully lamellar microstructures [1985Lip, 1995Kim, 1995Sau, 1998Bra, 1998Ton, 2000App, 2011App]. For duplex microstructures, the focus is on improving the creep resistance, oxidation resistance and fatigue strength of the alloys [1985Lip, 1995Kim, 1995Sau, 2000App, 2011App]. In the case of fully lamellar microstructures, the focus has been on refining the grain size and thus improving ductility [1985Lip, 1995Kim, 1995Sau, 2000App, 2011App]. No research has been done on the microalloying of single-phase gamma alloys as they are considered to have little engineering value.

The selected alloying elements to TiAl need to be soluble in the solid solutions of the γ-TiAl and α-Ti_3Al phases to enhance mechanical properties such as high temperature strength, room temperature ductility and creep resistance [1994Has, 2011App]. Also, the alloying elements need to minimize the precipitation of the β phase (bcc titanium phase which nucleates above 882°C) to improve the room temperature ductility and toughness [1994Has, 2000App, 2011App]. The addition of third alloying elements such as Cr, Mn, Mo and V, together with subsequent heat treatment has been found to improve the ductility of γ-TiAl [1994Has].

There are three groups of alloying elements for titanium aluminides [1989Kim, 2011App, 2012Kot], all of which generally affect the position of the phase boundaries in the Ti-Al phase diagram. They are categorised in the following composition (in at.%): Ti(45-52) – Al(42-49) – X(0.1-3.0) – Y(0.5-5.0) – Z (<1.0) where X = Cr, Mn or V, Y = Nb, Ta, W or Mo, and Z = Si, B or C.

X elements (Cr, Mn and V) are used to increase ductility by lowering the stacking fault energy, thereby increasing the propensity for twinning [2012Kot]. The Y elements (Nb, Ta, W and Mo) are added to increase oxidation and creep resistance at high temperatures [2012Kot]. The Z elements (Si, B and C) are added to refine the grain size and therefore can be used to form fully lamellar microstructures with a finer grain size, and carbon addition can increase strength by precipitating the Ti_3AlC phase [2012Kot].

Alloying elements can improve ductility by influencing the energies of planar defects and the diffusion coefficients in γ-TiAl [1994Has, 2011App]. Other alloying elements, such as boron and tungsten, are added to titanium aluminides to obtain precipitation hardening, grain refinement and stabilisation of microstructure against grain growth [1994Has, 2011App]. The only problem is that elements that improve ductility decrease the oxidation resistance of titanium aluminides, and elements that improve oxidation resistance reduce ductility. Nevertheless, extensive research on the alloying of titanium aluminides has yielded some superior alloys (Table 2.2) with good high temperature properties [2012Kot]. Table 2.2 summarizes the effect of different alloying elements on titanium aluminides. Table 2.3 lists the state-of-the-art titanium aluminide alloys that are commercially available [2004Bir, 2005Voi, 2012Kot].

Table 2.2: Effect of selected alloying elements on mechanical propertiesofTiAl[1994Has, 2011App, 2012Kot].

Elements	**Effect**
Cr (small amounts), Mn, V and Mo	Improve ductility
Cr (in range of 8%, Nb (small amounts), Ta, W, Mo, Ni, C, N and Si	Increase oxidation and creep resistance
Nb (in range of 5% - 10%) and Mo	Increase high temperature strength
B and W (small additions)	Refine grain size

Table 2.3: Commercial titanium aluminide alloys [2012Kot].

Alloy name	**Developers**	**Composition (at.%)**	**Alloy strengths**
GE 48-2-2	General Electric, USA	Ti-48Al-2Cr-2Nb	Ductility, fracture toughness, oxidation resistance
γ-MET	Plansee, Austria	Ti-45Al-(5-10)Nb	High temperature strength, creep, fatigue and oxidation resistance
TNB alloy	GKSS Research Centre, Germany	Ti-(45-47)Al-10Nb	High temperature strength, creep and oxidation resistance
XD^{TM} TiAl	Martin Marietta Labs, USA	Ti-45Al-2Mn-2Nb-0.8B	Ductility, high temperature strength, stiffness, creep and oxidation resistance

2.2.5 Effect of aluminium content

The amount of Al determines the initial phase to precipitate and the phase transformations that occur on solidification [2011App, 2012Kot]. Depending on the Al content, titanium aluminides can form α_2-Ti_3Al, dual α_2-Ti_3Al + γ-TiAl and pure γ-TiAl phases on cooling (Figures 2.6 - 2.10). Titanium aluminides with less than 40 at.% Al consist of the α_2-Ti_3Al phase. They have no engineering use as they are very brittle at room temperature. Alloys with >50 at.% Al, consisting of γ-TiAl phase, are also brittle at room temperature, but they have good high temperature oxidation and creep resistance. The dual phase alloys with Al in the range 46 - 49 at.%, consisting of γ-TiAl and α_2-Ti_3Al, exhibit the best ductility at room temperature (Figure 2.13) [2011App, 2012Kot]. As a result, most titanium aluminide alloys used for structural applications have some α_2-Ti_3Al to maximise thermo-physical properties.

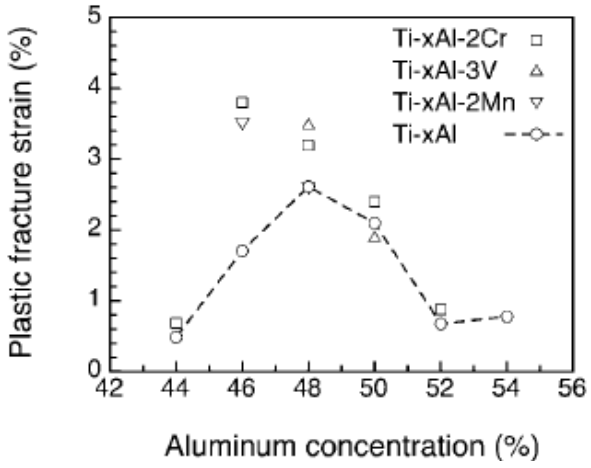

Figure 2.13: Effect of Al content on the room temperature ductility of wrought Ti-Al metals [2011App].

2.2.6 Effect of noble metal additions

There is limited research on noble metals as alloying elements for titanium aluminides [2000Van, 2012Mwa, 2013Mwa]. Most of the research on titanium aluminides has been focused on improving room temperature ductility and high temperature strength [1993Jha, 1994Kim]. Noble metals are usually used as alloying elements to improve corrosion resistance [1959Ste, 1996Sch]. In titanium and titanium alloys, the addition of small amounts of noble metals, such as Pt, Pd, Ag and Rh, has improved corrosion

resistance in reducing acids [1959Ste, 1996Sch, 2000Van]. Titanium and titanium alloys are susceptible to corrosion in aqueous reducing acids such as chloride and fluoride solutions [1959Ste, 1996Sch, 2000Van]. In oxidizing media, they spontaneously form protective oxide films on the surface, although in reducing media, they can show pitting and crevice corrosion [1959Ste, 1996Sch, 2000Van].

Alloying titanium with PGMs, such as platinum, palladium and ruthenium, produces alloys with a passive mixed potential with more positive values, as shown in Figure 2.14 [1959Ste]. On immersion in acid, the alloy undergoes cathodic polarization which initiates the dissolution of the alloy [1959Ste]. As the alloy is dissolved, the noble metal accumulates on the surface until the electrode potential changes to a more positive (noble) value and the alloy passivates by forming a slightly soluble, protective and hydrated oxide film.

For titanium aluminides, the addition of 1.0 at.% of the PGMs Pt, Pd and Ir to Ti-47.5 at.% Al in HCl generally improved the corrosion resistance by increasing the corrosion potential to nobler values [2013Mwa].

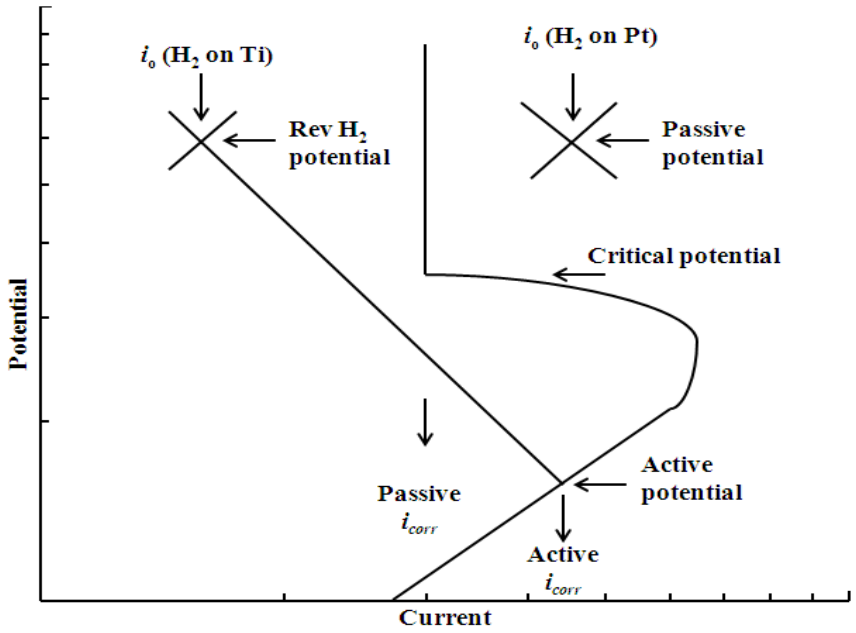

Figure 2.14: Schematic diagram showing how alloying with a noble metal produces a passive mixed potential and a marked reduction in corrosion rate [1959Ste].

2.3 The Ti-Al-Ni and Ti-Al-Ru ternary systems

The isothermal section at 1000°C of the Ti-Al-Ni ternary phase diagram in Figure 2.15 [2007Sch] shows the existence of five ternary phases, τ_1 - τ_5. The τ_3 phase Ti_2NiAl_3 melts congruently at 1289°C. At Ti-52.5Al-10.0Ni (at.%), there is a TiAl, $TiAl_2$ and Ti_2NiAl_3 (τ_3) phase field at 1000°C, and a wide two-phase region between TiAl and Ti_2NiAl_3 (τ_3).

The isothermal section at 950°C of Ti-Al-Ru in Figure 2.16 [1989Kha] shows a wide two-phase field of γ-TiAl + τ at low ruthenium and high Al compositions.

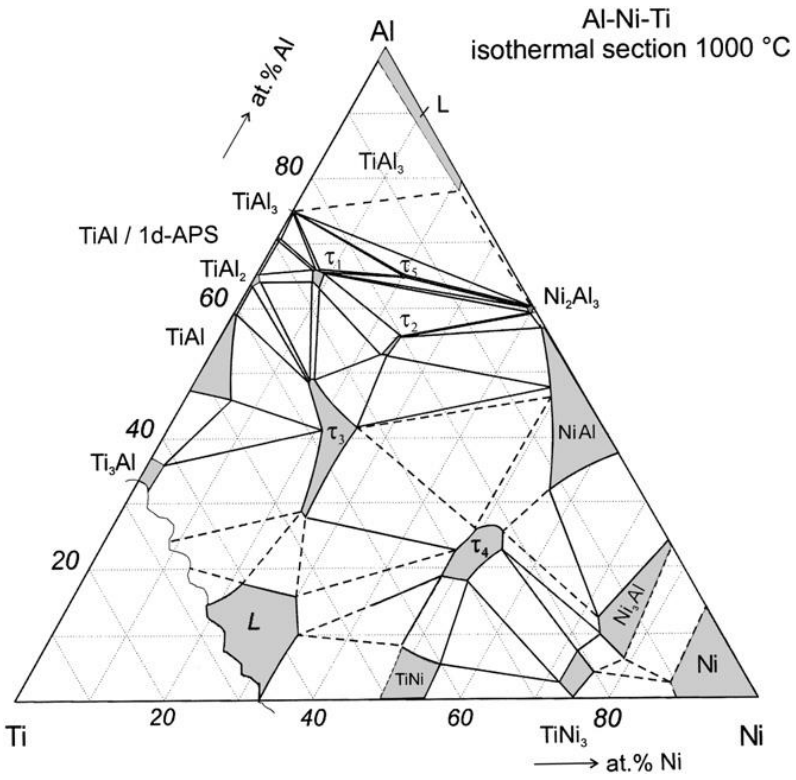

Figure 2.15: Isothermal section of Ti-Al-Ni at 1000°C [2007Sch].

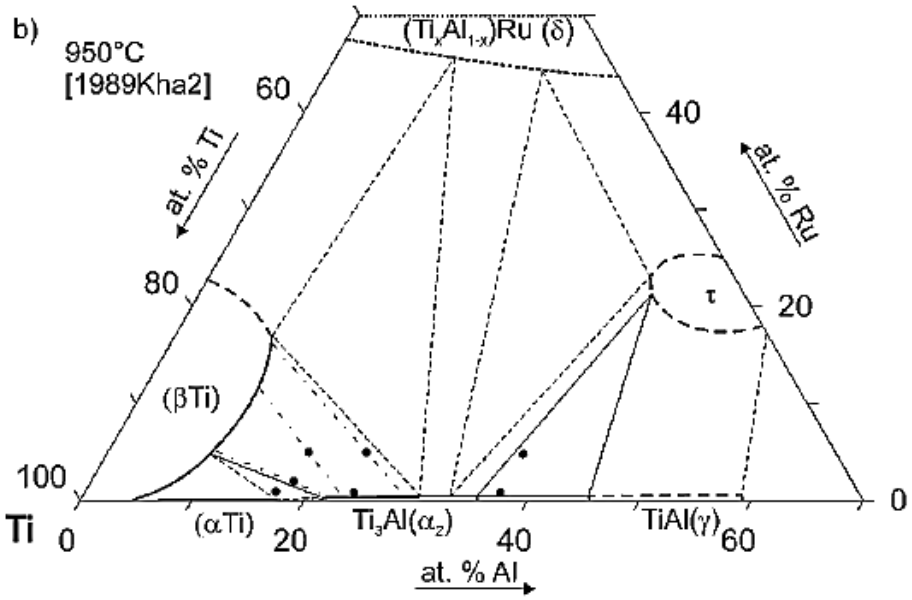

Figure 2.16: Isothermal section of Ti-Al-Ru at 950°C [1989Kha].

2.4 Manufacturing of titanium aluminides

The manufacturing of titanium aluminides is a fairly expensive process because these alloys have long range ordering up to their melting point [2011App, 2012Kot]. This means they have to be manufactured at high temperatures (>1460°C) and the equipment used must have good high temperature strength. Conventional processing techniques are investment casting, ingot metallurgy and powder metallurgy. These techniques have successfully produced titanium aluminide components which then require further processing like hot isostatic pressing (HIP), ageing, annealing and hot working. This adds to the manufacturing costs of titanium aluminides [2011App, 2012Kot].

Investment casting and ingot metallurgy produce inhomogeneous components with segregated microstructures [2011App, 2012Kot]. This is because the elements making up the titanium aluminide alloys have different densities and melting points. Thermo-mechanical treatments, such as hot rolling, forging and extrusion, are then conducted in the $\alpha + \beta$ phase field (1200 - 1350°C) to homogenize and refine the microstructure. Besides thermo-mechanical treatments, ingots can be subjected to HIP and ageing to relieve residual stresses, and homogenise and refine the microstructure.

The powder metallurgy route is considered another manufacturing option as it costs less than investment casting and ingot metallurgy [2011App, 2012Kot]. It is also a faster

process which produces more homogenous components with less porosity, and new alloys that cannot be produced via ingot metallurgy and casting can be made. The powder metallurgy route generally involves gas atomisation of pre-alloyed powder followed by HIP or extrusion.

Other successful recently-developed manufacturing techniques are laser forming, direct rolling and plasma sintering [2011App, 2012Kot]. These techniques have been successful in reducing the post-processing steps and therefore also the manufacturing time. However, they still produce components with some porosity, and the components are not easily scalable in size.

Mechanical alloying is another successful technique to manufacture titanium aluminide components [2011App, 2012Kot]. It involves high energy ball- and attrition- milling of pre-alloyed metal powder for up to 50 hours. The powder particle size can be reduced to the sub-micrometre and nanometre ranges. The challenge with this technique is the metal powder contamination from milling media and the milling container.

In manufacturing it is important to eliminate impurities such as oxygen and nitrogen as they can introduce porosity in the final fabricated components [2011App, 2012Kot]. In order to optimise mechanical properties, it is also important to use a processing technique that can minimise the grain size.

2.5 Uses and applications of titanium aluminides

Most titanium aluminide applications are in the aerospace and automobile industry [1976Cho, 1989Nis, 1997Kel, 2000Cha, 2011App, 2012Kot]. Their low density and high temperature strength make them good candidate materials to make lighter hot components jet engine gas turbines and automobile engine valves. They can especially be used in low pressure turbine blades and high pressure compressor blades, which are shown in Figures 2.17 and 2.18 [2014Gea, 2003Dim]. These components are conventionally made from NBSAs whose density is nearly twice that of TiAl based alloys. NBSAs are already operating at their melting point of 1360°C, and the TiAl-based alloys have a higher melting point (~1460°C) [1992Fro, 1995Imm, 1999Voi, 2012Kot]. They are being considered to replace 21-2N high temperature steel in

automobile engine valves, as they are 50% lighter, and have a higher thermal conductivity and exhibit high tensile strength at 700°C - 800°C [1989Nis, 1997Kel, 2000Cha].

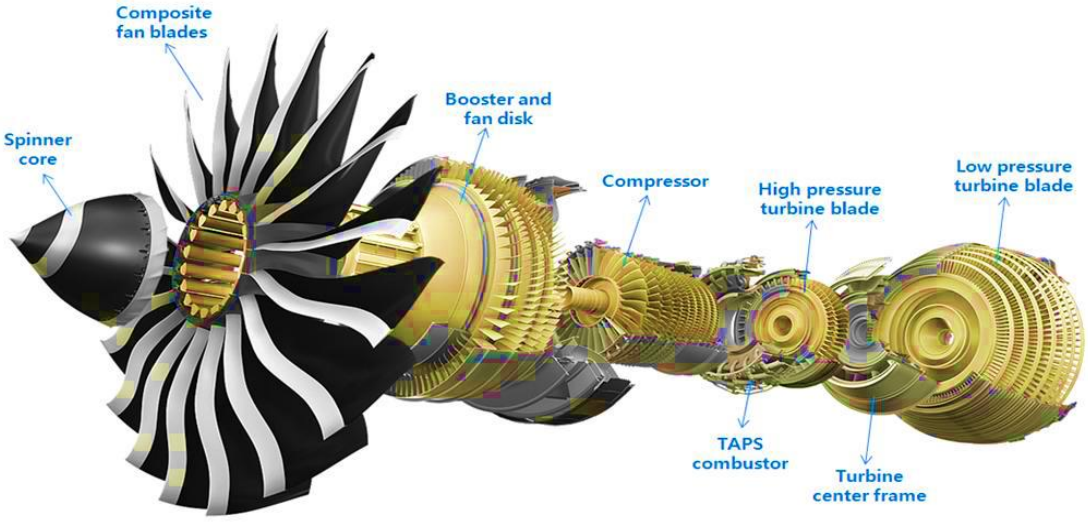

Figure 2.17: General Electric GEnX engine [2014Gea].

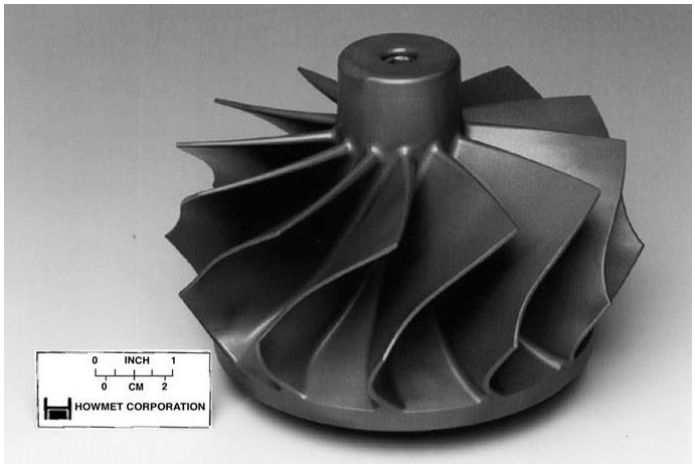

Figure 2.18: TiAl turbocharger wheels made by Howmet Corporation [2003Dim].

The challenge with the widespread use of titanium aluminide alloys is their production costs which are higher than steel and NBSAs [1992Fro, 1995Imm, 1999Voi, 2012Kot]. They are also more difficult to manufacture due to their low ductility and high melting points. However, their production costs are projected to decrease, and several novel techniques, mentioned earlier, have successfully produced titanium aluminide

components with good mechanical properties. Table 2.4 lists the potential applications for titanium aluminide alloys.

Table 2.4: Potential applications for titanium aluminides [2003Das].

Vehicle	Component	No. of vehicles	Projected usage [kg]
Global first strike/ Tomahawk missiles	Hot structures, compressor, nozzle	>2000	>30,000
Comanche helicopter	Nozzles, IR suppression systems	>500	>10,000
F-22, JSF	Nozzles, exhaust structures, engine components	>700	>100,000
Military space plane	Thermal protection systems, wing box and vertical tail hot structures	>2	>5,000
Re-usable launch vehicles		2 - 8	20,000 – 80,000

Due to their high productions costs, low ductility at room temperature and difficulty in manufacturing, titanium aluminides are mainly used for specialized military [2003Das] and aerospace industries [1999Sch, 1997Cle, 2015Gup].

2.6 High temperature oxidation of titanium aluminides

Oxidation is described as the process whereby an unstable metal reacts with oxygen to form a thermodynamically favoured metal oxide. The mechanism of oxidation for any metal or alloy can be described by the following chemical reaction [1974Law]:

$$xM_{(s)} + \frac{y}{2}O_{2(g)} = M_xO_y \qquad \text{(Equation 2.3)}$$

where M is the reacting metal and M_xO_y is the metal/alloy oxide.

The driving force for oxidation reactions is the Gibbs standard free energy (ΔG) described in Equation 2.4 [1983Bit]:

$$\Delta G = \Delta G^\circ + RT\ln\left[\frac{a_{M_xO_y}}{a_M^x P{O_2}^{1/2}}\right] \qquad \text{(Equation 2.4)}$$

where R is the universal gas constant, T is the absolute temperature, PO_2 is the oxygen partial pressure and a_i is the chemical activity of component *i*.

At equilibrium, $\left[\frac{a_{Mx}O_y}{a_M^x PO_2{}^{1/2}}\right]$ is constant and $\Delta G = 0$, so Equation 2.4 becomes:

$$\Delta G^\circ = -RT\ln\left[\frac{a_{Mx}O_y}{a_M^x PO_2{}^{1/2}}\right] \qquad \text{(Equation 2.5)}$$

Taking the natural logarithms:

$$\left[\frac{a_{Mx}O_y}{a_M^x PO_2{}^{1/2}}\right] = e^{\frac{-\Delta G^\circ}{RT}} \qquad \text{(Equation 2.6)}$$

Rearranging Equation 2.6 gives the equilibrium dissociation pressure for the metal oxide M*x*O*y*:

$$PO_2{}^{1/2} = e^{\frac{\Delta G^\circ}{RT}} . \frac{a_{MxOy}}{a_M^x} \qquad \text{(Equation 2.7)}$$

Equation 2.7 gives the minimum oxygen potential required to form the metal oxide M*x*O*y*. The Ellingham diagram (Figure 2.19) graphically shows how the Gibbs free energy (ΔG°) changes as a function of temperature [2011App]. The diagram is often used to compare the thermodynamic stability of various oxides. Oxides with a more negative ΔG° are considered more stable than oxides with a less negative or more positive ΔG°. Therefore, using the Ellingham diagram, Al_2O_3 is more stable than Cr_2O_3 and SiO_2.

The development of an oxidation-resistant alloy is based on the addition of an element that will readily oxidize and form a protective metal oxide on the surface of the base metal. For this to happen, the surface oxide formed should be more stable than the lowest oxide of the base metal [1962Kub, 1970Woo, 1974Law, 1983Bir]. The Gibbs free energy of formation of the surface oxide formed should be more negative than the lowest oxide of the base metal. When designing an oxidation resistant alloy, the aim should be to design an alloy that forms a stable, slow-growing, protective oxide layer

with good adherence to the substrate [1962Kub, 1970Woo, 1974Law, 1983Bir, 2011App].

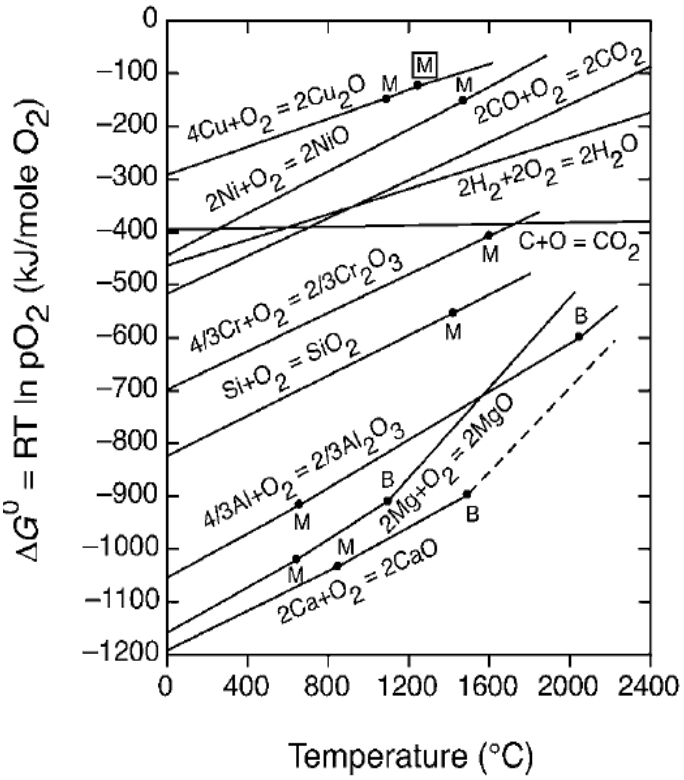

Figure 2.19: Ellingham diagram showing the standard free energy of formation of selected oxides at a function of temperature [2011App].

2.6.1 Mechanisms of oxidation

Dual phase titanium aluminides have good oxidation resistance, although above 800°C, the oxidation resistance is inadequate [1985Lip, 1995Kim, 1995Sau, 1996Tan, 2000App]. Micro-alloying with Nb, Ta and W is typically used to improve oxidation resistance. Single-phase (γ TiAl-based) titanium aluminides exhibit good oxidation resistance, but they are brittle at room temperature. Therefore, most research is focused on improving the oxidation resistance of dual phase (duplex) titanium aluminides, as they have the optimal ductility [2000App, 2011App, 2012Kot].

Meier and Petit [1993Mei] found that with micro-alloying, titanium aluminides form stable Al_2O_3 oxides below 1000°C. Above 1000°C, they form mixed oxides of Al_2O_3 and TiO_2. Zhou et al. [2008Zho] found that oxidation of titanium aluminide alloys can

be divided into two stages. Stage 1 is the selective growth of alumina, characterised by a linear growth in mass gain. Stage 2 is the simultaneous oxidation of Ti and Al to form the oxides TiO_2 and Al_2O_3, which is characterised by the parabolic increase in mass gain. They found that adding Nb did not change the two stage mechanism, but delayed the transition from stage 1 to stage 2.

The mechanism of oxidation in titanium aluminide alloys is believed to occur in four modes dependent on oxidation temperature, shown in Figure 2.20 [1994Bey], starting with TiO_2 forming only. An increase in temperature results in thicker and more complex scales. Above 800°C, complex scales with internal oxides, voids, sub-scales, porous and intermixed Al_2O_3/ TiO_2 can form.

Titanium aluminide alloys have a high affinity for oxygen [1996Bey], therefore even at room temperature, a thin (~200nm), continuous and stable TiO_2 oxide will form on the surface of the alloy. This is generally accepted as mode I (Figure 2.20) oxidation in γ-based TiAl alloys.

Mode II occurs at 800 - 950°C (Figure 2.20), although for γ-TiAl with higher Al contents, the temperature can be higher [1996Bey]. At this stage, an alumina scale and some TiO_2 form on the surface of the alloy. The alumina scale passivates and protects the substrate, ensuring minimal loss of the alloy.

At higher temperatures up to ~1100°C, mode III oxidation occurs (Figure 2.20) and most aircraft applications occur at this temperature range [1996Bey]. Here, a tri-layer oxide scale is formed, consisting of an outer TiO_2 layer, an intermixed TiO_2/Al_2O_3 layer underneath the TiO_2 layer, and a stationary Al_2O_3 at the interface of the substrate and oxide layer. Passivation is minimal and breakaway oxidation occurs.

Mode IV occurs above 1100°C (Figure 2.20), where internal oxidation occurs, resulting in even more rapid deterioration of the alloy [1996Bey].

Taniguchi and Shibata [1996Tan] proposed that titanium aluminides form a scale with two layers after mode III oxidation (Figure 2.21). The scale consists of an outer TiO_2 layer and an inner, porous and intermixed TiO_2/Al_2O_3 layer. The two layers are separated by a non-continuous Al_2O_3 layer which can act as a barrier to oxidation. Also,

at the interface between the layers, large voids can be present (Figure 2.21 [1996Tan]). In the substrate adjacent to the substrate/scale interface, Al_2O_3 platelets are present as internal oxides. The areas between the internal oxides have titanium which transforms to lamellar Ti_3Al and is oxidized as oxidation proceeds. After long oxidation times, cracks develop near the substrate/scale interface. During oxidation, titanium ions and oxygen ions diffuse through the outer TiO_2 layer [1983Kof]. Oxygen ions diffuse much faster than titanium ions, so the outer TiO_2 layer grows by the outward diffusion of titanium ions and the inner TiO_2/Al_2O_3 layer grows by the diffusion of oxygen ions.

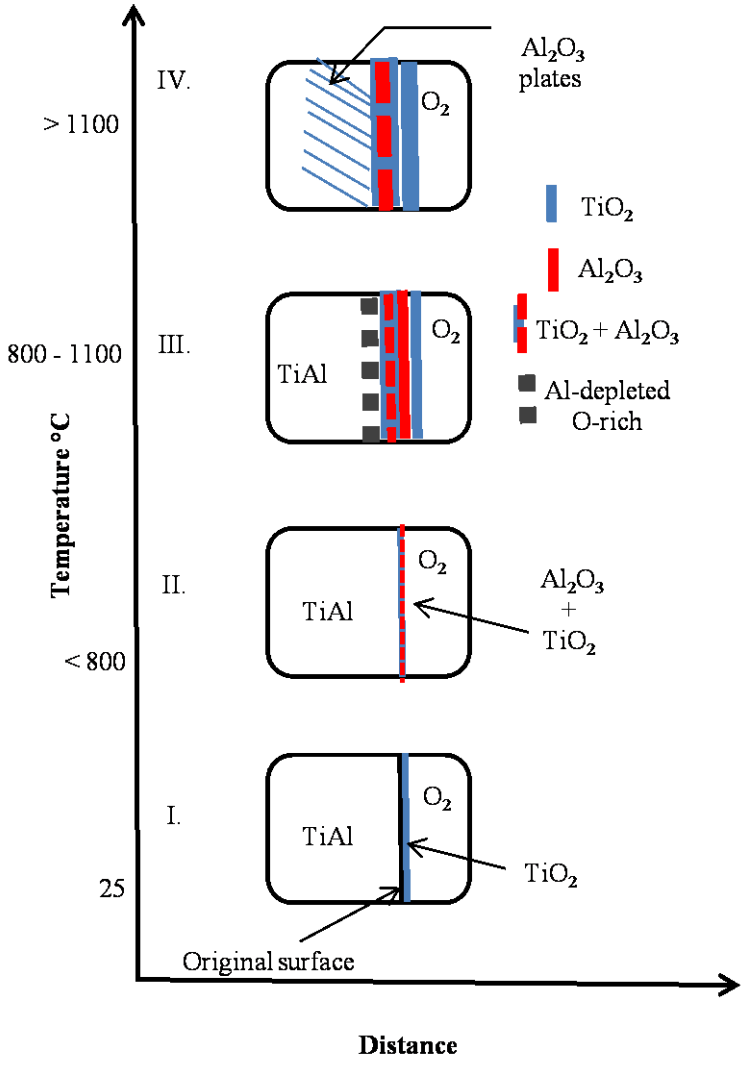

Figure 2.20: Mechanism of oxidation in γ-based titanium aluminides [1996Bey].

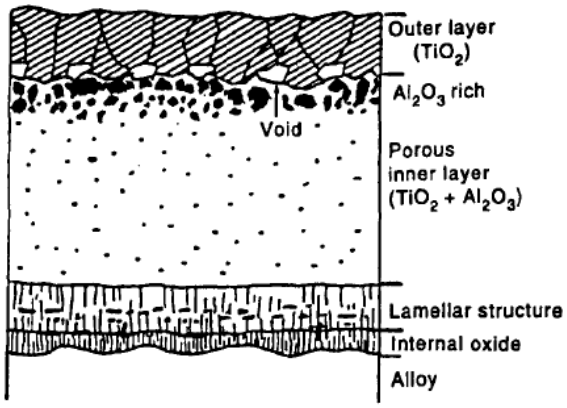

Figure 2.21: Model for the structure of the scale and the substrate near the scale/substrate interface [1996Tan].

2.6.2 Thermodynamics of oxidation

Like titanium alloys, titanium aluminides have a high affinity for oxygen [1993Mei, 1996Bra, 1996Tan, 2011App]. From room temperature, they react with oxygen and air to form oxide scales with varying amounts of TiO_2 and Al_2O_3 depending on the oxidation temperature and the Al content of the TiAl alloy [1993Mei, 1996Bra, 1996Tan, 2011App]. Pure γ-TiAl alloys (Al content >52 at.%), do not form a continuous Al_2O_3: instead in air and in oxygen under atmospheric pressure at 820 - 1150°C, they form an intermixed scale of TiO_2 + Al_2O_3 [1993Mei, 1996Bra, 1996Tan, 2011App]. This is due to the thermodynamic stability of TiO (which rapidly oxidises to TiO_2) and Al_2O_3 being very similar. Figure 2.22 [2011App] indicates that the oxygen equilibrium pressures of Al/$Al_2O_3$and Ti/TiO are similar, making it difficult to predict the most stable oxide.

In titanium aluminides, TiO_2 oxide grows faster than Al_2O_3 (1 mole of TiAl produces 1 mole of TiO_2 and 1/2 mole Al_2O_3) [1996Bra, 1996Tan, 2011App]. The presence of TiO_2 should be suppressed as the TiO_2 grains provide quick diffusion paths for oxygen and less protection for the substrate material. Brady et al. [1996Bra] proposed that the TiO_2 may also act as a short-circuit transport path, enabling the interstitial dissolution of O_2 and nitrogen particles into the alloy at elevated temperatures. This results in the embrittlement of the alloy and degradation of the mechanical properties such as the fatigue life of the alloy.

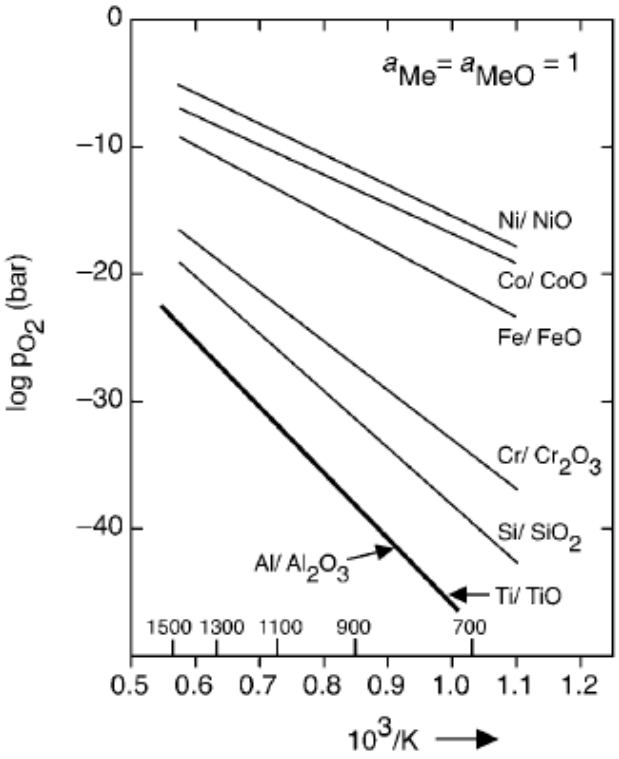

Figure 2.22: Oxygen equilibrium pressures of selected metal/oxide system [2011App].

2.6.3 Kinetics of oxidation

During oxidation, the base metal reacts with its surrounding atmosphere and starts to form various types of oxides and corrosion products as per Equation 2.3. The kinetics of this oxidation reaction are dependent the material, temperature and time and can be described as linear, parabolic, cubic and logarithmic [2011App]. Linear oxidation kinetics are typical for metals that form oxides with no protection of the underlying material. Parabolic oxidation kinetics are observed when the oxide scale growth is diffusion-controlled, and this is typical of oxidation-resistant alloys. As oxidation time progresses, the kinetics of oxidation can change, i.e. alloys can change from parabolic to linear oxidation kinetics with time. Also, if sufficient stress is built up within a scale with time, then cracking or spallation can occur [2011App]. The kinetics of the system, rather than the thermodynamics, control the oxidation rate [2011App].

It is generally accepted that titanium aluminides follow parabolic kinetics in short, isothermal oxidation conditions and may experience breakaway kinetics (cracking and

spallation) at longer oxidation times [1989Kas, 1989Uma, 1992Bec]. As mentioned above, titanium aluminide alloys react and form an oxide scale when exposed to an oxidizing environment (air/O_2) at high temperatures [1996Bey]. The weight changes which occur due to the formation of the scale can be plotted against time. Graphs similar to Figure 2.23 [2011App] can be plotted for different alloys. Depending on material and temperature, different rate laws can be observed (linear, parabolic, cubic and logarithmic) [1962Kub].

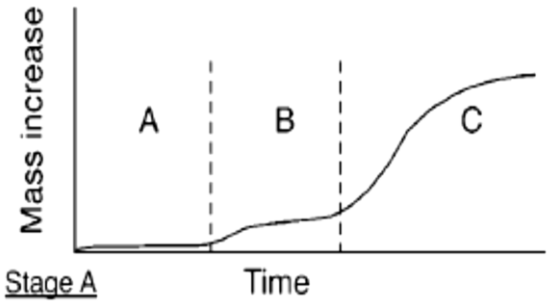

Figure 2.23: Schematic diagram showing the kinetics of oxidation for TiAl alloys [2011App].

In Figure 2.23 [1992Bec, 1995Rah, 2011App], Stage A indicates the growth of the protective oxide Al_2O_3 with very little oxidation of the material (low mass increase). As time progresses, stage B occurs where the Al_2O_3 scales starts to break down and a mixed TiO_2 + Al_2O_3 scale forms. At stage C, breakaway oxidation occurs due to a complete breakdown in the Al_2O_3 scale and the formation of a non-protective TiO_2 oxide scale.

The linear rate law is described by [1962Kub]:

$y = k_1 t$ (Equation 2.8)

where y = scale thickness, t = time and k_1= linear rate constant.

A linear oxidation rate is observed during initial scale growth. It occurs when an oxide layer does not act as a solid state diffusion barrier and does not protect the substrate. The oxidation of the metal/alloy proceeds at a constant rate and a phase boundary process controls the overall rate of reaction [2011App].

The parabolic rate law is described by [1962Kub]:

$(\Delta m/A)^2 = k_p t$ (Equation 2.9)

where m = mass (g) of metal, A = surface area (cm^2), t = time (s) and k_p = parabolic oxidation rate constant in $mg^2.cm^{-4}.s^{-1}$.

A parabolic oxidation rate applies when the diffusion of ions through the scale is the rate controlling process as the initial rapid scale growth rate decreases with time. It occurs during high temperature oxidation, and is usually observed in oxidation-resistant alloys. Materials with low k_p values have slower oxidation kinetics and are considered more oxidation resistant [2011App].

The logarithmic rate law is expressed by [1962Kub] as:

$$y = k_{log} log(t + t_0) + A \qquad \text{(Equation 2.10)}$$

and $$1/y = B - k_{il} log t \qquad \text{(Equation 2.11)}$$

where y = thickness, A, B, k_{log} and k_{il} are constants at time t.

Logarithmic oxidation rate is characterized by the formation of thin oxide scales between 0.0020 – 0.0040 μm due to a quick reduction of the initial rapid rate of scale formation to a very low rate of reaction. It usually occurs to metals or alloys oxidised at low temperatures ~400°C.

Most metals oxidise at a more rapid rate than the measured bulk diffusion rate [1996Bra, 2011App]. This is because the transport of reactants through the scale is by bulk lattice diffusion and diffusion along low resistance, short circuit paths such as grain boundaries, dislocations, pores and micro-cracks. The presence of cracks and pores in the scale provide direct access for oxygen. For oxidation resistance, it is thus important to have a continuous oxide scale with minimal cracks and pores.

2.6.4 Oxide scales

Oxidation resistance of high temperature alloys depends on the formation of continuous, slow growing oxide scales. The scales Al_2O_3 and Cr_2O_3 are mostly stoichiometric oxides [1992Mei, 2011App] with low defect concentrations and they thus develop relatively more protective oxide scales. Alloys of Al_2O_3, SiO_2 and BeO are of principal interest because they exhibit low diffusivities for both cations and anions, as well as

being highly stable [1992Mei]. In Ti-based alloys, the oxides of the base metal (TiO/TiO_2) are almost as stable as those of Al, Si and Be. This can prevent selective oxidation.

In alloys, there should be a sufficient supply of Al and Cr [1992Mei, 2011App] to form a protective Al_2O_3 and Cr_2O_3. An ideal scale should be highly stable, free from stress, cracks and pores at high temperatures. It must be coherent and remain adherent to the surface, even after cyclic conditions. A major setback with Al_2O_3 scales is that they crack and spall under cyclic oxidation conditions.

In titanium aluminides, the formation of the stable α-Al_2O_3 (corundum) rather than the metastable alumina phases (γ, θ, δ and κ) is required. Metastable alumina transforms to corundum upon heating to above 900°C. The ease of formation of corundum on the surface of an alloy depends on the alloy grain size, surface finish, and amount of cold work, initial oxide present and the method of heating the alloy [1962Kub, 1965Hau, 1970Woo, 1974Gig, 1983Bir].

Two other factors are also significant in the formation, composition and structure of the oxide layer: the thermodynamic stability of the oxide layer formed [1965Hau] and the crystal structures of the oxide scale and substrate which determine the adhesion between them. An essential requirement for the formation of a non-porous and adherent scale is the capability of the substrate and oxide scale to withstand stresses that develop from the growth of a scale [1965Hau]. The scale needs to have vacant lattice positions or interstitial sites to allow the infiltration of reactants such as cations and oxygen. The diffusion of reactants through the scale enables scale growth and internal oxidation.

2.6.5 Hot salt oxidation

Hot salt corrosion is accelerated oxidation which affects alloys that are exposed to high temperature combustion gases with impurities [1997Nic]. It is noticeable in turbines at 700 – 900°C with Na_2SO_4 as the corrosive media [1997Nic]. The source of Na_2SO_4 can be from salt ingestion into the engine from atmospheric aerosols, alkali metals in the fuel and sulphur gases from combustion of the fuels [1997Nic]. Hot corrosion usually affects alloys exposed to gas turbines and incinerators, and occurs in two stages

[1997Nic]. The initial stage occurs by the destruction of the protective oxide layer [1997Nic], which can occur by thermal cycling, mechanical stressing or abrasion and impact, as well as by dissolving in molten salt.

The propagation stage occurs by the sulphidation of the TiAl alloy [1997Nic]. Sulphur from combustion gases combines with reactive metals in the alloys to form a dispersion of sulphide particles within the metal. These sulphide particles oxidise rapidly and release sulphur in the oxidation reaction. The sulphur penetrates further into the metal, so that the process becomes self-propagating.

Typical reactions in turbine engines include [1997Nic]:

$$2NaCl + SO_2 + \frac{1}{2}O_2 + H_2O = Na_2SO_4 + 2HCl \qquad \text{(Equation 2.12)}$$

$$2NaCl + SO_3 + H_2O = Na_2SO_4 + 2HCl \qquad \text{(Equation 2.13)}$$

Reactions 2.12 and 2.13 are common in the temperature range of 650 - 1040°C.

Hot corrosion of TiAl alloys is believed to occur by the mechanism explained above [1997Nic]. It is detrimental, especially if the continuous and protective alumina coating is not formed and the intermixed Al_2O_3/TiO_2 scale is present.

2.7 Aqueous corrosion of titanium aluminides

Most of the research on titanium aluminides has been focused on the high temperature aerospace and automobile applications, due to weight savings which can be achieved and their good high temperature performance [1976Cho, 2011App, 2012Kot]. There is therefore limited research on the room temperature aqueous corrosion of titanium aluminides. Titanium aluminides could be used to replace titanium alloys in petrochemical processing, offshore oil and gas, marine environments and the fabrication of medical implants.

Titanium and titanium alloys have excellent corrosion resistance in most neutral and oxidizing aqueous environments [1959Ste, 1996Sch, 2000Van]. However, in reducing environments, such as low pH chloride solutions, titanium alloys are susceptible to crevice and pitting corrosion. Thus, palladium-containing titanium alloys are being

used in low pH chloride solutions to improve corrosion resistance, although palladium is increasingly being replaced by ruthenium to reduce costs [1983Lum, 1996Yan, 2000Van]. The Ti-Ru alloys can be used to make lighter and cost effective components for: down-hole oil and geothermal sour wells, hot brine plate exchangers, chlor-alkali and chlorate cell anodes and liners. The pH in these environments can be similar to that of 5 wt% HCl and 25 wt% HCl.

As stated above, there has been limited research on the room temperature aqueous corrosion of titanium aluminides. Most of the research has focused on the corrosion performance in Ringer's solution as gamma titanium aluminide alloys could be used for bone repair and replacement [1996Saf, 2006Del, 2009Ham]. Gamma titanium aluminide has good corrosion resistance in Ringer's solution, especially after surface modification (oxidation in air at 500°C and 550°C) [2006Del, 2009Ham]. Oxidized gamma titanium aluminide also has good corrosion resistance in sea water and 3.5 wt % NaCl [2007Del]. Saffarian et al. [1996Saf] found that titanium aluminide alloys were susceptible to pitting corrosion in aqueous NaCl and that the pitting potential was dependent on the pH or Cl^- concentration. In this study, aqueous corrosion tests were done on two HCl concentrations (5 wt % and 25 wt %) to assess the effect of solution concentration on the corrosion rate.

2.7.1 Corrosion mechanisms

Corrosion is a chemical reaction where metals and materials deteriorate under an attack from their surrounding environment [1971Den, 1973Wes, 1982Shr]. Most corrosion reactions are electrochemical reactions as they involve the transfer of electrons between the electrode (metal) and electrolyte (liquid containing ions). There are two types of electrochemical reactions: anodic, where the reaction transfers electrons to the electrode, and cathodic, where the reaction takes electrons from the electrode.

Corrosion has four sub-reactions which act in series [1971Uhl], and if one of them is retarded, then the overall corrosion process is also retarded. The sub-reactions involved are illustrated in Figure 2.18 [2004McE] and include the electrochemical reactions, electron transfer and an electrical connection (ion flow).

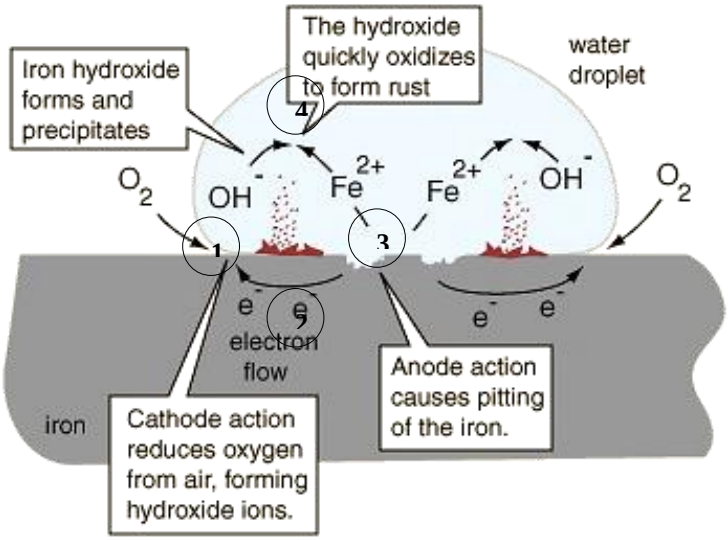

Figure 2.24: Schematic of the four sub-reaction which occur when a metal (iron) corrodes in contact in with an electrolyte (water) [2004McE].

Anodic reaction

The anodic reaction is also known as the oxidation reaction, whereby the metal is changed into a charged species and goes into solution.

The anodic reaction releases electrons and a loss of metal occurs [1971Uhl].

$M \rightarrow M^{2+} + 2e^-$ (Equation 2.14)

where M = atom on metal surface, M^{2+} = ion in solution and $2e^-$ = electrons in metal. Equation 2.14 shows that electrons (e^-) are released by the anodic reaction.

Electron flow

Electrons released by the anodic reaction flow through the metal (electrode) from the anodic site to the cathodic site. This movement of electrons represents a current, I, which by convention, flows in the opposite direction of electron flow, i.e. the current flows towards the site of anodic reaction [1971Uhl].

Cathodic reaction

The electrons are used by one or more cathodic reactions, also known as reduction reactions [1971Uhl]. In different environments, typical cathodic reactions are:

$O_2 + 2H_2O + 4e^- \rightarrow 4OH^-$ (Equation 2.15)

$2H^+ + 2e^- \rightarrow H_2$ (Equation 2.16)

$O_2 + 4H^+ + 4e^- \rightarrow 2H_2O$ (Equation 2.17)

Equation 2.15 is the typical cathodic reaction in neutral or alkaline environments. Equations 2.16 and 2.17 are typical cathodic reactions in acidic environments.

Ion flow

To close the electrical circuit between the anodic and cathodic sites, the current I must also flow through the electrolyte [1971Uhl]. Any ions that may be dissolved in the electrolyte (such as OH^-, H^+, Cl^-, Ti^{2+} and Al^{3+}) carry the current I between the anodic and cathodic sites.

For corrosion to occur, all four sub-reactions must happen simultaneously 1971Uhl]. If one of the reactions is halted, then the whole corrosion process is halted. Hence most corrosion protection methods are based on retarding one or more of the sub-reactions.

Importance of current (I)

The corrosion current is directly proportional to the rate a metal is corroded [1971Uhl]. This relationship is given as:

Rate (moles/second) = I/zF (Equation 2.18)

where F = Faraday constant = 96.485 C/mol, z = valence of the corroded metal, and I = current.

Since the corrosion rate will be the same whether for a large or small area of a metal, the corrosion current density *i* (current divided by the total exposed area of metal) is used in Equation 2.18.

Therefore the rate of corrosion becomes:

Rate (moles/second.mm^2) = *i*/zF (Equation 2.19)

where the corrosion rate is directionally proportional to the corrosion current density.

Importance of potential (E)

The potential of the corroding metal affects the rates of the anodic and cathodic reactions [1971Uhl]. The rate of the anodic reaction increases as the potential becomes more positive, and similarly the rate of the cathodic reaction increases as the potential

decreases (Figure 2.25 [1971Den]). The potential where the rate of the anodic reaction is equal to the rate of the cathodic reaction (equilibrium) is the corrosion potential (E_{corr}). At equilibrium, the rates of the anodic and cathodic reactions are equal and opposite and are referred to as the *exchange current density* which is the corrosion rate (i_{corr}) of the metal [1971Uhl, 1987Fon, 1992Jon]. For metals in solution, the larger the exchange current density, the faster the redox reaction will be, as expressed in Equation 2.19. The exchange current density is dependent on the nature of the redox reaction, the electrode composition/surface, temperature and the concentration ratio of oxidised and reduced species.

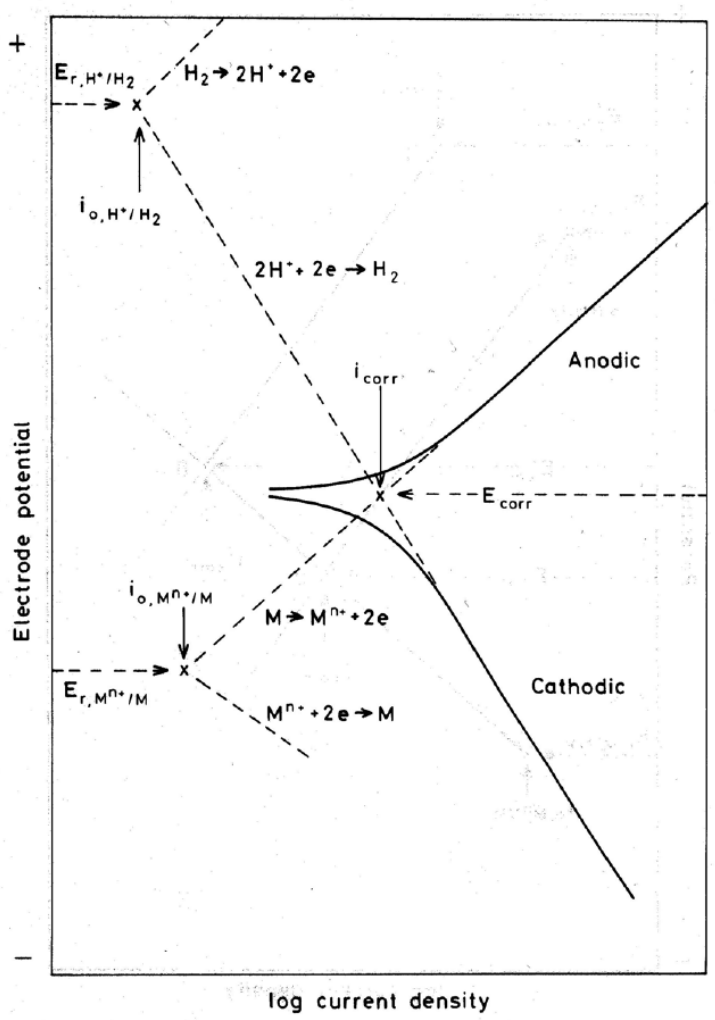

Figure 2.25: Schematic anodic and cathodic polarisation curves for a metal corroding in an acid solution [1971Den].

2.7.2 Kinetics of electrochemical reactions

Polarisation

Electrochemical reactions can be limited by physical and chemical environmental factors such as temperature, pressure, metal ion concentration and electrolyte pH [1987Fon, 1992Jon]. An electrochemical reaction is thus said be polarised or retarded by these environmental factors. Polarisation is classified into two types – activation and concentration polarisation. Activation polarisation (η) occurs when the electrochemical process is controlled by the reaction sequence at the metal-electrolyte interface [1987Fon, 1992Jon]. For examples, the hydrogen evolution reaction (Equation 2.16) can occur in three major steps [1987Fon, 1992Jon]. In step 1 (Equation 2.20), H^+ reacts with an electron from the metal and forms an adsorbed hydrogen atom (H_{ads}) on the surface [1992Jon]. In step 2 (Equation 2.21), two H_{ads} react to form a hydrogen molecule. In step 3, the hydrogen molecules combine and form a bubble on the surface.

$$H^+ + e^- \rightarrow H_{ads} \qquad \text{Equation 2.20}$$

$$H_{ads} + H_{ads} \rightarrow H_2 \qquad \text{Equation 2.21}$$

Any one of these steps (the slowest step) can control the rate of hydrogen evolution (Equation 2.16) and cause activation polarisation. Polarisation is also commonly known as *overpotential* [1992Jon].

Concentration polarisation occurs in electrochemical reactions that are controlled by the diffusion of ions in the electrolyte. In the case of hydrogen evolution (Equation 2.16), the reduction rate is controlled by the diffusion of H^+ to the metal surface. Therefore, the reduction rate is controlled by a process occurring in the bulk solution, rather than at the metal-electrolyte surface [1987Fon, 1992Jon].

Passivity

Passivity occurs when metals/alloys cease to react with their surrounding environments by forming thin surface films [1986Fon, 1992Jon, 1996Hin]. The metals used to constitute the alloys in this study (titanium, nickel, aluminium and ruthenium) are among some of the common engineering metals and alloys which are susceptible to passivation [1986Fon, 1992Jon, 1996Hin]. Figure 2.26 illustrates the typical behaviour of an alloy that shows passivity in a corrosive environment. The behaviour of the alloy

can be divided into active, passive and transpassive regions. In the active region (points A to B), the alloy behaves like a typical metal where a slight increase in the oxidizing power (electrode potential) of the solution causes a rapid increase in the corrosion rate and reaches a maximum at the passivation potential (E_{pp}) [1986Fon, 1992Jon, 1996Hin]. The critical current density (i_{crit}) is at the passivation potential. The passive region (points C to F) begins after the corrosion rate suddenly decreases (points B to C) and remains fairly low (< 1μA.cm^{-2}) and constant with an increase in electrode potential [1986Fon, 1992Jon, 1996Hin]. At very high electrode potential (high concentrations of oxidizing agent), the transpassive region (points F to I) begins where the corrosion rate increases again with increasing oxidizing power (electrode potential).

The passivation region ends at the pitting potential E_b, where the current density increases rapidly with an increase in potential (DE). The value of E_b is dependent on the concentration ratio of inhibitive anions (stabilize the oxide film) and aggressive anions (break down the oxide film) in the electrolyte. If there is sufficiently more inhibitive anions than aggressive anions in solution, the break-down of the passivating oxide film can be completely suppressed and no pitting potential will be observed. As the ratio of inhibitive anions to aggressive anions decreases, the pitting potential becomes more negative [1986Fon, 1992Jon, 1996Hin].

In some metals, transpassive dissolution is observed (FG) where the oxide film remains stable, the metals produces soluble ions and the current density increases with a more positive electrode potential. As the electrode potential increases, the rate of transpassive dissolution may decrease due to secondary passivity (point G) [1996Hin]. As the electrode potential increases further, the breakdown of water occurs, and the current density increases with potential (HI) due to the evolution of oxygen (Equation 2.22).

$$2H_2O \rightarrow O_2 + 4H^+ + 4e^- \qquad \text{Equation 2.22}$$

In corrosion experiments [1996Hin], polarisation curves (potentiodynamic scans or Evans diagrams) similar to Figure 2.26 are obtained and used to find the corrosion potential, corrosion rate (corrosion density) and corrosion behaviour of metals and alloys.

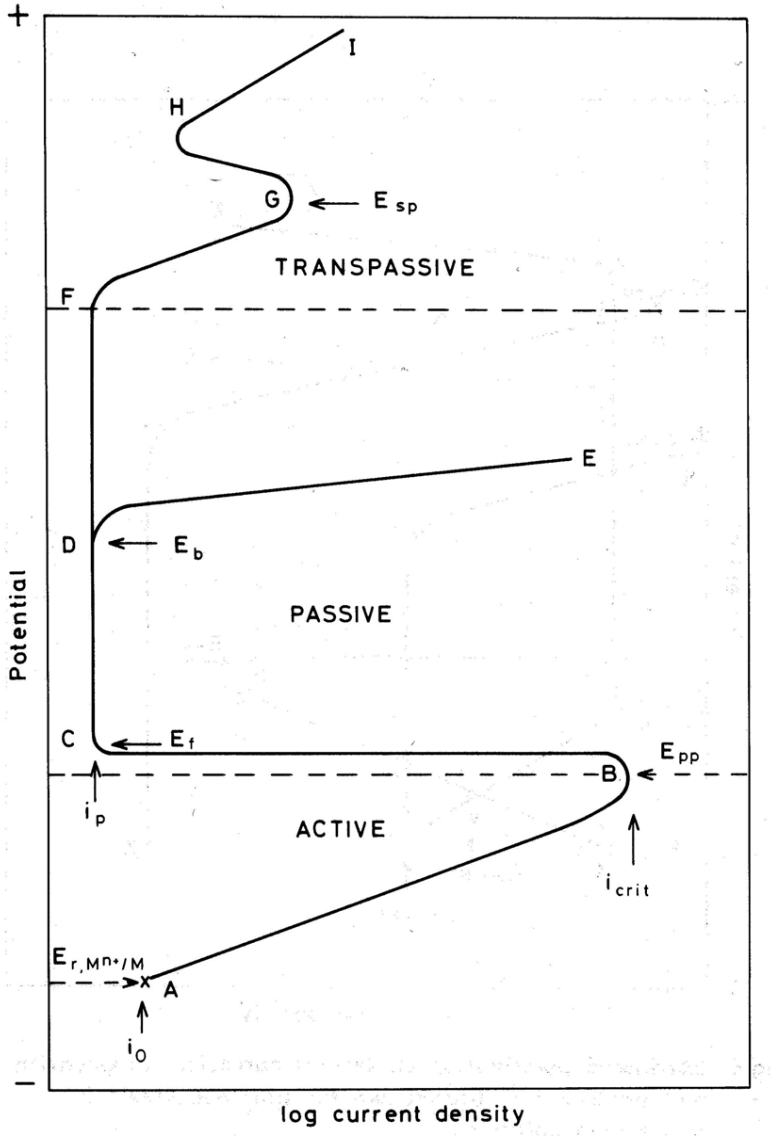

Figure 2.26: Corrosion characteristics of an active-passive metal as a function of solution oxidizing power (electrode potential) [1996Hin].

Oxide film formation during corrosion [1996Hin]

At the onset of corrosion (Figure 2.26), the metal/alloy surface reacts with water to form an oxide. The oxide gradually spreads over the surface and forms a thin film completely covering the metal/alloy (AB). The oxide film slows the flow of metal ions and thus decreases the current density to a small value (BC). The metal/alloy is thus protected against corrosion by a passivating oxide film which starts forming at E_{pp}. The E_{pp} value is dependent on the pH value of the electrolyte and the concentration of anions in the electrolyte. Oxide films generally become more stable with increasing pH and therefore the critical current density (i_{crit}), generally decreases considerably as the pH

increases. Thus the value of i_{crit} can give a measure of the ease of passivation; the smaller the current, the easier is passivation.

When the metal surface is completely covered with a passivating oxide film, the oxide film thickness increases to an equilibrium value and the current of metal ions passing through the film becomes independent of potential (CD). As time passes and the electrode potential increases, the oxide film starts to breakdown and form anions (usually chloride ions) which increase the current again (DE). The dissolution of the oxide film is usually localised or initiates at weak points such as grain boundaries, dislocations, cracks and inclusions in the metal/alloy. The underlying metal (substrate) is then exposed to the corrosive environment and can dissolve leading to an increase in current density. In some metals/alloys, like titanium and titanium alloys in reducing environments [1959Ste, 1996Sch, 2000Van], continued dissolution can lead to the formation of pits.

As mentioned above, some metals/alloys can have very stable oxide films and undergo transpassive dissolution, along FG in Figure 2.26. This phenomenon is usually observed in strong oxidising solutions such as nitric acid. If potential is increased further, secondary transpassive dissolution can occur in some metals/alloys.

2.7.3 Cathodic modification

Cathodic modification is an electrochemical technique used to improve the corrosion resistance of mostly titanium alloys and stainless steels in reducing media [1990Pot]. In cathodic modification, a noble metal (such as gold, silver, ruthenium, rhodium, palladium, osmium, iridium and platinum) having a high cathodic exchange current density (rate of reaction at equilibrium) for the reduction of H^+ ($2H^+ + 2e^- \rightarrow H_2$), is added to a base alloy to induce passivity in the new metal matrix [1961Gre].

Cathodic modification was first discovered by Monnartz in 1911 when he found that winding a platinum wire around stainless steel, or alloying it with platinum, improved its corrosion resistance in certain acids [1911Mon]. Tomashov *et al.* [1948Tom] further confirmed the cathodic modification concept for stainless steels, titanium and titanium alloys.

The presence of platinum in the stainless steel produces a more noble alloy by increasing the electrode potential to a value higher than the passivity potential. In a corrosive environment, the alloy passivates by forming a sparingly soluble, protective and hydrated oxide film on the surface. Figure 2.27 [1990Pot] shows the effect of cathodic modification, where line A_0 represents the cathodic polarization curve of a base metal, and line A_1 the same metal which has been alloyed and therefore cathodically modified. Therefore, the addition of corrosion-resistant noble metals to A_0 should produce the cathodically modified alloy A_1, where the corrosion potential is more noble and lies in the passive region of alloy A_0.

For an alloy to be corrosion resistant by cathodic modification, the following criteria must be met in the base alloy [1990Pot]:

- The base alloy must have a small critical current density (i_{crit}) that can be exceeded by the current of the hydrogen cathodic reaction on the addition of a noble metal at the given passivation potential.
- The passivation potential of the base metal must be sufficiently negative to allow the noble metal to change the corrosion potential to a value within the passive range of the base alloy. Also, the passive region of the base alloy should extend to potentials that are more negative than the redox potential of the environment.
- The transpassive potential of the base metal should be sufficiently positive to allow a wide passive range

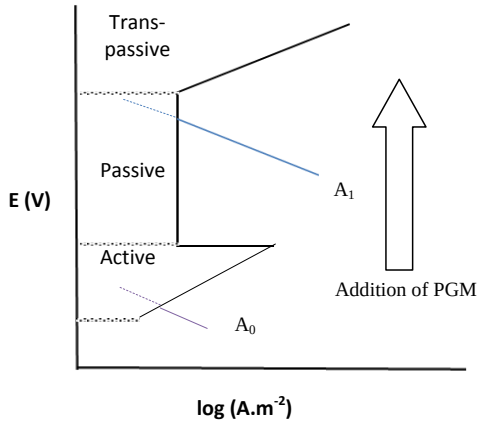

Figure 2.27: Schematic diagram of the effect of cathodic modification [1990Pot].

Stern and Wissenberg [1959Ste] found that only small amounts of PGMs were required to drastically improve the corrosion resistance of titanium in boiling dilute sulphuric and hydrochloric acids (Table 2.6). Pt, Pd, Rh and Ru produced the best corrosion resistance; Os, Ir and Re had an intermediate effect, Au was effective at higher concentrations and Cu and Ag were detrimental.

Table 2.6: Effect of various alloying additions on corrosion resistance of titanium [1959Ste].

	Weight loss in 24 h (mil/yr)			
	Boiling Sulphuric Acid		**Boiling**	**Hydrochloric**
Composition	**1%**	**10%**	**3%**	**10%**
Titanium	460	3950	242	4500
Ti + 0.064% Pt	<2	145	<2	128
Ti + 0.54% Pt	<2	48	3	120
Ti + 0.080% Pd	<2	166	3	100
Ti + 0.44% Pd	<2	45	<2	67
Ti + 0.10% Rh	<2	26	5	96
Ti + 0.50% Rh	3	48	<2	55
Ti + 0.10% Ru	3	187	5	280
Ti + 0.50% Ru	<2	48	<2	113
Ti + 0.11% Ir	<2	359	3	120
Ti + 0.60% Ir	<2	45	3	88
Ti + 0.10% Os	5	480	3	1820
Ti + 0.48% Os	<2	82	3	208
Ti + 0.11% Re	235	-	345	-
Ti + 0.36% Re	9	-	30	-
Ti + 0.11% Au	1050	-	1500	-
Ti + 0.48% Au	3	-	9	146
Ti + 0.040% Ag	500	-	334	-
Ti + 0.34% Ag	-	-	-	4850
Ti + 0.17% Cu	470	-	340	-
Ti + 0.44% Cu	660	-	550	-

*The possible weighing error of these tests is ± 2 mil/y.

Also, for the alloy to be corrosion resistant [1990Pot], the cathodic alloying component (noble metal) should have a higher exchange current density (and lower overpotential) for the reduction of H^+ ($2H^+ + 2e^- \rightarrow H_2$) than the base metal or alloy. The noble metal should also be corrosion resistant under the given conditions. In reducing acids

[1990Pot], such as sulphuric and hydrochloric acids, titanium based alloys (along with Cr-based alloys and stainless steels) have a sufficiently negative passivation potential and PGMs have the required high exchange current density (and low overpotential) for the hydrogen ion reduction. Therefore, when a sufficient amount of PGM is added to a Ti-based alloy, there will be an increase in hydrogen evolution, the corrosion potential of the cathodically modified alloy will increase to a passive region and the modified alloy will spontaneously passivate [1990Pot].

2.8 Rationale of the study

The Ti-52.5Al-10.0Ni (at.%) and Ti-52.5Al-10.0Ni-0.2Ru (at.%) alloys were manufactured to investigate whether the high Al content (52.5 at.%), could promote formation of the protective Al_2O_3 oxide instead of the non-protective TiO_2 oxide on the surface of the alloys. Nickel was added to the alloys to improve corrosion resistance, because it improves corrosion resistance in nickel aluminides by promoting the formation of the protective Al_2O_3 oxide [1996Bra]. Ruthenium was added to the alloys as its presence in ferritic steels [1977Str] and some titanium alloys [1959Ste] improves corrosion and oxidation resistance.

The behaviour of Ti-52.5Al-10.0Ni (at.%) and Ti-52.5Al-10.0Ni-0.2Ru (at.%) alloys under typical service conditions experienced in aerospace engines was investigated. The alloys were exposed to air or Na_2SO_4 at 950°C.

The alloys were also exposed to dilute (5 wt%) and concentrated (25 wt%) HCl to investigate their corrosion behaviour in a reducing environment at room temperature. Titanium and titanium alloys are susceptible to pitting and crevice corrosion in reducing environments [1959Ste, 1996Sch, 2000Van]. It was investigated whether the presence of nickel and ruthenium would encourage passivation of the Ti-52.5Al (at.%) alloy by cathodic modification.

CHAPTER 3: EXPERIMENTAL PROCEDURE

3.1 Alloy synthesis

The alloys were made by mixing and melting pure (99.96%) elemental powders of titanium, aluminium, nickel and ruthenium in a button arc furnace under an argon atmosphere. The alloys were re-melted three times to attempt the production of homogeneous buttons of the base alloy Ti-52.5Al-10.0Ni (TAN) and Ti-52.5Al-10.0Ni-0.2Ru (TAN+Ru) in at.%. A titanium oxygen-getter button was first melted to react with any residual oxygen or nitrogen which might have been present. The alloys were cut using a water-jet line cutter into samples which were used for subsequent tests.

Some samples of each alloy were annealed at 1050°C for 120 hours in a Carbolite tube furnace under an argon flow, where they were heated at a rate of 10°C/min and subsequently furnace cooled. The rest of the alloy samples were left in the as-cast condition and were used for subsequent isothermal oxidation, cyclic oxidation and corrosion test work.

3.2 Metallography

All samples were mounted and ground flat using 200, 600, 800 and 1200 grit SiC paper consecutively. The exposed surface of the sample was then diamond polished to a 1 µm finish. The samples were not etched.

3.3 Characterisation of alloys

The as-cast, heat treated and samples obtained after oxidation and corrosion tests were characterised in terms of microstructure and hardness. A Future-tech® FV-800 Vickers hardness tester, using a 10 kg load, was used for the hardness test work. Five measurements were taken on each sample, and the samples were analysed for cracks.

The composition and phases of the samples were determined using a combination of energy dispersive X-ray spectroscopy (EDX) in the SEM and X-ray diffraction (XRD).

A Carl Zeiss Sigma® field emission scanning electron microscope (FE-SEM) was used for EDX analysis, and at least five measurements were taken for each reported phase analysis. The PANAlytical X'Pert Pro® powder diffractometer was used for XRD. Phase identification was conducted using X'Pert Highscore Plus® software.

3.4 Oxidation testing

3.4.1 Thermogravimetric analysis

Thermogravimetric analysis (TGA) using a NETZSCH STA® instrument was done to investigate the oxidation behaviour of the TAN and TAN+Ru alloys in air. The samples were heated from room temperature to 1050°C at a rate of 10°C/min and subsequently furnace cooled. The mass gains of the alloys were recorded with increasing temperature.

3.4.2 Isothermal oxidation tests in air

The longer term effect of oxidation in air was determined by heating the alloys in a pre-heated front loading muffle furnace for 120 hours and 720 hours at 950°C. After the oxidation tests, the samples were taken out of the furnace and allowed to cool in air at room temperature. Each sample was weighed before and after the oxidation tests using a Mettler Toledo® analytical balance. The mass gain of the samples was calculated and the surfaces as well as the cross-sections of the samples were examined using a PANAlytical X'Pert Pro®X-ray diffractometer and a Carl Zeiss Sigma SEM® with EDX.

3.4.3 Cyclic oxidation tests

Samples were oxidised in air under thermal cycling between room temperature and 950°C for intervals of 1, 5, 10, 25, 50, 80 and 120 hours in a tube furnace. Each cycle entailed:

- Weighing the polished sample,
- Heating the sample for the required interval at 950°C,
- Air cooling the sample for 10 minutes, and

- Weighing the sample and then repeating the cycle.

After 120 hours, the samples and resulting oxides were analysed by XRD and SEM with EDX to determine their compositions and structures.

3.4.4 Hot salt oxidation tests

Polished samples were weighed and then completely immersed in Na_2SO_4 in an alumina crucible with a lid. The sample, salt and crucible were exposed to cyclic loading in a furnace at 950°C in air. Exposure times of 1, 5, 10, 25, 50, 80 and 120 hours were used. After each exposure time, the samples were cooled to room temperature and then cleaned by immersing in boiling water to remove the salt melt (Na_2SO_4 melts at 884°C [2014Sci]). The cleaned samples were weighed on an analytical balance to determine the weight gain from hot corrosion. The salt was replenished after each oxidising test. After 120 hours, the samples and resulting oxides were analysed by XRD and SEM with EDX to determine their compositions and structures.

3.5 Aqueous corrosion testing

The surfaces of the samples were ground to a 1200 grit SiC paper finish, degreased with methanol, rinsed with distilled water, and dried. The surfaces were prepared just prior to starting the polarisation experiment to limit long-term oxidation. Before conducting the scan, each sample was immersed in the HCl solution for an hour to obtain a stable corrosion potential.

Potentiodynamic scans were conducted on the TAN and TAN+Ru alloys in dilute HCl (5 wt%) and concentrated HCl (25 wt%) at 25°C. An ACM AutoTafel® potentiostat/galvanostat system with a conventional three-electrode system with a saturated calomel electrode (SCE) was used. Potentiodynamic scans were done from -1000 mV to + 400 mV at a scanning rate of 10 $mV.min^{-1}$, for two hours. All electrochemical tests were repeated once for each sample because of a lack of material.

CHAPTER 4: RESULTS

4.1 Microstructure and morphology of TAN alloy

The targeted composition (Ti-52.5Al-10.0Ni at.%) of the TAN alloy was obtained (Table 4.1). The alloy formed dendrites of γ-TiAl surrounded by a eutectic of γ-TiAl and Ti_2NiAl_3 (τ_3), as shown in Figures 4.1 and 4.2. Most of the nickel was present in the Ti_2NiAl_3 (τ_3) phase, with only trace amounts in the γ-TiAl dendrites.

The eutectic coarsened with heat treatment (Figure 4.3), and the composition of the γ-TiAl dendrites was slightly enriched in Ti (~1%) and slightly depleted in Al (~3%). In the eutectic, the titanium and aluminium contents decreased slightly and the nickel content increased by ~5% after heat treatment (Tables 4.1 and 4.2). Like the as-cast alloys, the heat treated alloys were brittle and contained cracks.

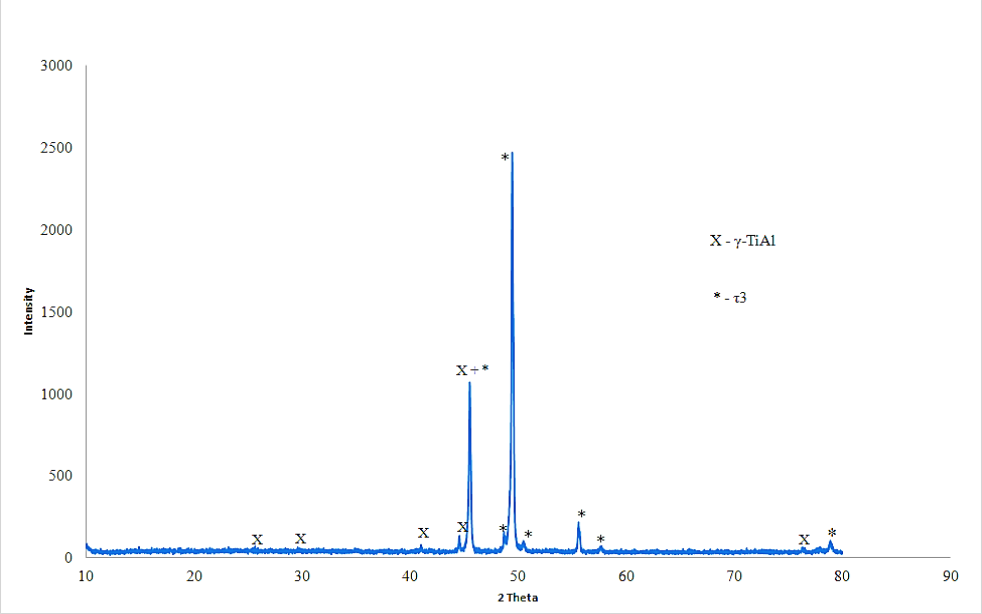

Figure 4.1: XRD pattern of as-cast TAN, showing dendrites (dark) in a TiAl + Ti_2NiAl_3 (τ_3) (light) eutectic.

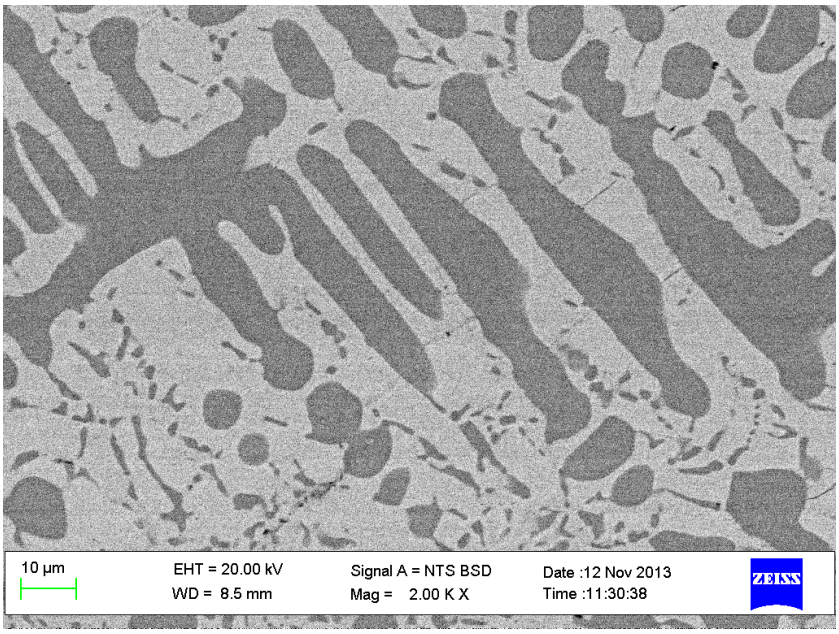

Figure 4.2: SEM-BSE image of as-cast TAN showing γ-TiAl dendrites (dark) in a TiAl + Ti_2NiAl_3 (τ_3)(light) eutectic.

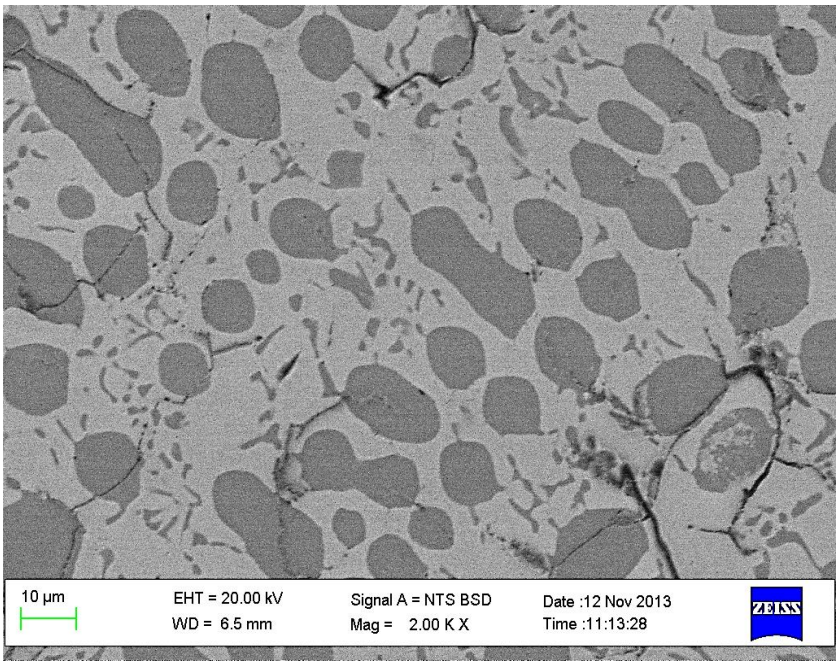

Figure 4.3: SEM-BSE image of annealed TAN showing γ-TiAl dendrites (dark) in a TiAl + Ti_2NiAl_3 (τ_3) (light) eutectic.

Table 4.1: EDX analyses for *as-cast* alloy TAN.

Area	Composition (at.%)			Phase
	Ti	Al	Ni	
Overall	37.4 ± 1.1	52.8 ±1.2	9.8 ± 0.5	-
Dendrites	43.9 ± 1.3	55.6 ± 0.8	0.5 ± 0.1	γ-TiAl
Eutectic (light)	37.8 ± 1.1	49.9 ± 0.5	12.3 ± 1.2	$Ti_2NiAl_3(\tau_3)$
Eutectic (overall)	41.2 ± 0.9	52.2 ± 0.8	6.6 ± 1.3	γ-TiAl+$Ti_2NiAl_3(\tau_3)$

Table 4.2: EDX analyses for *heat treated* alloy TAN.

Area	Composition (at.%)			Phase
	Ti	Al	Ni	
Overall	38.9 ± 1.1	51.4 ±1.1	9.6 ± 0.5	-
Dendrites	44.9 ± 1.3	52.2 ± 0.8	0.7 ± 0.1	γ-TiAl
Eutectic (light)	35.3 ± 1.1	49.1 ± 0.5	16.2 ± 1.2	$Ti_2NiAl_3(\tau_3)$
Eutectic (overall)	37.5 ± 1.1	50.5 ± 0.8	12.0 ± 1.1	γ-TiAl+$Ti_2NiAl_3(\tau_3)$

4.2 Microstructure and morphology of TAN+Ru alloy

The targeted composition (Ti-52.5Al-10.0Ni-0.2Ru at.%) of the TAN+Ru alloy was obtained (Table 4.2) and all elements were present in two phases. The alloy (Figures 4.4 and 4.5) also formed dendrites of γ-TiAl surrounded by a eutectic of γ-TiAl and Ti_2NiAl_3 (τ_3). Most of the nickel and ruthenium were present in the Ti_2NiAl_3 (τ_3) phase, with only trace amounts in the dendrites (Tables 4.3 and 4.4).

The eutectic coarsened with heat treatment (Figure 4.6) and the composition of the γ-TiAl dendrites remained the same. In the eutectic, the titanium content decreased slightly and the nickel and ruthenium content increased after heat treatment (Tables 4.3 and 4.4). The alloy was very brittle, even after heat treatment because the samples would easily break at room temperature.

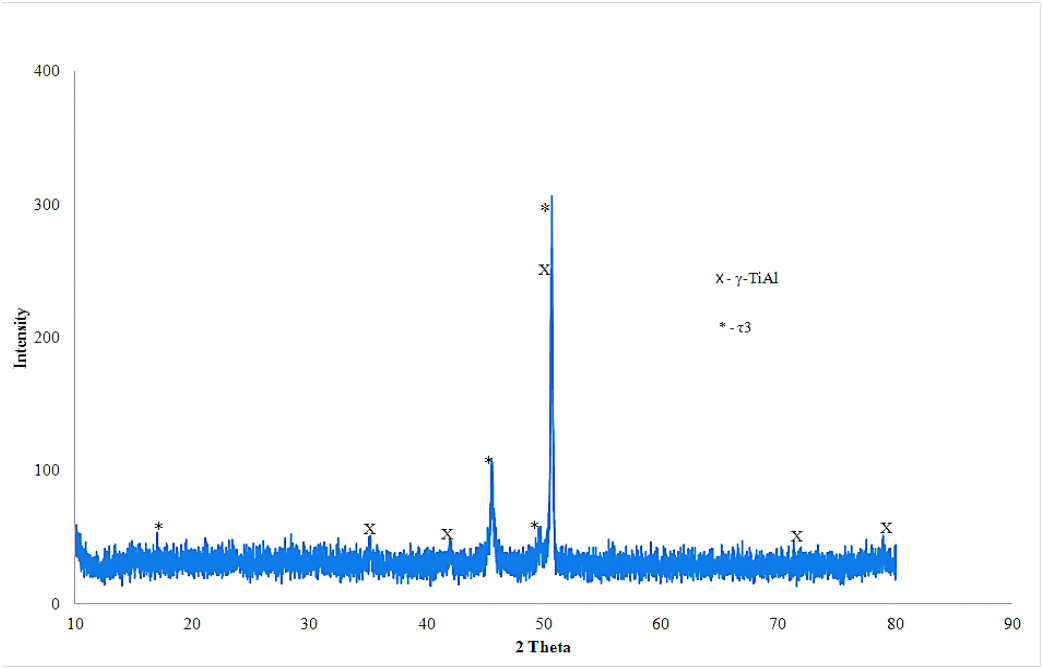

Figure 4.4: XRD pattern of as-cast TAN+Ru.

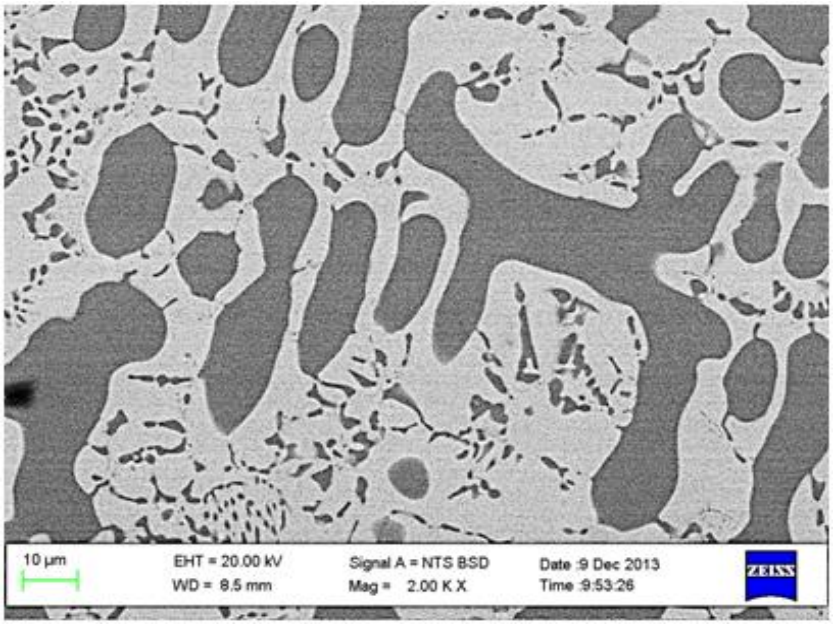

Figure 4.5: SEM-BSE image of as-cast TAN+Ru showing γ-TiAl dendrites (dark) in a TiAl+ Ti_2NiAl_3 (τ_3) (light) eutectic.

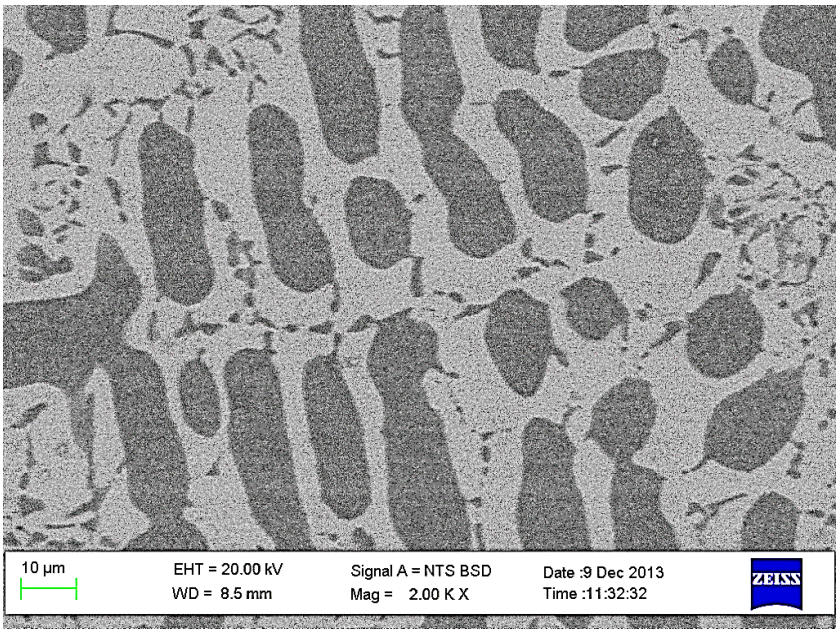

Figure 4.6: SEM-BSE image of annealed TAN+Ru showing γ-TiAl dendrites (dark) in a TiAl + Ti_2NiAl_3 (τ_3) (light) eutectic.

Table 4.3: EDX analyses for *as-cast* alloy TAN+Ru.

Area	Composition (at.%)				Phase
	Ti	Al	Ni	Ru	
Overall	39.7 ± 1.4	50.6 ± 1.3	9.6 ± 1.0	0.2 ± 0.1	-
Dendrites	45.2 ± 1.5	53.6 ± 1.1	1.1 ± 0.2	0.1 ± 0.1	γ-TiAl
Eutectic (light)	36.2 ± 1.8	48.4 ± 0.7	15.1 ± 1.1	0.3 ± 0.1	$Ti_2NiAl_3(\tau_3)$
Eutectic (overall)	42.1 ± 1.1	50.3 ± 0.6	7.6 ± 1.1	0.1 ± 0.1	γ-TiAl+$Ti_2NiAl_3(\tau_3)$

Table 4.4: EDX analyses for *heat treated* alloy TAN+Ru.

Area	Composition (at.%)				Phase
	Ti	Al	Ni	Ru	
Overall	38.9 ± 1.4	51.0 ± 1.3	9.9 ± 1.0	0.2 ± 0.1	-
Dendrites	45.8 ± 1.5	53.5 ± 1.1	0.6 ± 0.2	0.1 ± 0.1	γ-TiAl
Eutectic (light)	35.2 ± 1.8	48.6 ± 0.7	15.5 ± 1.1	0.3 ± 0.1	$Ti_2NiAl_3(\tau_3)$
Eutectic (overall)	37.5 ± 1.1	49.7 ± 0.6	12.5 ± 1.1	0.3 ± 0.1	γ-TiAl+$Ti_2NiAl_3(\tau_3)$

4.3 Hardness

The Ti-52.5Al-10.0Ni (at.%) and Ti-52.5Al-10.0Ni-0.2Ru alloys were quite hard and brittle (Table 4.5) and heat treatments slightly decreased the hardness. However, the decrease in hardness was within experimental error. The samples had extensive cracks and would sometimes crack during hardness testing. The Vicker's indentations of the alloys did not display any Palmqvist-type cracks [1985She] characteristic of hard materials such as cemented carbides. Therefore, the crack resistance and toughness of the models suggested by Shetty et al. [1985She] could not be used.

For both alloys, oxidation at high temperatures decreased the hardness (Figure 4.7). Under isothermal conditions, a longer oxidation time (720 hours) slightly reduced the hardness of both alloys than the shorter oxidation time of 120 hours, although the errors showed that the results could overlap. A reduction in hardness was most severe under cyclic oxidation between room temperature and 950°C. The hardness of TAN remained fairly similar to that of TAN+Ru under the different oxidation conditions.

Table 4.5:Vickers hardness (HV_{10}) of TAN and TAN+Ru, in at.%.

Condition	**Hardness HV_{10}**	
	TAN	TAN+Ru
As-cast	579 ± 15	561 ± 17
Annealed in argon (120 h, 1050°C)	556 ± 15	546 ± 12
Oxidized in air (120 h, 950°C, isothermal)	495±16	481 ±12
Oxidized in air (720 h, 950°C, isothermal)	475 ±14	468 ±15
Oxidized in air (120h, between room temperature and 950°C cyclic)	369 ±12	376 ± 15

Under cyclic oxidation, the TAN+Ru had a slightly higher hardness than the TAN alloy. Under all the other conditions, the TAN+Ru alloy had a slightly lower hardness, although the errors show that the hardnesses are very similar.

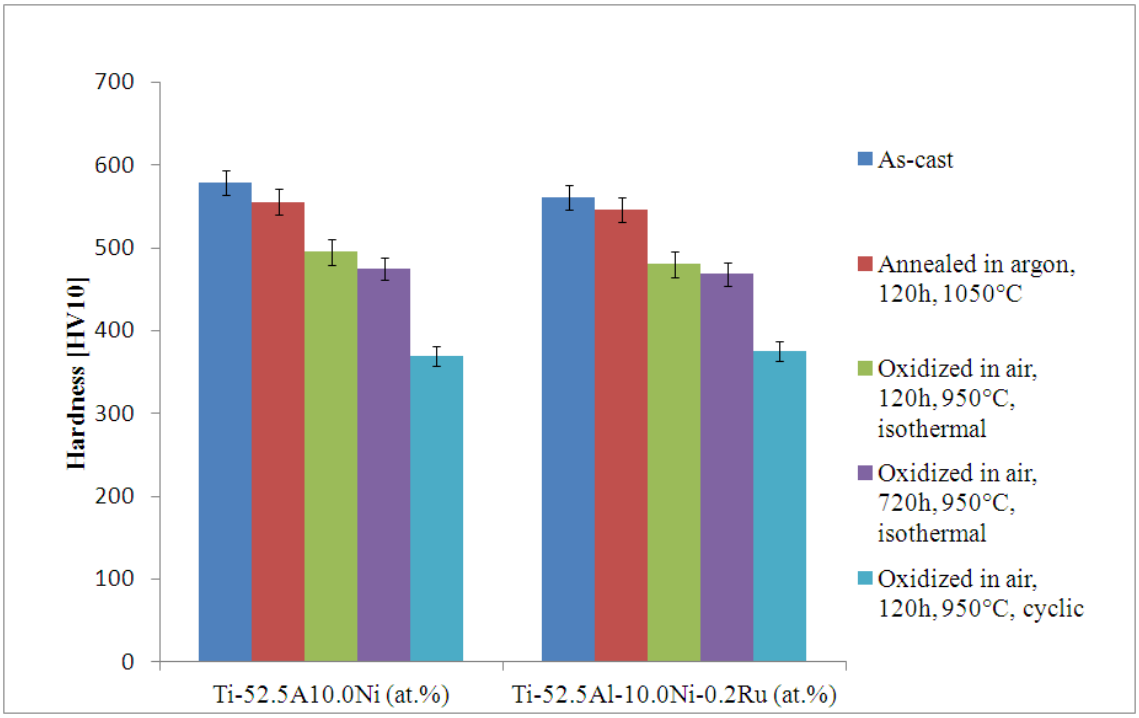

Figure 4.7: Hardness of gamma titanium aluminide alloys TAN and TAN+Ru.

4.4 High temperature oxidation results

4.4.1 Thermogravimetric analysis (TGA)

The TGA curves show the mass gain of the alloys with time, and the DSC curves shows the heat flow data (Figures 4.8 and 4.9). Overall, both the TAN and TAN+Ru alloys were fairly nonreactive when exposed to air from room temperature up to 1050°C. The alloys had a slight mass gain, indicating that they readily oxidized in air, although both alloys had a mass gain of less than 2%. The TAN alloy had small endothermic peaks at ~580°C and ~700°C (Figures 4.8), which were close to the oxide nucleation peaks [1993Mei, 1996Bra]. The TAN+Ru (at.%) alloy had a lower mass gain than the TAN (at.%) alloy (Figure 4.10) in both the as-cast and heat treated conditions.

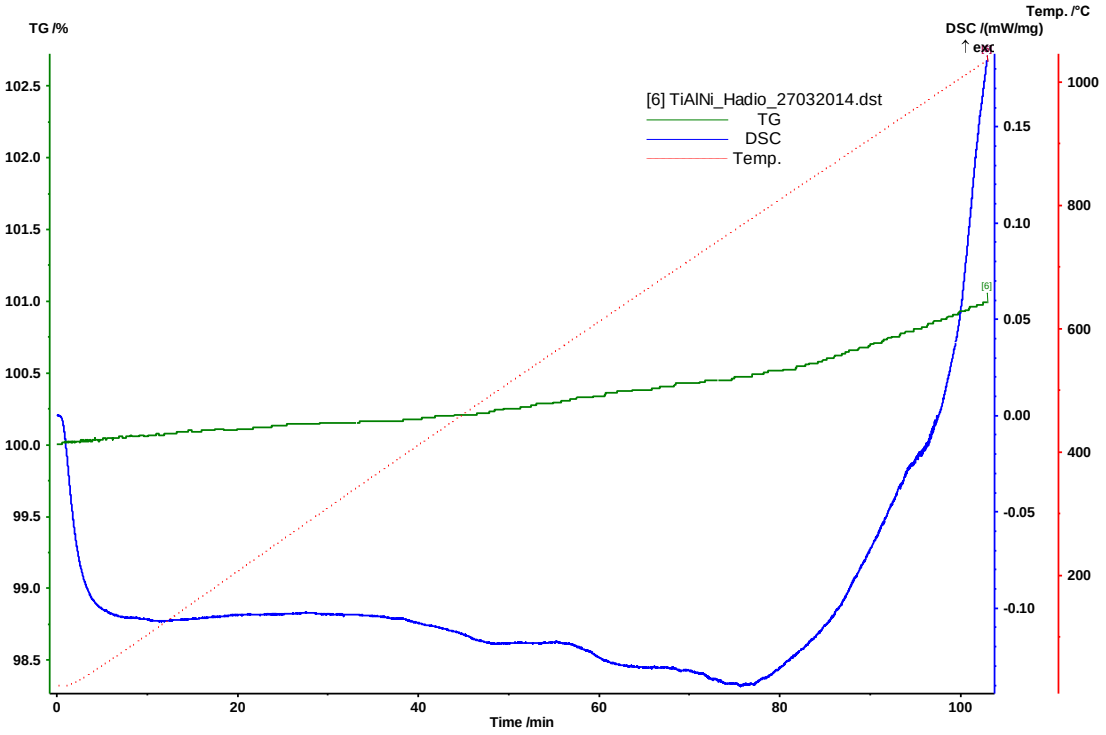

Figure 4.8: DSC/TGA curves for the TAN alloy.

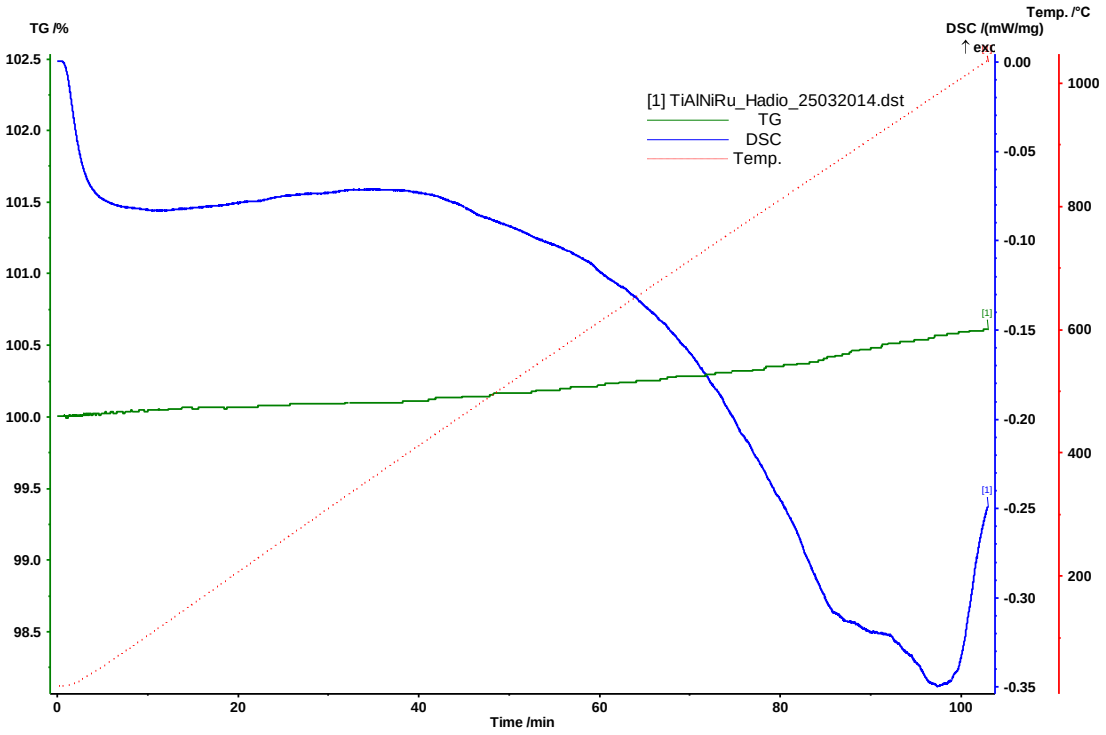

Figure 4.9: DSC/TGA curves for the TAN+Ru alloy.

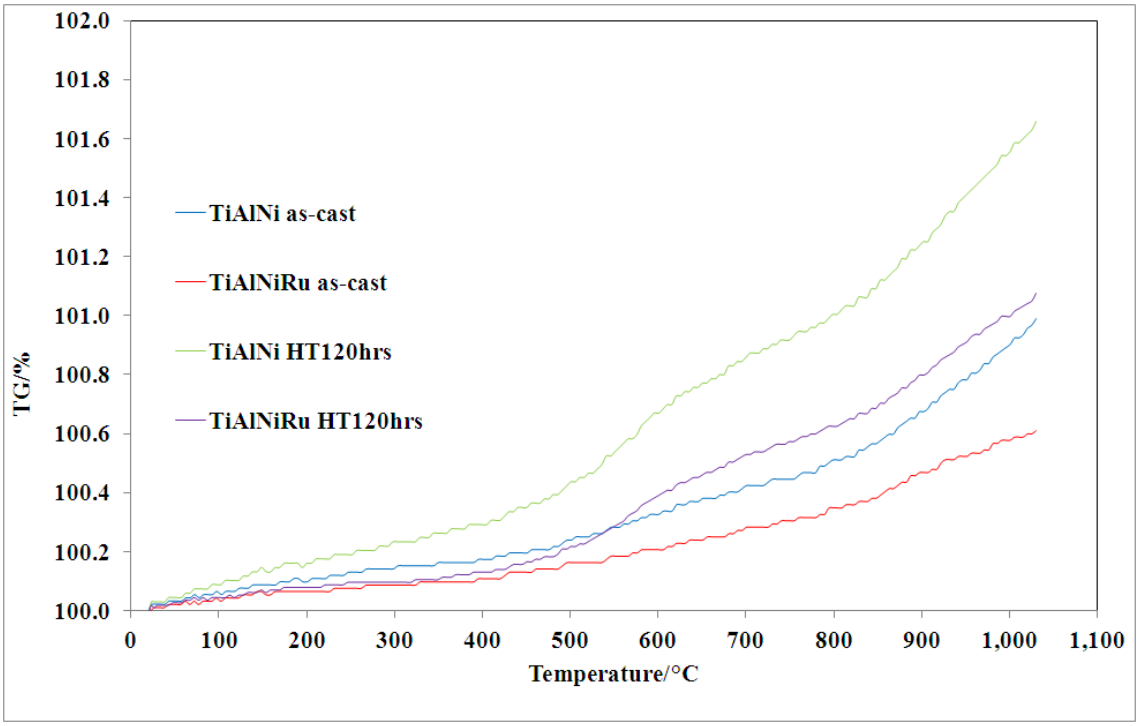

Figure 4.10: Thermogravimetric analysis curves for TAN and TAN+Ru.

For both the TAN and TAN+Ru alloy, the as-cast alloys showed slightly different behaviour from the heat treated alloys. The heat treated alloys had pronounced bumps between 550°C - 750°C. This feature in the heat treated alloys was independent of composition.

4.4.2 Isothermal oxidation of TAN

Oxidation of TAN in air at 950°C resulted in the formation of TiO_2 and Al_2O_3 scales on the surface of the alloy (Figure 4.11), where the TiO_2 occurred on the eutectic and the Al_2O_3 on the dendrites. After oxidising for 120 hours (Figures 4.11 and 4.13), the alloy formed a thin, non-continuous, blue-grey scale with good adherence to the substrate. After 720 hours (Figures 4.12 and 4.14), the scale exfoliated from the substrate on cooling after removal from the furnace. The remaining grey scale appeared severely degraded and contained trace amounts of nickel, which decreased with increased exposure time (Tables 4.6 and 4.7). The substrate (γ-TiAl dendrites in a eutectic of γ-TiAl + Ti_2NiAl_3 (τ_3)) showed extensive cracks and pores, especially adjacent to the

oxide layer. A small amount of oxygen was observed in the eutectic and the dendrites remained oxygen-free.

The alloy had a mass gain of 0.19% after 120 hours and 12.39% after 720 hours of isothermal oxidation in air at 950°C. XRD showed the different phases present in the alloy after oxidation (Figures 4.15 and 4.16): γ-TiAl, Ti_2NiAl_3 (τ_3), TiO_2 and Al_2O_3. A longer oxidation time increased the intensity of the peaks of the oxide scale, indicating more oxides.

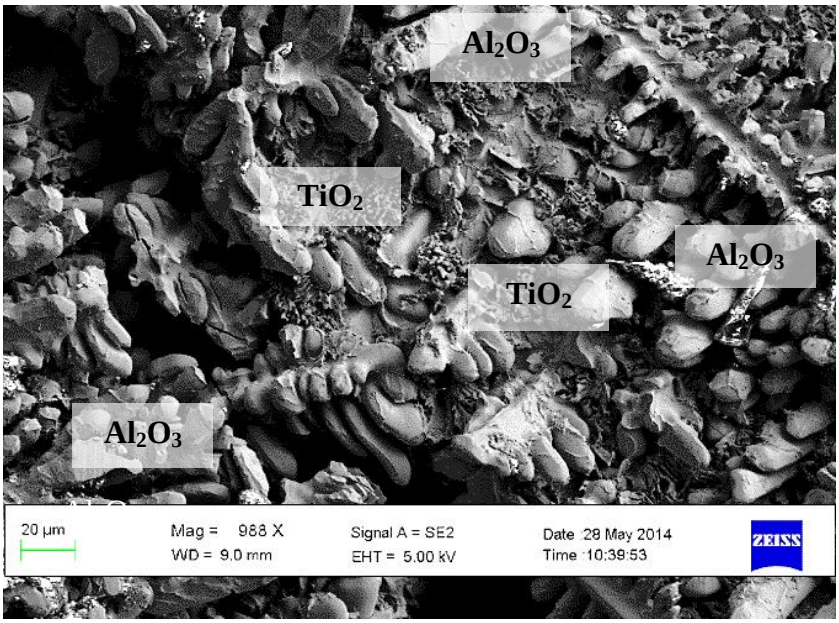

Figure 4.11: SEM-SE image of TAN surface after 120 hours oxidation in air at 950°C, showing TiO_2 and Al_2O_3 scales.

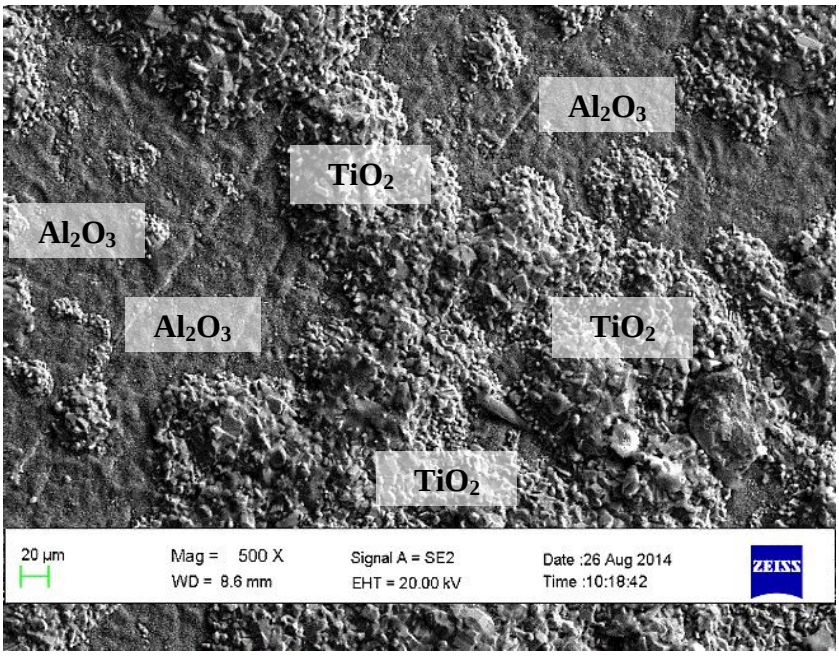

Figure 4.12: SEM-SE image of TAN after 720 hours oxidation in air at 950°C, showing degraded TiO_2 and Al_2O_3 scales.

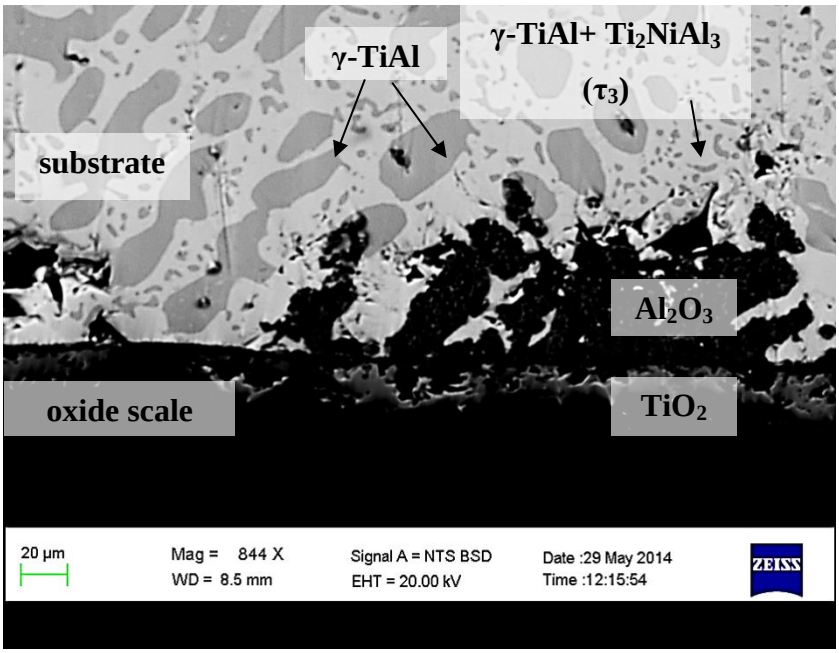

Figure 4.13: SEM-BSE image of a cross-section of TAN after 120 hours oxidation in air at 950°C, showing TiO_2 and Al_2O_3 scales.

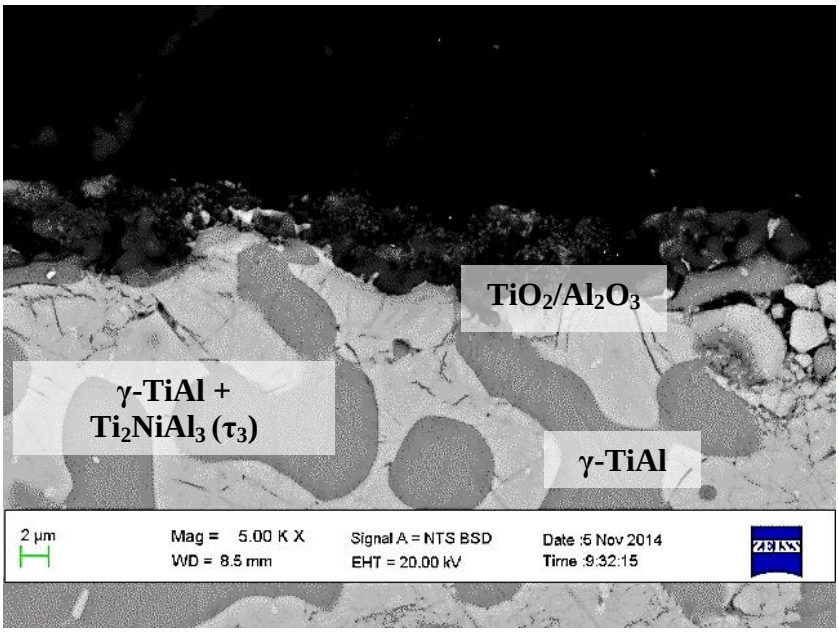

Figure 4.14: SEM-BSE image of a cross-section of TAN after 720 hours oxidation in air at 950°C, showing extensive cracks and pores in the alloy with a TiO_2/Al_2O_3 scale.

Table 4.6: EDX analyses for TAN after 120 hours oxidation in air at 950°C.

Area	Composition (at.%)			
	Ti	Al	Ni	O
Oxide (light outer layer)	27.9 ± 0.7	1.4 ± 0.1	0.1 ± 0.1	70.6 ± 1.1
Oxide (dark inner layer)	4.7 ± 0.1	27.9 ± 0.5	0.1 ± 0.1	67.3 ± 1.1
Dendrites	45.2 ± 1.3	54.2 ± 1.1	0.6 ± 0.1	-
Eutectic	34.6 ± 1.2	49.9 ± 1.1	13.7 ± 1.2	1.8 ± 0.1

Table 4.7: EDX analyses for TAN after 720 hours oxidation in air at 950°C.

Area	Elemental composition (at.%)			
	Ti	Al	Ni	O
Oxide (light outer layer)	21.2 ± 0.1	1.6 ± 0.1	-	77.2 ± 1.2
Oxide (dark inner layer)	6.5 ± 0.1	24.4 ± 0.1	0.7 ± 0.1	68.3 ± 1.0
Dendrites	43.4 ± 0.1	55.1 ± 1.4	1.5 ± 0.1	-
Eutectic	43.9 ± 1.2	42.9 ± 1.1	10.6 ± 0.1	2.7 ± 0.3

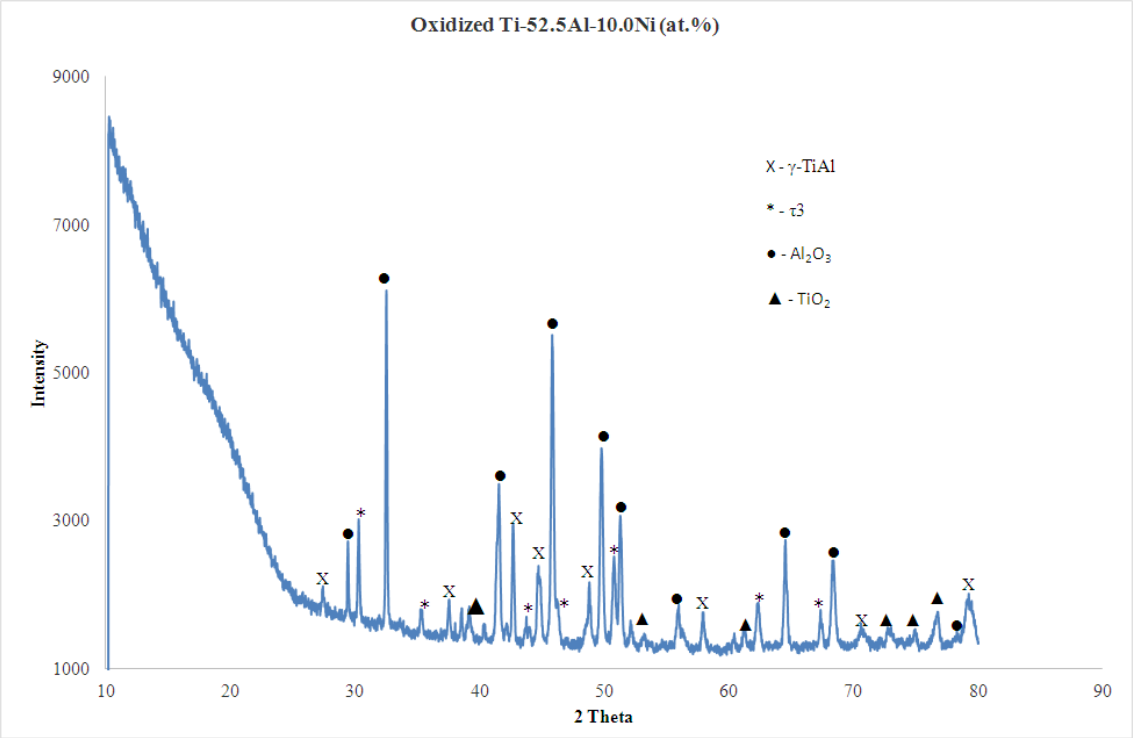

Figure 4.15: XRD pattern of TAN after oxidation in air for 120 hours at 950°C.

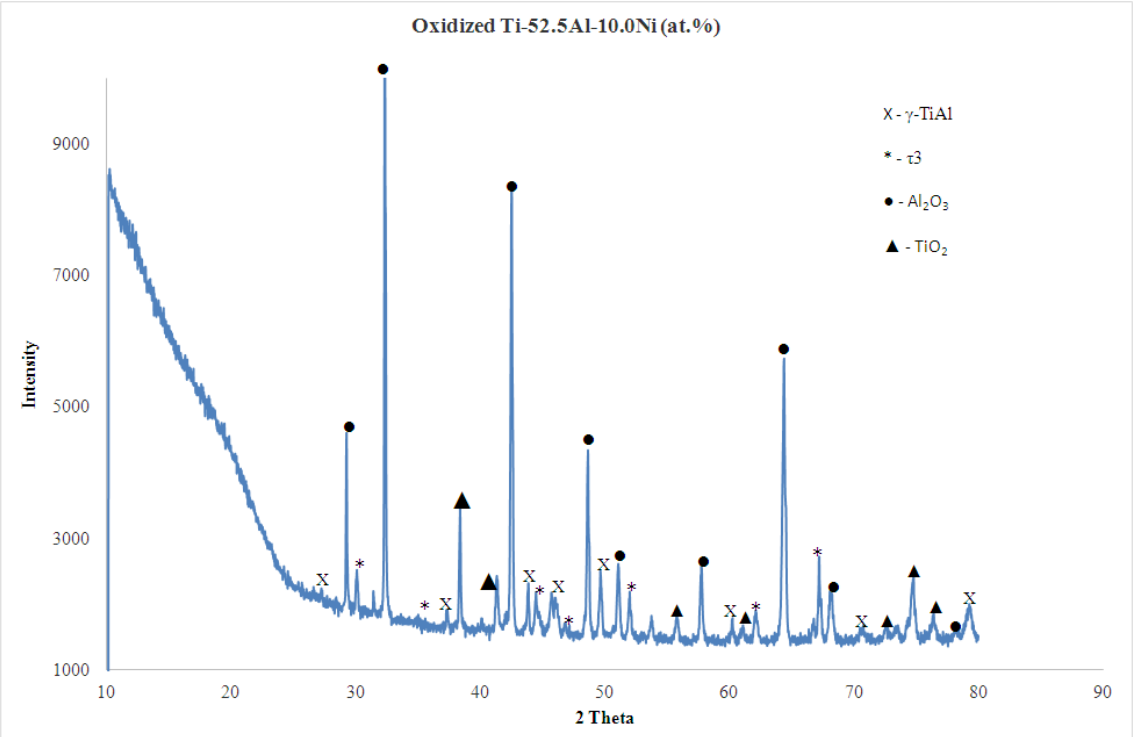

Figure 4.16: XRD pattern of TAN after oxidation in air for 720 hours at 950°C.

4.4.3 Isothermal oxidation of TAN+Ru

Oxidation of TAN+Ru in air for 120 hours at 950°C also resulted in the formation of a TiO_2 and Al_2O_3 scale on the surface of the alloy (Figure 4.17). The TiO_2 was on the eutectic and the Al_2O_3 was on the dendrites. The scale formed was thin with a good adherence to the substrate (Figures 4.17 and 4.19) and it appeared more continuous in the TAN+Ru alloy.

A longer oxidation time of 720 hours resulted in a severely degraded, scale of TiO_2 and Al_2O_3 (Figure 4.18). The scale had more of the less protective TiO_2 phase. On cooling, the scale exfoliated from the substrate material. In some areas of the alloy, the scale penetrated deeply into the substrate and seemed to consume the dendrites (Figure 4.20). The substrate still consisted of γ-TiAl dendrites in a eutectic of γ-TiAl + Ti_2NiAl_3 (τ_3). The scale had trace amounts of ruthenium and nickel. The alloy had a mass gain of 0.14% after 120 hours and 11.45% after 720 hours of isothermal oxidation in air at 950°C (Table 4.8). The ruthenium content was not accurate, because it was below 0.1 at.% (and this was also true in Table 4.9).

After 120 hours oxidation in air, the TAN+Ru alloy had no oxygen in the dendrites and eutectic (Table 4.8). After 720 hours oxidation, internal oxidation commenced in the alloy as trace amounts of oxygen were in the dendrites and eutectic (Table 4.9). XRD showed the different phases present in the alloy after oxidation (Figures 4.21 and 4.22).

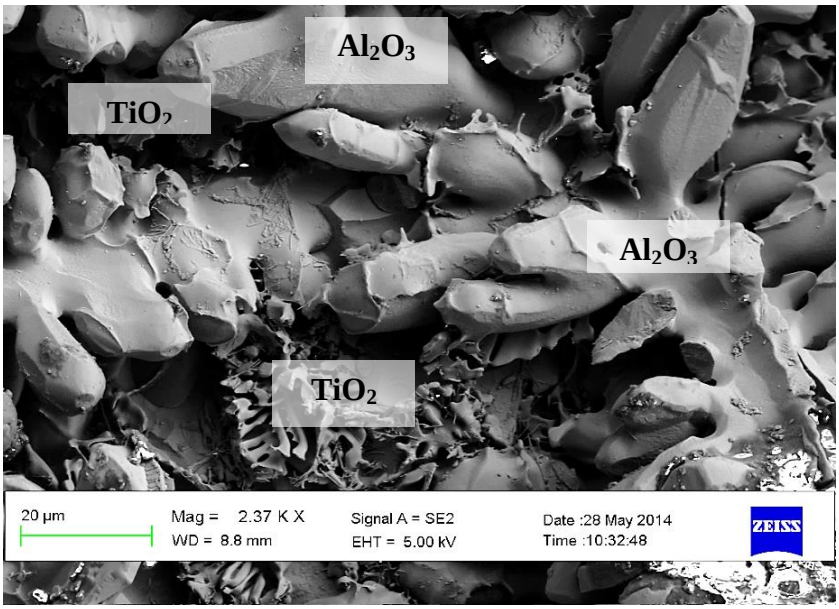

Figure 4.17: SEM-SE image of TAN+Ru surface after 120 hours oxidation in air at 950°C, showingTiO_2 scale on the eutectic and Al_2O_3 scale on the dendrites.

Table 4.8: EDX analyses for alloy TAN+Ru after 120 hours oxidation in air at 950°C.

Area	Composition (at.%)				
	Ti	Al	Ni	Ru	O
Oxide (light outer layer)	19.8 ± 0.8	1.5 ± 0.1	0.1 ± 0.1	0.01 ± 0.1	78.6 ± 0.2
Oxide (dark inner layer)	6.0 ± 0.1	24.8 ± 0.1	0.5 ± 0.1	0.01 ± 0.1	68.7 ± 0.2
Dendrites	44.1 ± 1.4	54.7 ± 0.8	1.1 ± 1.0	0.05 ± 0.1	-
Eutectic	33.7 ± 1.4	50.9 ± 1.1	15.1 ± 1.2	0.30 ± 0.1	-

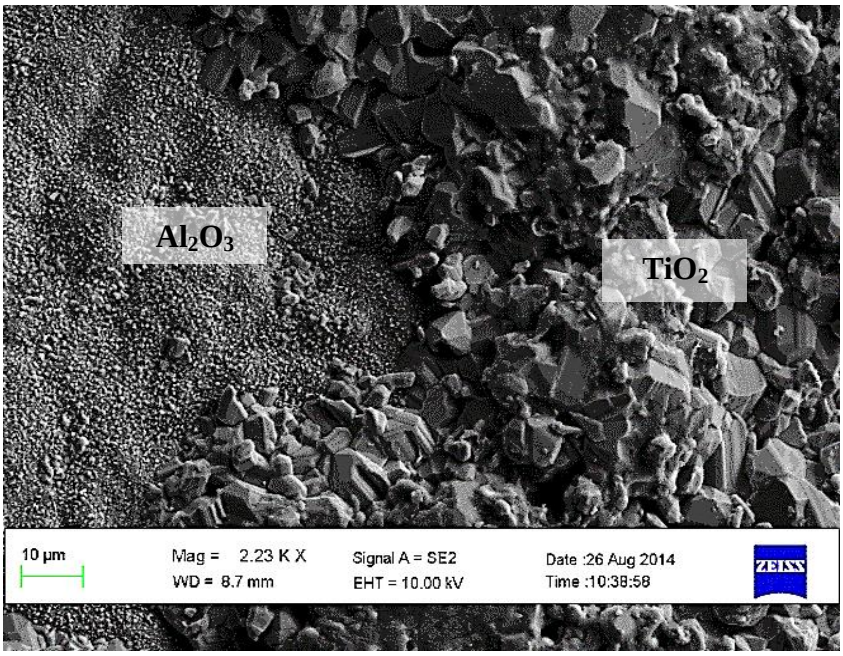

Figure 4.18: SEM-SE image of TAN+Ru surface after 720 hours oxidation in air at 950°C, showing severely degraded TiO_2 and Al_2O_3 scales.

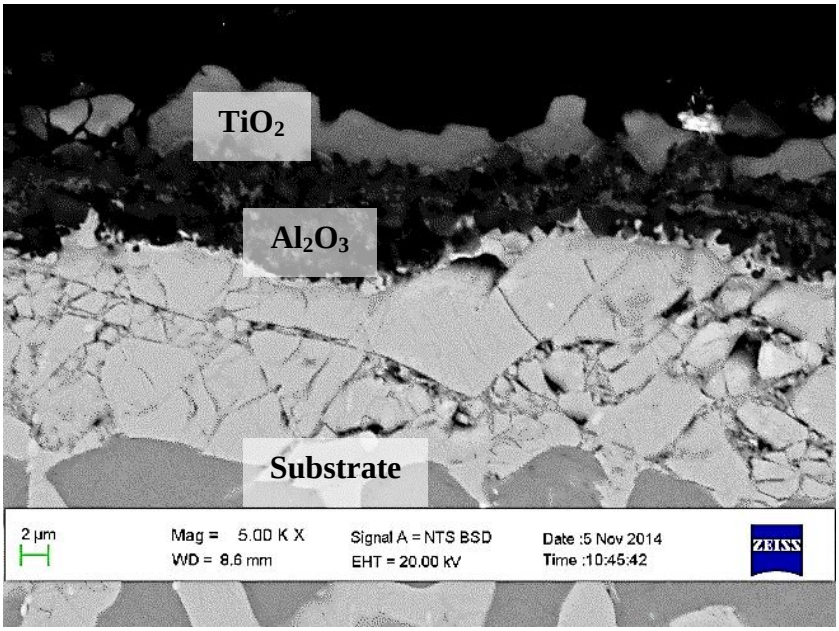

Figure 4.19: SEM-BSE image of a cross-section of TAN+Ru after 120 hours oxidation in air at 950°C, showing a substrate with extensive cracks and an oxide scale with an outer Ti-rich layer and an inner Al-rich layer.

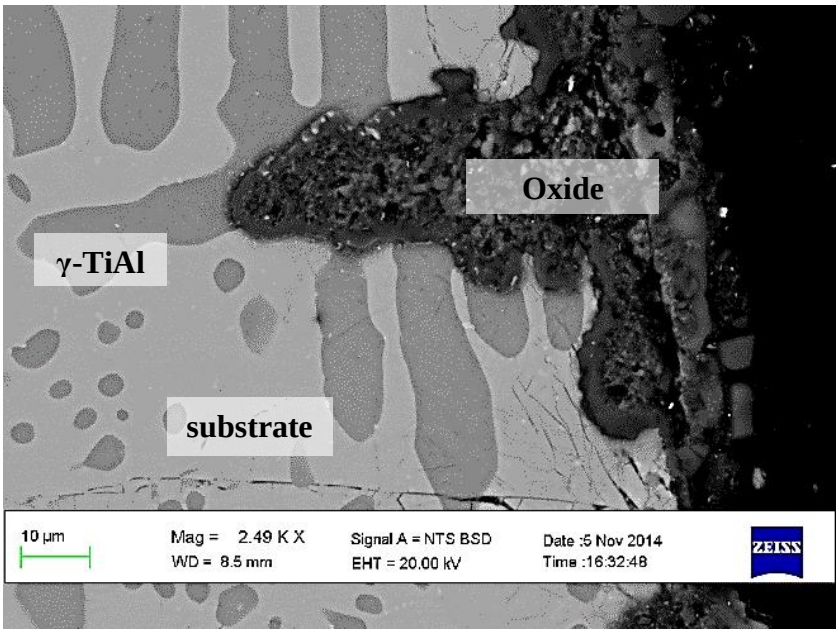

Figure 4.20: SEM-BSE image of a cross-section of TAN+Ru after 720 hours oxidation in air at 950°C, showing the oxide scale consuming a dendrite in the substrate.

Table 4.9: EDX analyses for alloy TAN+Ru after 720 hours oxidation in air at 950°C.

Area	Elemental composition (at.%)				
	Ti	Al	Ni	Ru	O
Oxide (light outer layer)	20.4 ± 1.2	6.2 ± 0.1	0.1 ± 0.1	0.01 ± 0.1	73.3 ± 1.1
Oxide (dark inner layer)	5.2 ± 0.1	26.1 ± 1.3	0.1 ± 0.1	0.02 ± 0.1	68.5 ± 1.2
Dendrites	44.4 ± 1.4	52.5 ± 1.4	0.5 ± 0.1	0.1 ± 0.1	2.1 ± 0.1
Eutectic	34.4 ± 1.4	48.2 ± 1.1	15.6 ± 1.2	0.3 ± 0.1	1.5 ± 0.2

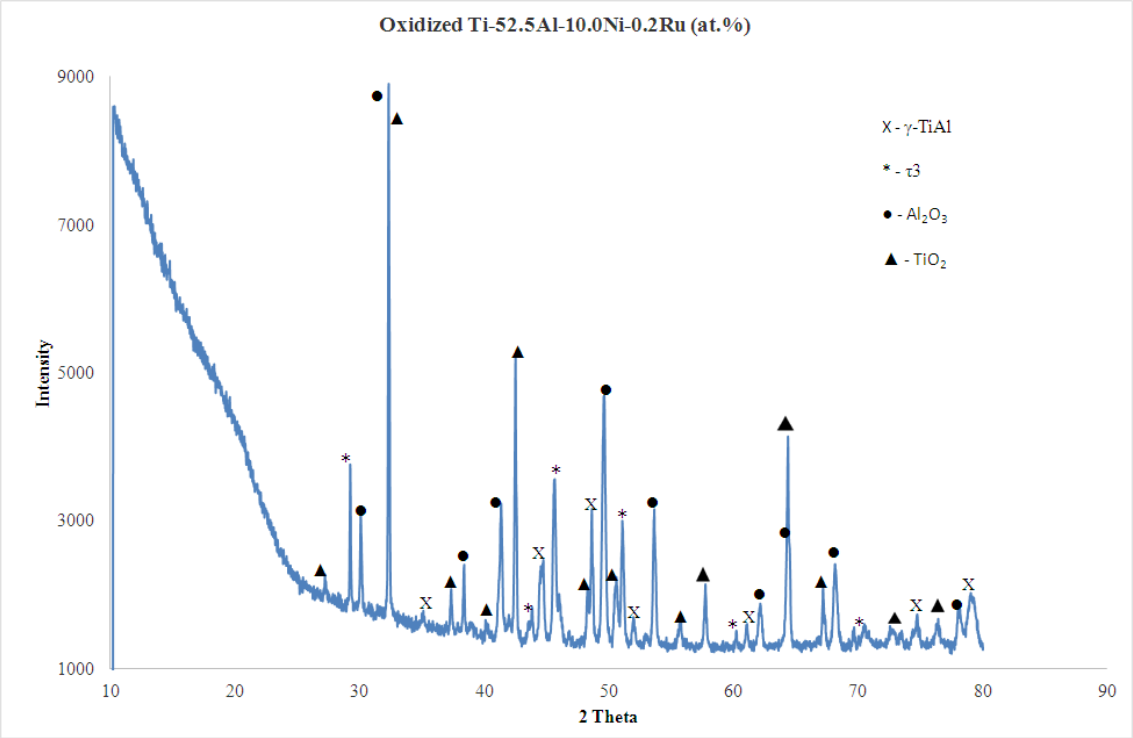

Figure 4.21: XRD pattern of TAN+Ru after oxidation in air for 120 hours at 950°C.

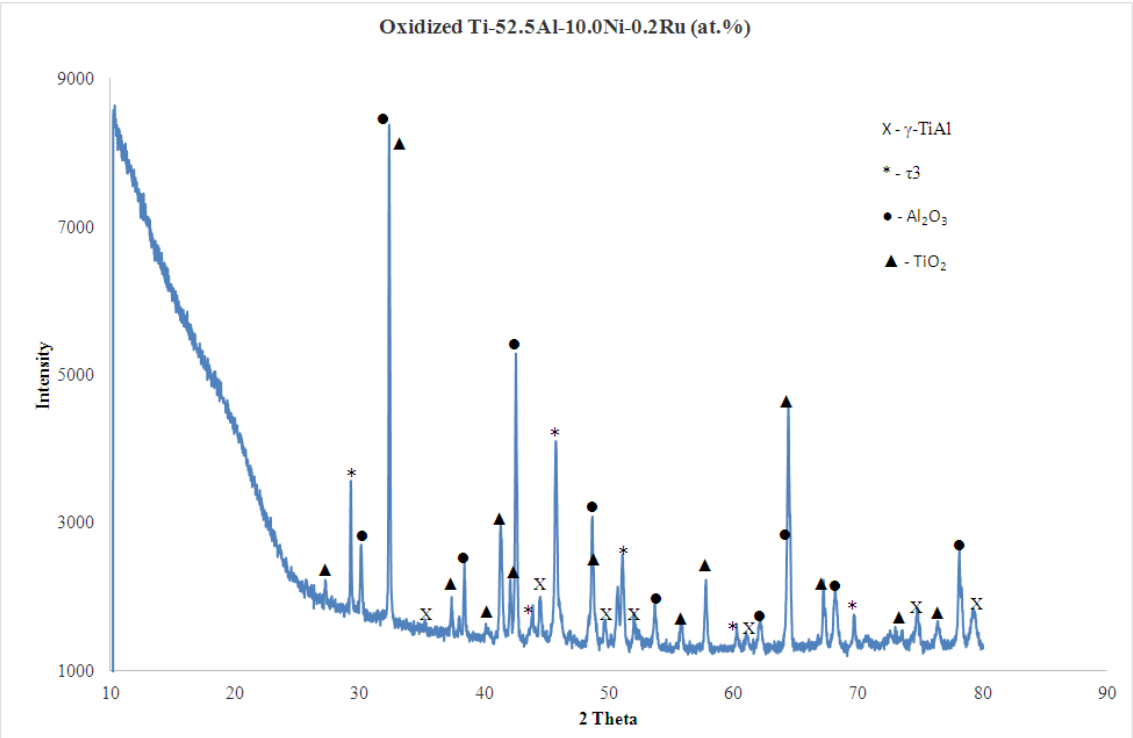

Figure 4.22: XRD pattern of TAN+Ru after oxidation in air for 720 hours at 950°C.

4.4.4 Cyclic oxidation of TAN and TAN+Ru

The TAN alloy was very brittle and had severe cracks (Figure 4.24). The substrate consisted of γ-TiAl dendrites in a eutectic of γ-TiAl + Ti_2NiAl_3 (τ_3). There was no oxide scale on the alloy as it had exfoliated from the surface (Figure 4.25). The alloy had no internal oxidation after cyclic oxidation in air (Table 4.10).

The TAN+Ru alloy was also brittle and consisted of γ-TiAl dendrites in a eutectic of γ-TiAl + Ti_2NiAl_3 (τ_3) (Figure 4.26). The alloy formed a more adherent intermixed scale of TiO_2/Al_2O_3 with an intermittent, nickel-rich (45.1 ± 0.2 at.%) sub-surface zone between the substrate and oxide layer (Figures 4.27). The sub-surface zone had a composition similar to the τ_4 phase in the isothermal Al-Ni-Ti phase diagram (Figure 5.1 [2007Sch]). The scale had trace amounts of nickel and ruthenium and had an outer TiO_2 layer and an inner Al_2O_3 oxide layer, as shown in Table 4.11. The TAN+Ru alloy had more oxides than the TAN alloy (Figures 4.21 and 4.22).

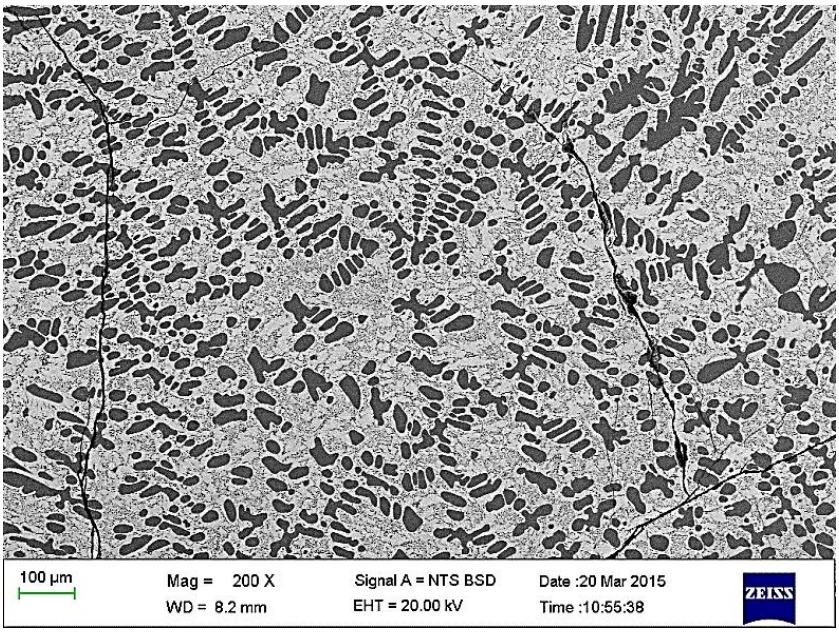

a) SEM-BSE image of TAN (200x) after cyclic oxidation in air.

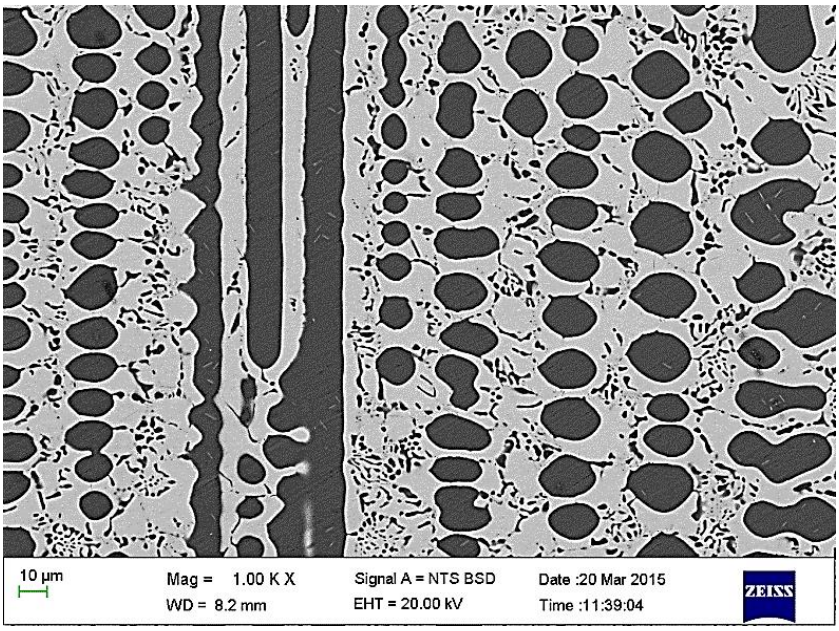

b) SEM-BSE image of TAN (1000x) after cyclic oxidation in air.

Figure 4.24: SEM-BSE images a) 200x and b) 1000x of TAN after cyclic oxidation in air, showing γ-TiAl dendrites in a eutectic of γ-TiAl + Ti_2NiAl_3 (τ_3).

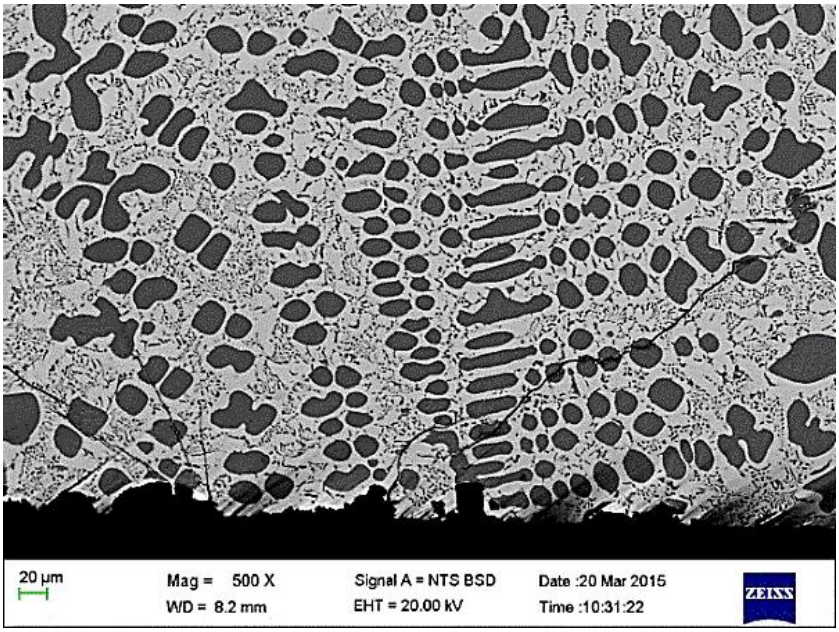

Figure 4.25: SEM-BSE image of the cross-section of TAN after cyclic oxidation in air, showing the substrate with cracks and without an oxide layer.

Table 4.10: EDX analyses for alloy TAN after 120 hours cyclic oxidation in air between room temperature and 950°C.

Area	Composition (at.%)				Phases
	Ti	Al	Ni	O	
Dendrites	47.0 ± 0.1	52.1 ± 0.1	1.0 ± 0.1	-	γ-TiAl
Eutectic (light)	37.1 ± 0.1	45.7 ± 0.1	17.2 ± 0.2	-	$Ti_2NiAl_3(\tau_3)$
Eutectic (overall)	39.2 ± 0.2	47.4 ± 0.1	13.5 ± 0.2	-	γ-TiAl + $Ti_2NiAl_3(\tau_3)$

Table 4.11: EDX analyses for alloy TAN+Ru after 120 hours cyclic oxidation in air between room temperature and 950°C.

Area	Composition (at.%)				
	Ti	Al	Ni	Ru	O
Oxide (light outer layer)	15.4 ± 0.1	8.3 ± 0.1	0.3 ± 0.1	0.02 ± 0.1	75.9 ± 0.1
Oxide (dark inner layer)	5.8 ± 0.1	21.8 ± 0.1	0.2 ± 0.1	0.10 ± 0.1	71.1 ± 0.1
Sub-surface zone	22.2 ± 0.2	32.0 ± 0.1	45.1 ± 0.2	0.20 ± 0.1	-
Dendrites	41.4 ± 0.1	57.7 ± 0.1	1.0 ± 0.1	0.10 ± 0.1	-
Eutectic	36.9 ± 0.1	53.6 ± 0.2	9.8 ± 0.1	0.20 ± 0.1	-

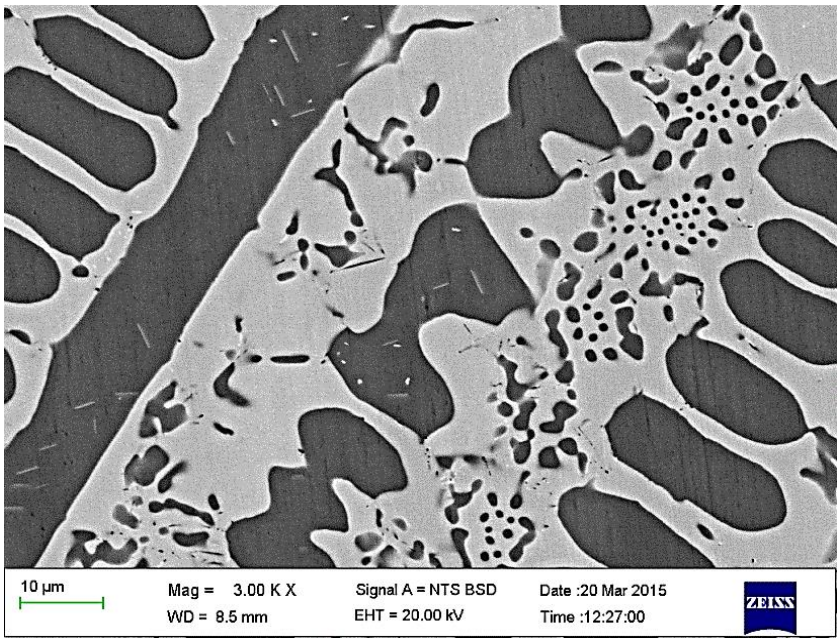

Figure 4.26: SEM-BSE image of TAN+Ru after 120 hours cyclic oxidation in air, showing γ-TiAl dendrites in a eutectic of γ-TiAl + Ti_2NiAl_3 (τ_3).

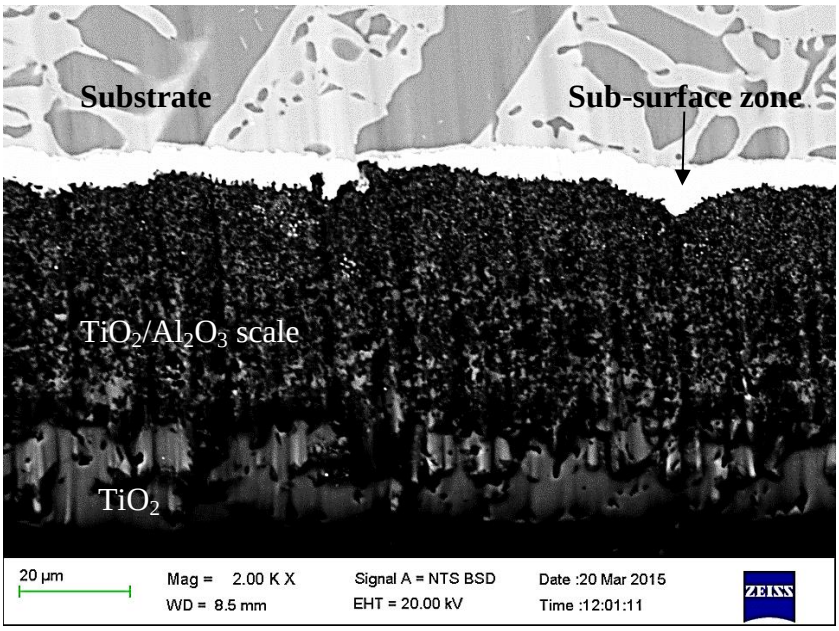

Figure 4.27: SEM-BSE image of a cross-section of TAN+Ru after 120 hours cyclic oxidation in air, showing an intermixed TiO_2/Al_2O_3 scale with a nickel-rich sub-surface zone between the substrate and oxide layer and an outer TiO_2 scale.

The alloys showed a higher amount of mass gain under cyclic oxidation conditions than in isothermal oxidation conditions. The mass gain was lower in air than in a hot salt environment for both alloys (Figure 4.28). The TAN+Ru alloy performed better than the TAN alloy in both environments.

In the hot salt environment, the TAN alloy formed a TiO_2 and Al_2O_3 scale which appeared severely degraded (Figure 4.29). The surface consisted of mostly TiO_2, significantly less Al_2O_3 and no nickel. The alloy had internal oxidation, with dendrites and a eutectic containing oxygen (Table 4.12).

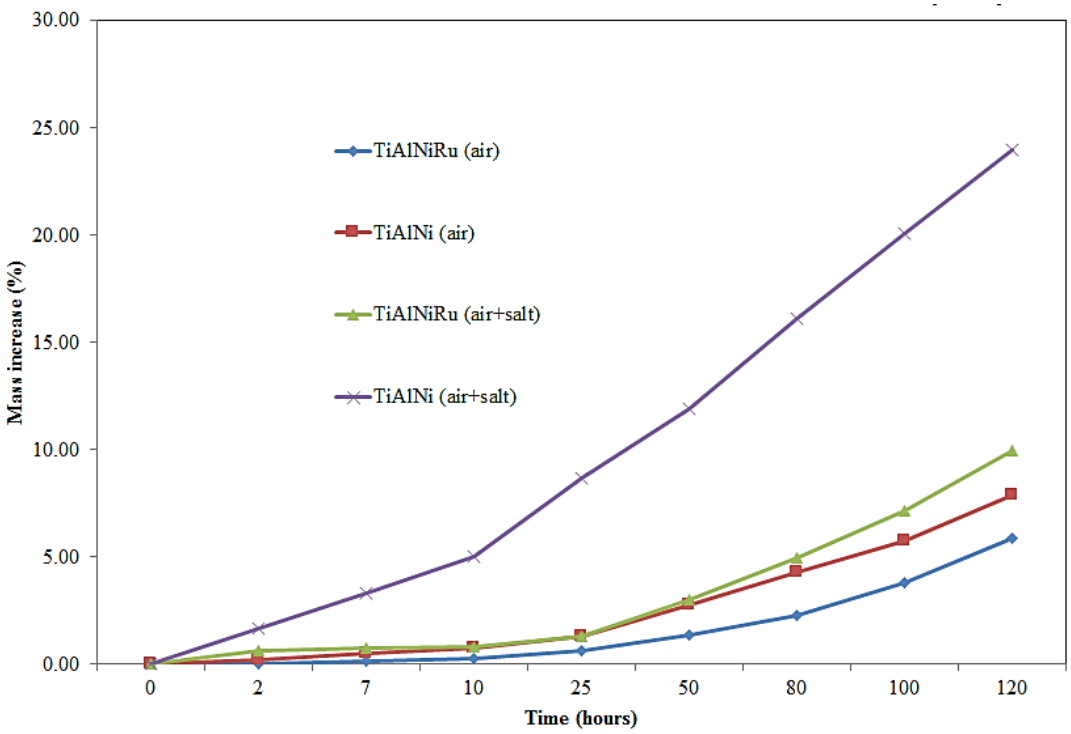

Figure 4.28: Mass gain data of TAN and TAN+Ru obtained during cyclic oxidation in air and salt (Na_2SO_4).

Table 4.12: EDX analyses for alloy TAN after 120 hours cyclic oxidation in Na_2SO_4.

Area	Composition (at.%)			
	Ti	Al	Ni	O
Oxide layer	30.2 ± 0.2	0.79 ± 0.1	-	67.2 ± 0.2
Dendrites	38.2 ± 0.1	53.1 ± 0.1	0.5 ± 0.1	8.2 ± 0.1
Eutectic	33.8 ± 0.1	45.7 ± 0.1	11.2 ± 0.2	9.3 ± 0.1

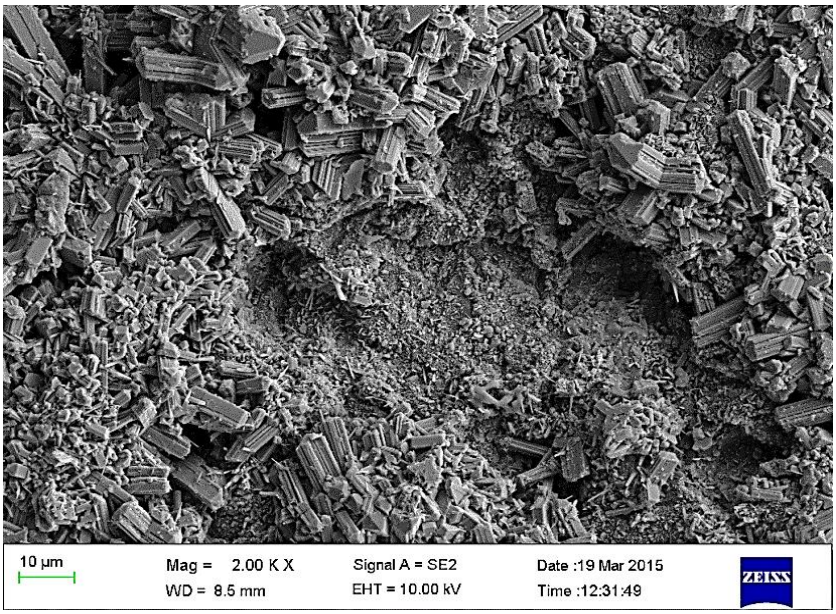

a) SEM-SE image of TAN (2000x).

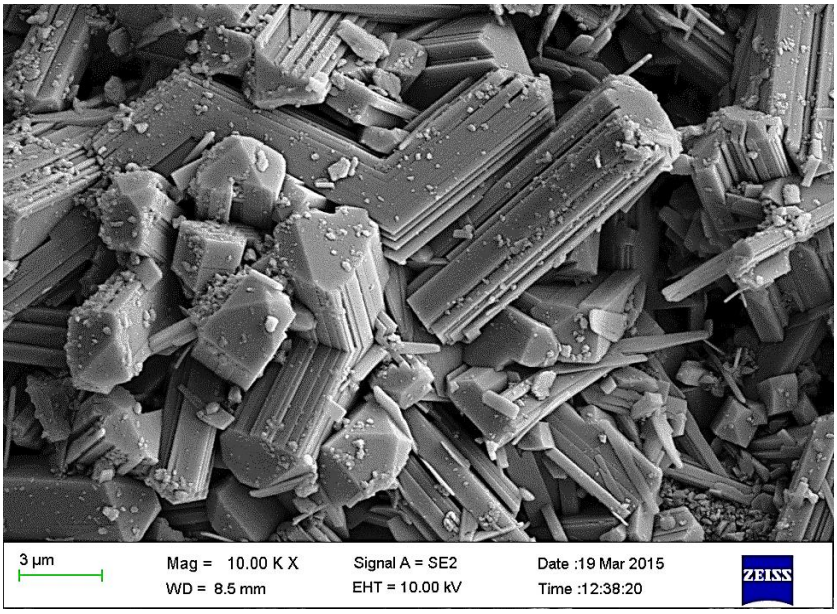

b) SEM-SE image of TAN (10000x).

Figure 4.29: SEM-SE images a) 2000x and b) 10000x of the surface of TAN after hot salt corrosion in Na_2SO_4 at 950°C, showing long, prismatic crystals on the surface.

In hot salt, the TAN+Ru alloy formed a TiO_2 and Al_2O_3 scale which appeared more adherent to the substrate (Figure 4.30). No ruthenium and nickel were detected in the scale and the alloy had some internal oxidation (Table 4.13).

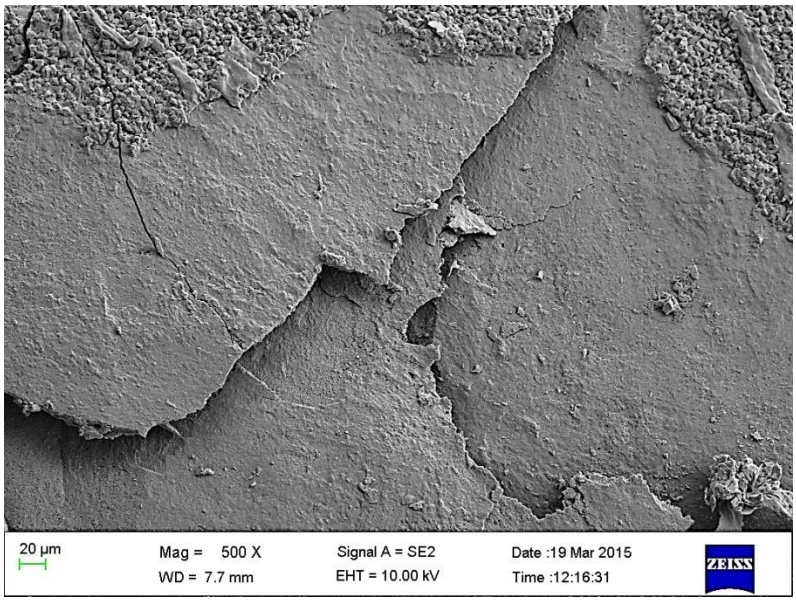

a) SEM-SE images (500x) of TAN+Ru after hot salt corrosion in Na_2SO_4 at 950°C.

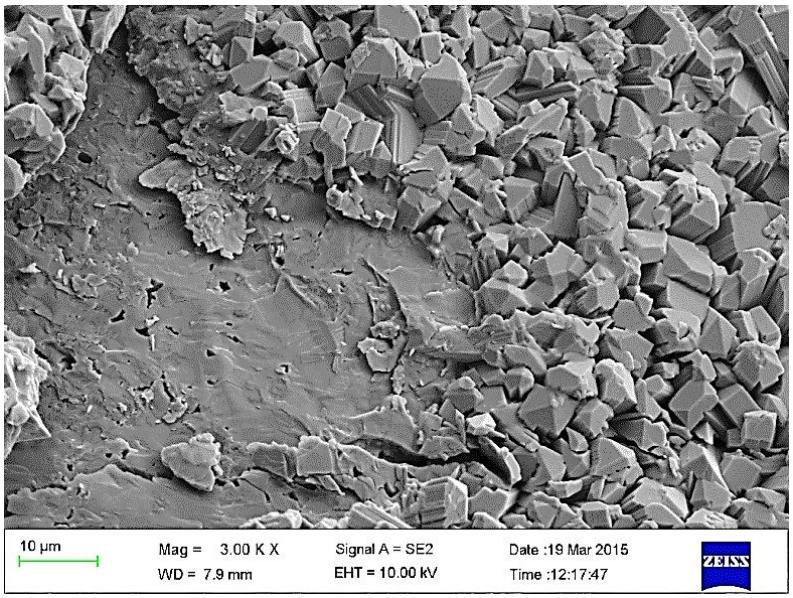

b) SEM-SE image (3000x) of TAN+Ru after hot salt corrosion in Na_2SO_4 at 950°C.

Figure 4.30: SEM-SE images a) 500x and b) 3000x of the surface of TAN+Ru after 120 hours hot salt corrosion in Na_2SO_4 at 950°C, showing $TiO_2$and Al_2O_3 scales, and crystals partially covering the surface.

Both alloys had the lowest oxidation resistance in hot salt under cyclic oxidation conditions. A longer exposure time reduced the oxidation resistance of the alloys (Figure 4.31).

Table 4.13: EDX analyses for alloy TAN+Ru after 120 hours cyclic oxidation in Na_2SO_4.

Area	Composition (at.%)				
	Ti	Al	Ni	Ru	O
Oxide layer	18.5 ± 0.1	0.35 ± 0.1	-	-	81.2 ± 0.2
Dendrites	42.3 ± 0.1	52.3 ± 0.1	1.0 ± 0.1	0.1 ± 0.05	4.3 ± 0.1
Eutectic	38.2 ± 0.1	42.1 ± 0.2	10.3 ± 0.1	0.2 ± 0.05	9.2 ± 0.1

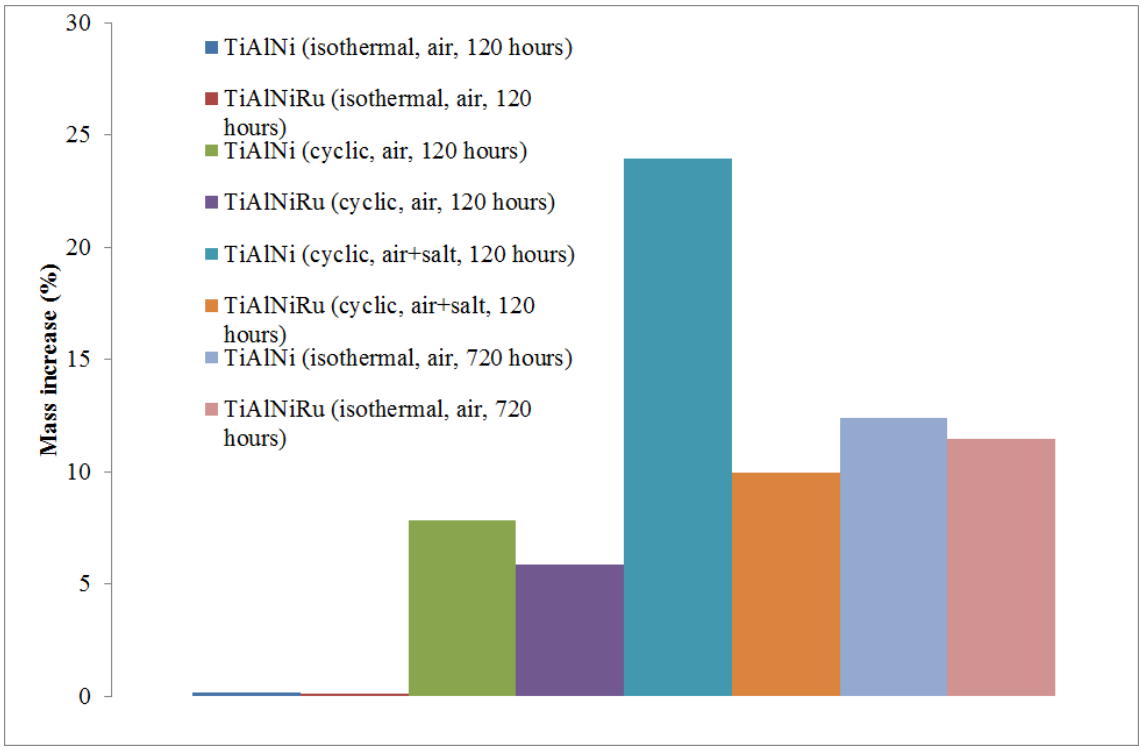

Figure 4.31 Comparison of mass gains for γ-TiAl alloys TAN and TAN+Ru in different oxidation environments.

4.5 Corrosion behaviour in hydrochloric acid

Gamma titanium aluminide (γ-TiAl) as-cast alloys TAN and TAN+Ru were evaluated for corrosion resistance in 5 wt% (dilute) and 25 wt% (concentrated) HCl solutions using potentiodynamic scans at room temperature. The alloys were assessed to determine whether the presence of nickel and ruthenium would cause TAN and TAN+Ru to passivate by cathodic modification, and become corrosion resistant in dilute and concentrated HCl.

4.5.1 Corrosion behaviour of TAN

In a non-oxidising, dilute (5 wt%) HCl environment, the TAN alloy formed a thin and non-continuous Al_2O_3 oxide scale on the surface of the γ-TiAl dendrites, with Ti_3NiAl_2O found in the γ-TiAl + Al_3NiTi_2 (τ_3) eutectic regions.

In concentrated (25 wt%) HCl, the Al_2O_3 oxide scale was present on the γ-TiAl dendrites, but to a lesser extent. In some areas, the alumina was clearly visible (Figure 4.32), and in other areas the layer was too thin to be observed in SEM (Figure 4.33). The acid mainly corroded the τ_3 phase, thus attacking the eutectic and leaving the γ-TiAl dendrites exposed (Figure 4.33). Alumina and Ti_3NiAl_2O were clearly shown by XRD (Figures 4.34and 4.35).

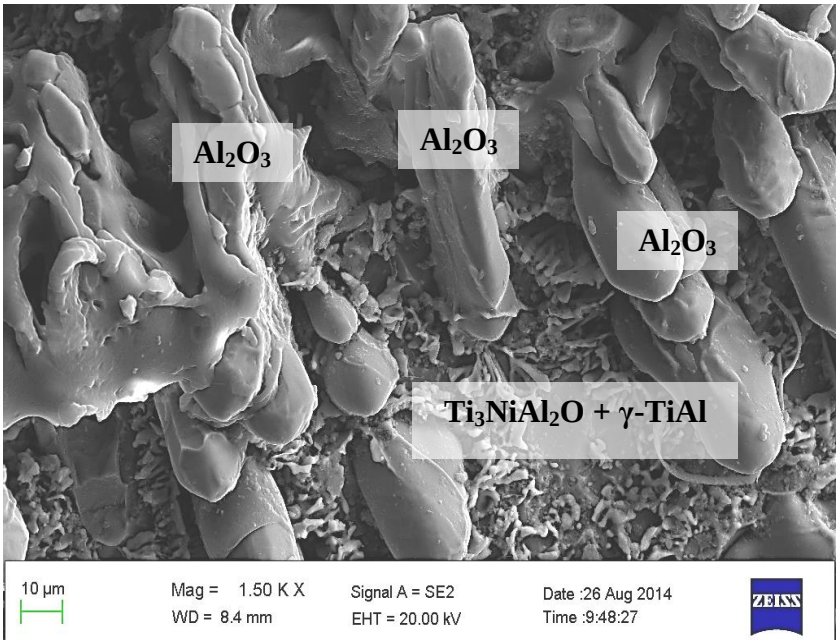

Figure 4.32: SEM-SE image of the corroded surface of TAN in 5 wt% HCl, showing a thin and non-continuous Al_2O_3 oxide scale on the surface of the γ-TiAl dendrites, with Ti_3NiAl_2O in the γ-TiAl + Ti_2NiAl_3 (τ3) eutectic.

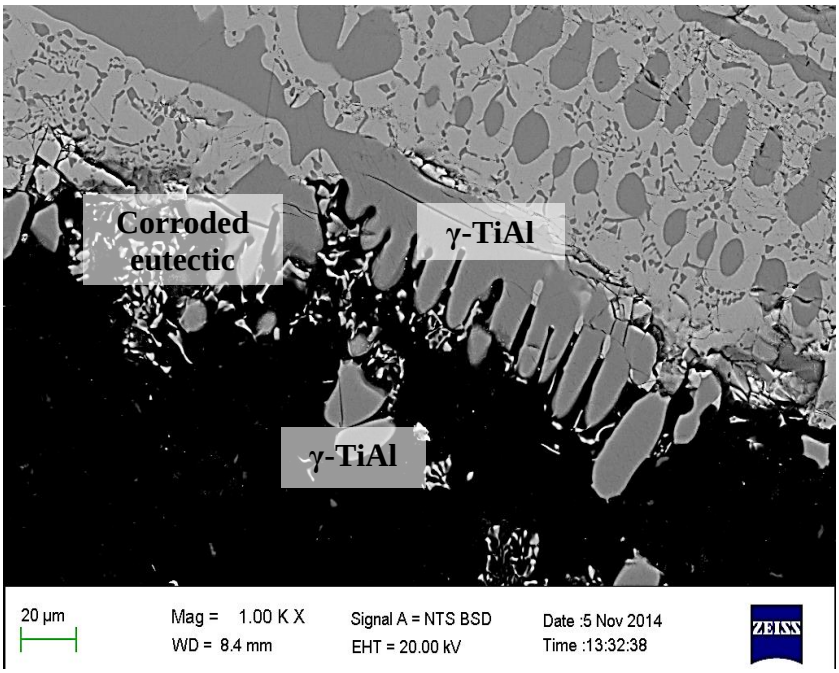

Figure 4.33: SEM-BSE image of a cross-section of corroded TAN in 5 wt% HCl, showing the corroded surface with exposed γ-TiAl dendrites.

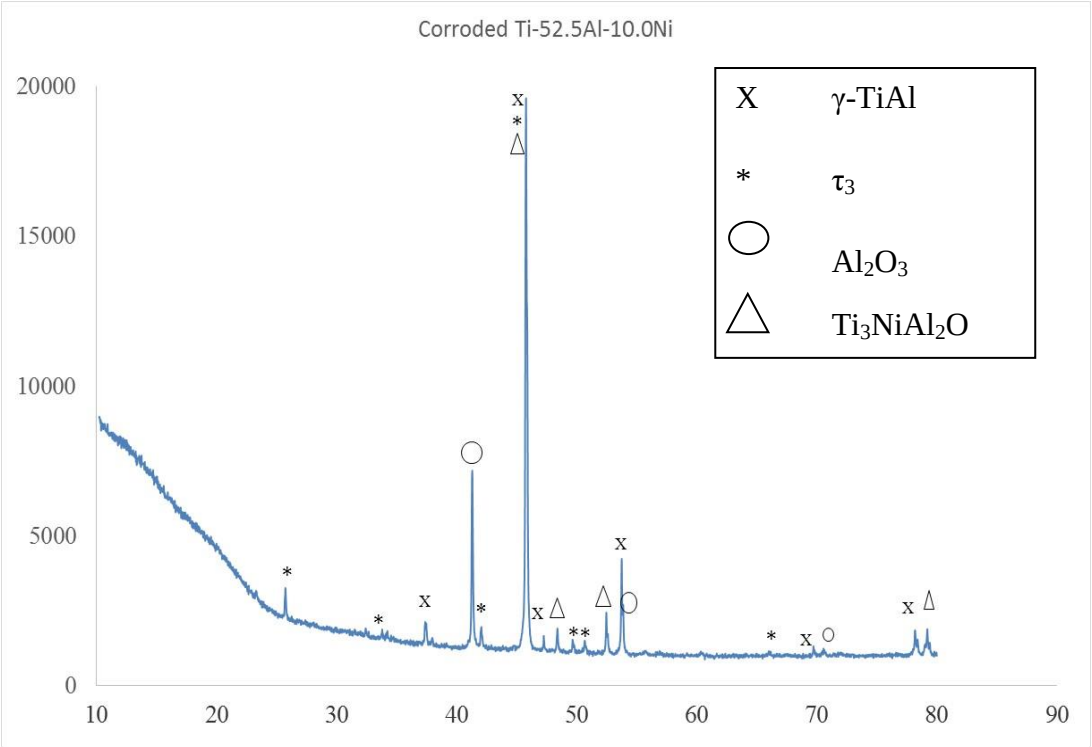

Figure 4.34: XRD pattern for TAN surface corroded in 5 wt% HCl.

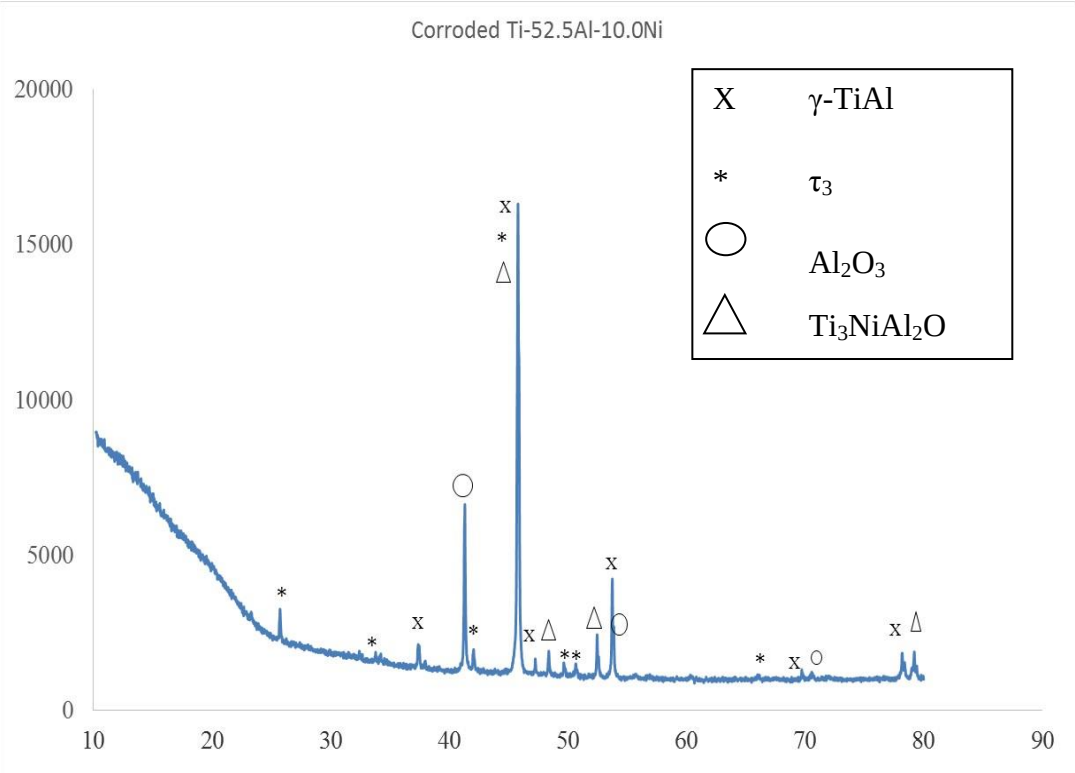

Figure 4.35: XRD pattern for TAN surface corroded in 25 wt% HCl.

4.5.2 Corrosion behaviour of TAN+Ru

The TAN+Ru alloy also formed a thin and non-continuous Al_2O_3 scale on the γ-TiAl dendrites, with Ti_3NiAl_2O found in the γ-TiAl + τ_3 eutectic regions (Figures 4.36 and 4.37). Ruthenium was not present in the γ-TiAl dendrites, but was present (0.3 ± 0.1 at.%) in the eutectic region. No ruthenium was found in the scale on the dendrites, although there were trace amounts of nickel (0.5 ± 0.1 at.%). In 5 wt% HCl, the scale on the TAN+Ru alloy (Figure 4.37) had better adherence to the substrate than the scale on the TAN alloy (Figure 4.33). In 25 wt% HCl, the scale on TAN+Ru appeared porous, unstable and was exfoliating (Figure 4.38), especially after exposure to the more concentrated HCl environment. Cracks were evident in the alloy (Figure 4.37), and mainly propagated along the surfaces of the γ-TiAl dendrites. Alumina and Ti_3NiAl_2O were clearly shown by XRD (Figures 4.39 and 4.40).

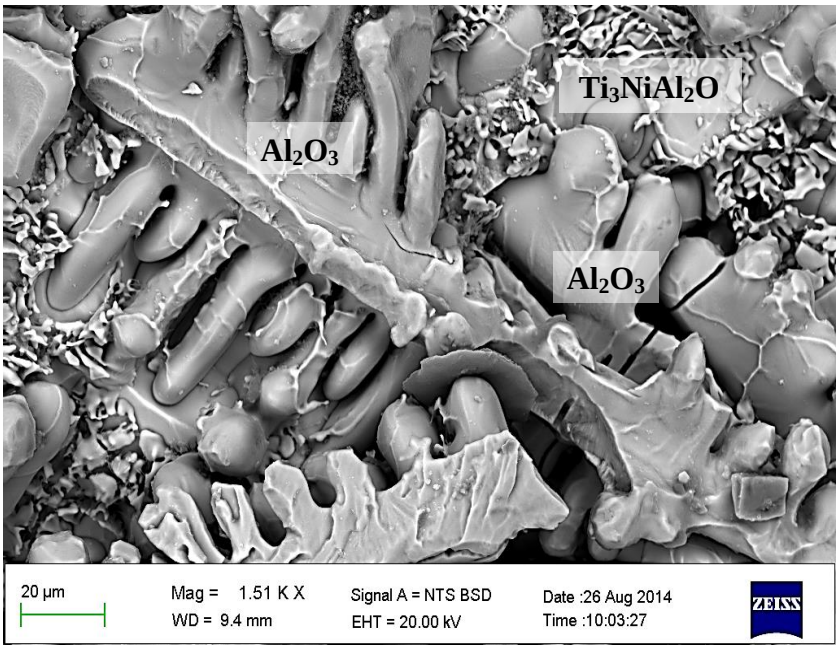

Figure 4.36: SEM-SE image of the corroded surface of alloy TAN+Ru in 5 wt% HCl, showing the Al_2O_3 and Ti_3NiAl_2O scales.

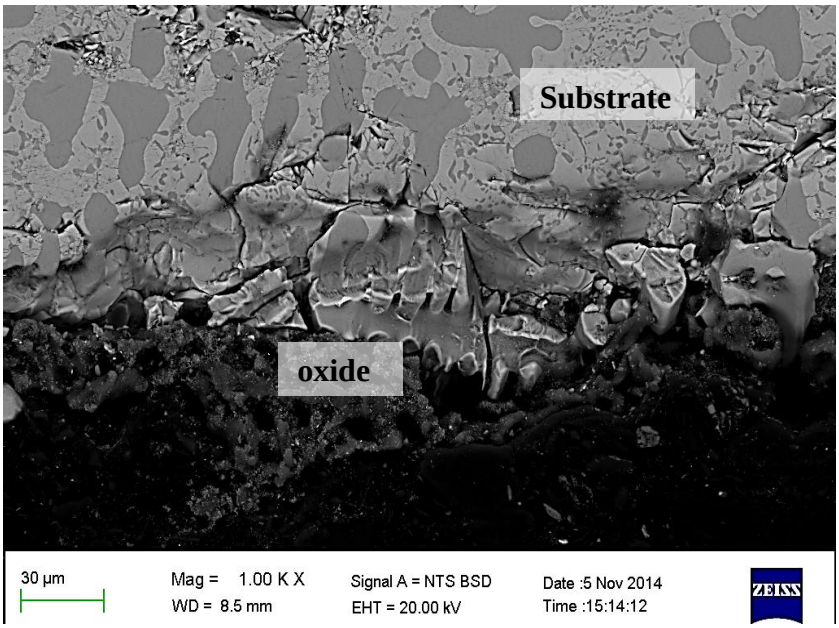

Figure 4.37: SEM-BSE image of a cross-section of corroded TAN+Ru alloy in 5 wt% HCl, showing a substrate with extensive cracks, a dendrite falling out and an unstable oxide layer.

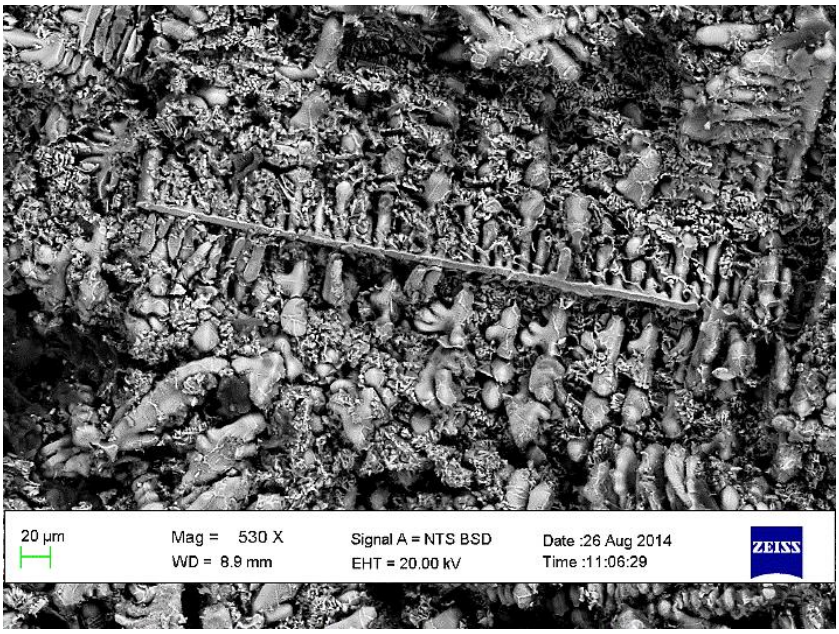

a) SEM-SE image of TAN+Ru (530x) after exposure to 25 wt% HCl.

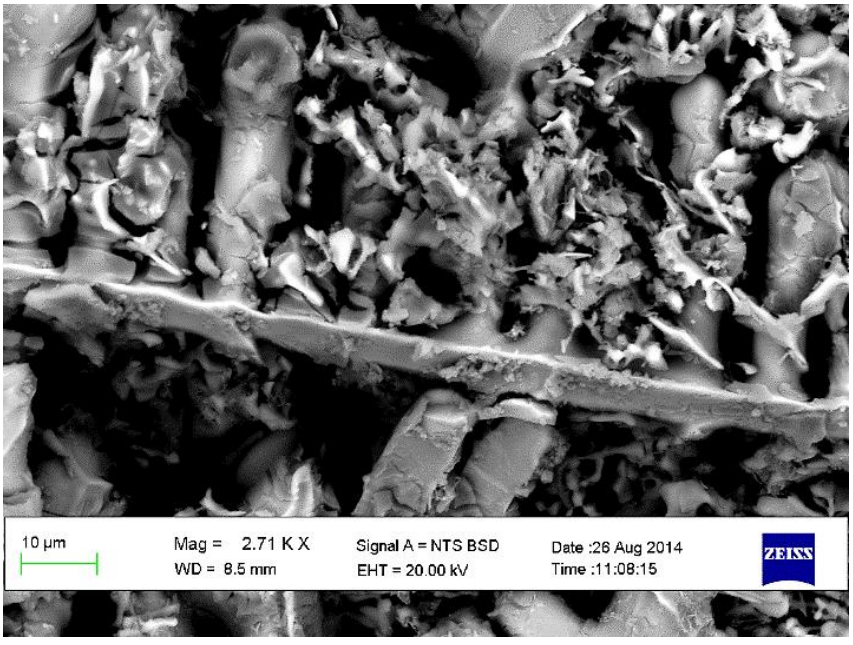

b) SEM-SE image of TAN+Ru (2710x) after exposure to 25 wt% HCl.

Figure 4.38: SEM-SE images a) 530x and b) 2710x of the corroded surface of alloyTAN+Ru in 25 wt% HCl, showing a discontinuous and unstable oxide layer.

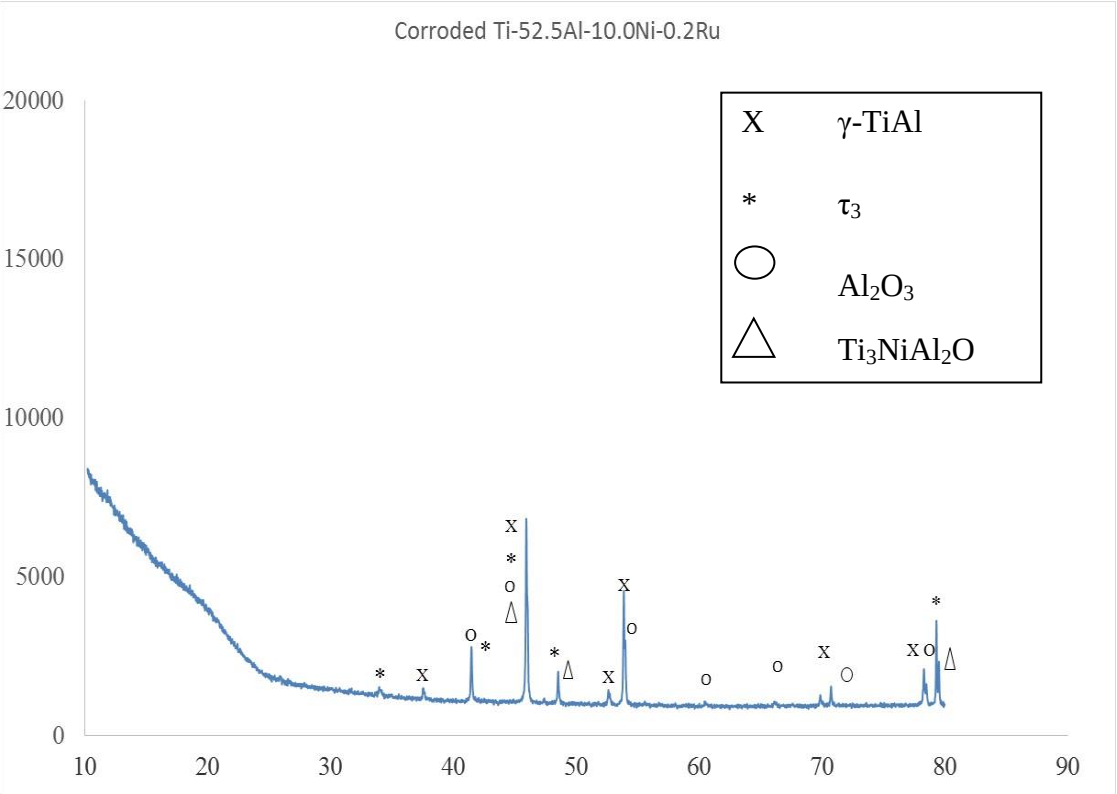

Figure 4.39: XRD pattern for TAN+Ru surface corroded in 5 wt% HCl.

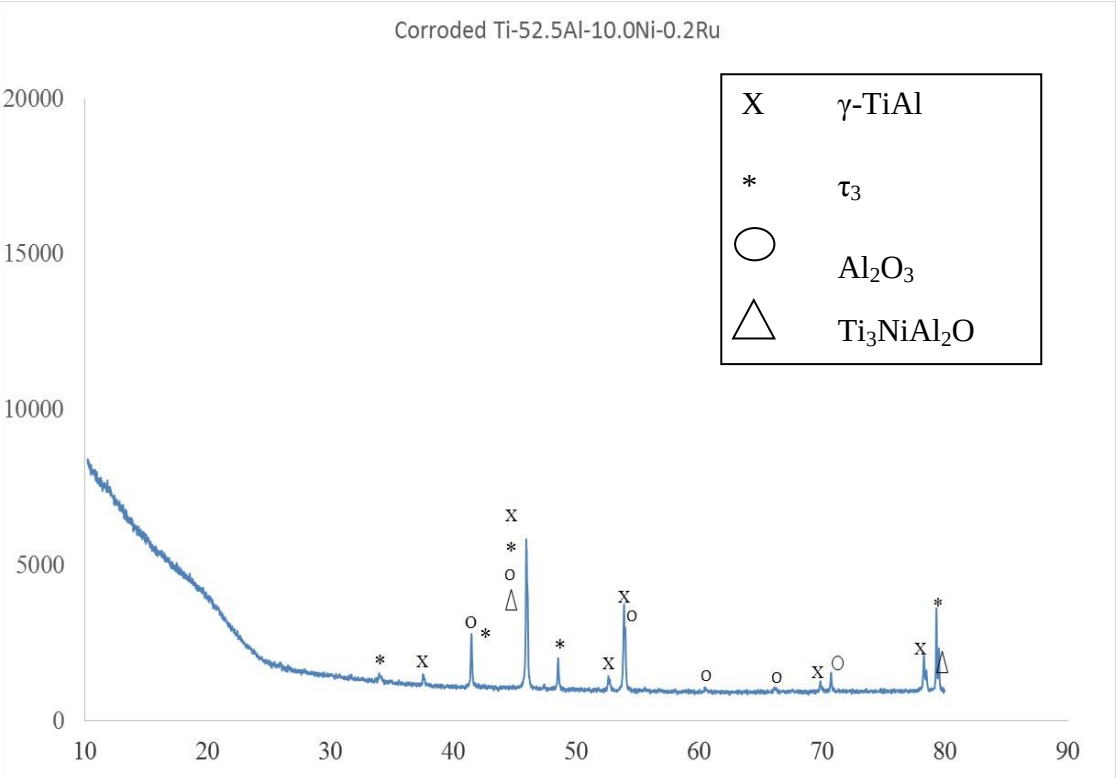

Figure 4.40: XRD pattern for TAN+Ru surface corroded in 25 wt% HCl.

4.5.3 Electrochemical results

The reproducibility of the electrochemical scans of TAN in 5 wt% HCl was good (Figure 4.41). However, the TAN+Ru alloy that solution was fairly unstable in the passive region, and the scan stopped before the transpassive region on the second run (Figure 4.42). The corrosion potential and corrosion current density of the γ-TiAl alloys TAN and TAN+Ru are shown in Table 4.14.

Table 4.14: Electrochemical characteristics of Ti-52.5Al (at.%) alloys in HCl.

Alloy	5 wt% HCl		25 wt% HCl	
	E_{corr} mV(SCE)	i_{corr} (mA.cm^{-2})	E_{corr} mV(SCE)	i_{corr} (mA.cm^{-2})
Plain γ-TiAl [2013MWA]	-677	$1.4x10^{0}$	-625	$1.0x10^{0}$
TAN	-454	$3.9x10^{-2}$	-440	$7.1x10^{-2}$
TAN+Ru	-454	$1.0x10^{-2}$	-620	$2.3x10^{-4}$

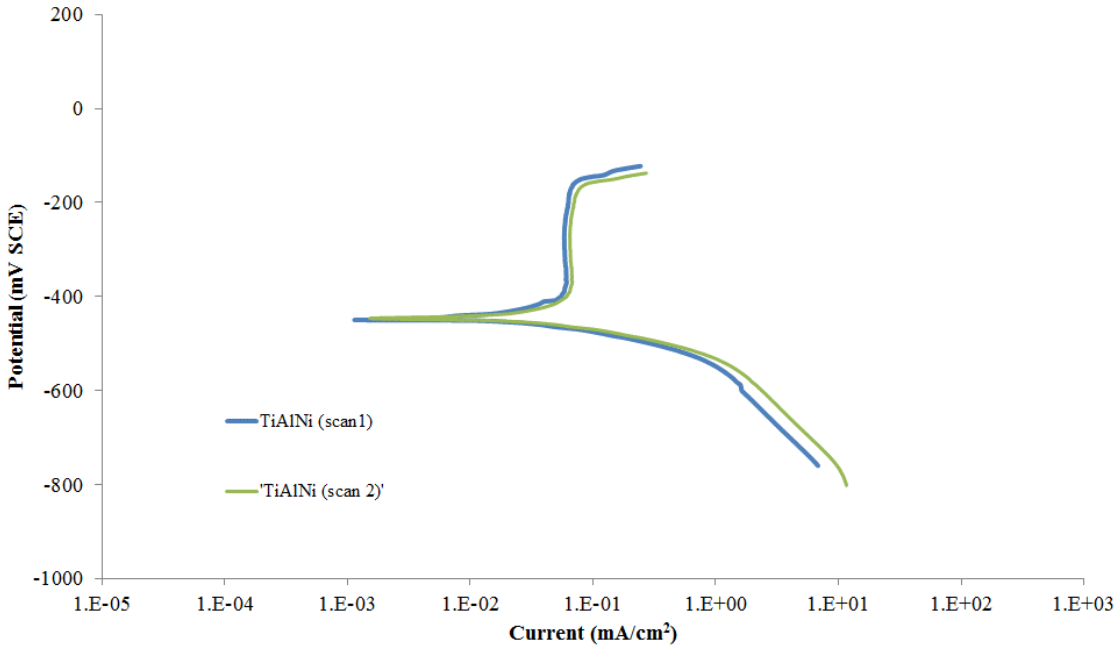

Figure 4.41: Electrochemical behavior of TAN in 5 wt% HCl.

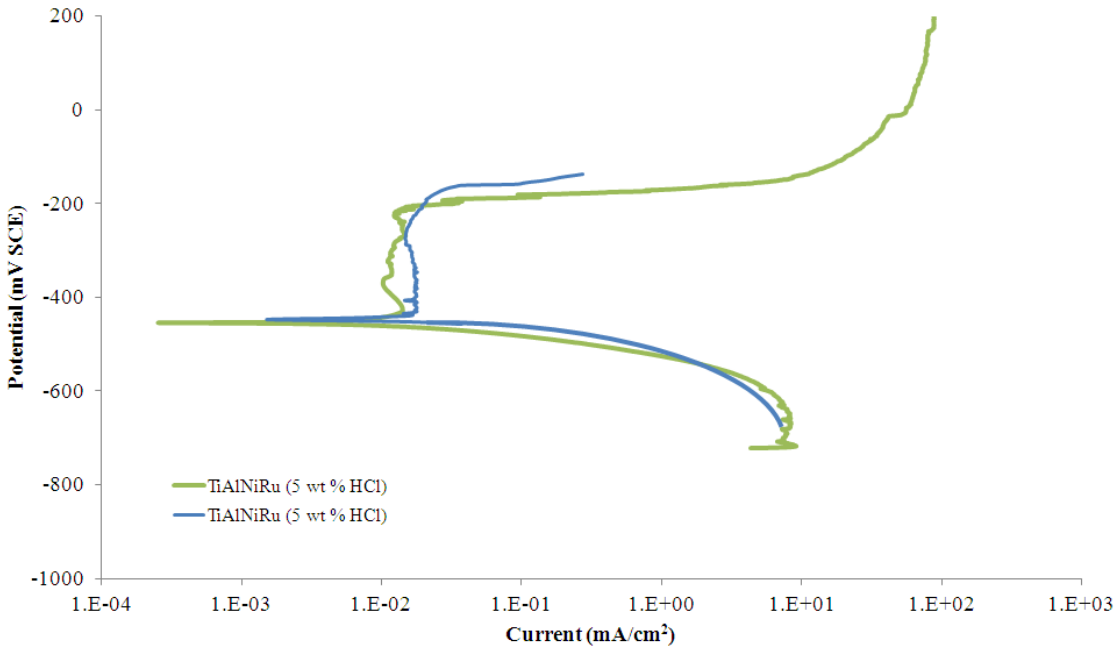

Figure 4.42: Electrochemical behaviour of TAN+Ru in 5 wt% HCl.

In 5 wt% HCl (Figure 4.43), the TAN alloy had a passive region from -400 mV (SCE) to -180 mV (SCE). The TAN+Ru alloy had unstable passivation, indicated by the irregular potentiodynamic curve, from -380 mV(SCE) to -220 mV(SCE). The addition of nickel and ruthenium decreased the corrosion current density and increased the corrosion potential (Table 4.14).

In 25 wt% HCl (Figure 4.44), there was no passive region in the scan of plain Ti-52.5Al (at.%) [2013Mwa], indicating that it would be difficult to cathodically modify by alloying with nickel and ruthenium. The addition of nickel decreased the corrosion current density and increased the corrosion potential of plain Ti-52.5Al (at.%) (Table 4.14). The addition of nickel and ruthenium decreased the corrosion current density and the corrosion potential remained the same. The TAN+Ru alloy had an irregular scan with more than one corrosion potential.

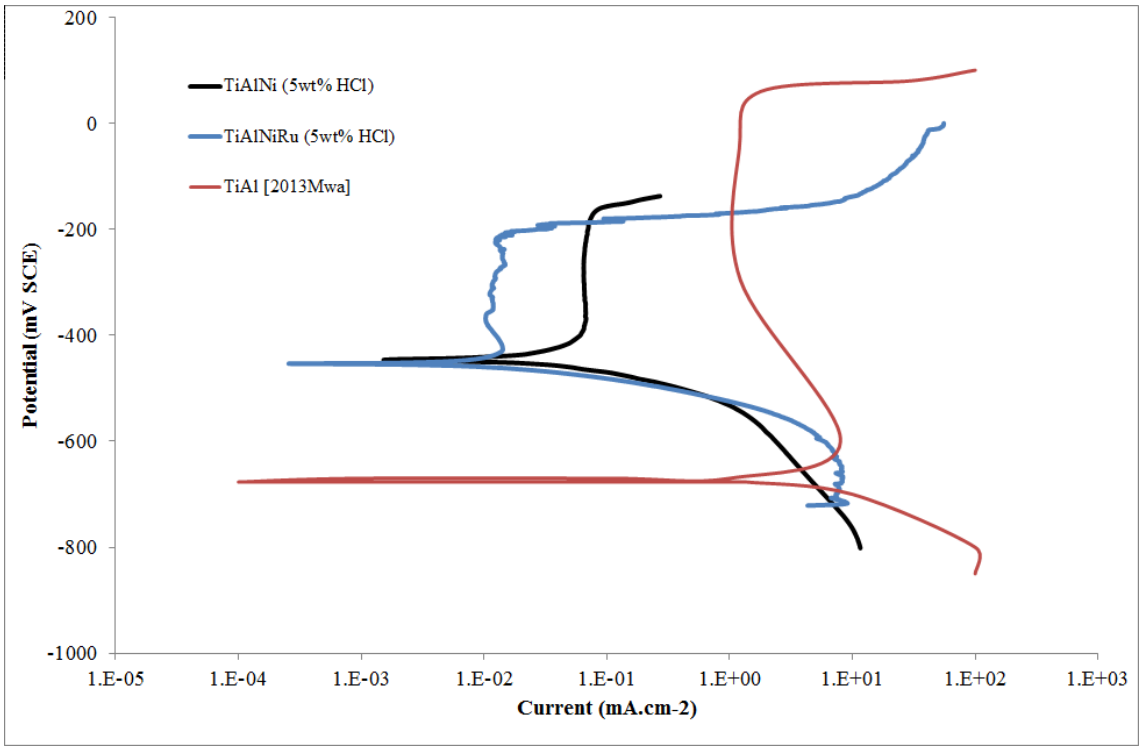

Figure 4.43: Potentiodynamic scans for plain Ti-52.5Al (at.%) [2013Mwa], TAN and TAN+Ru in 5 wt% HCl.

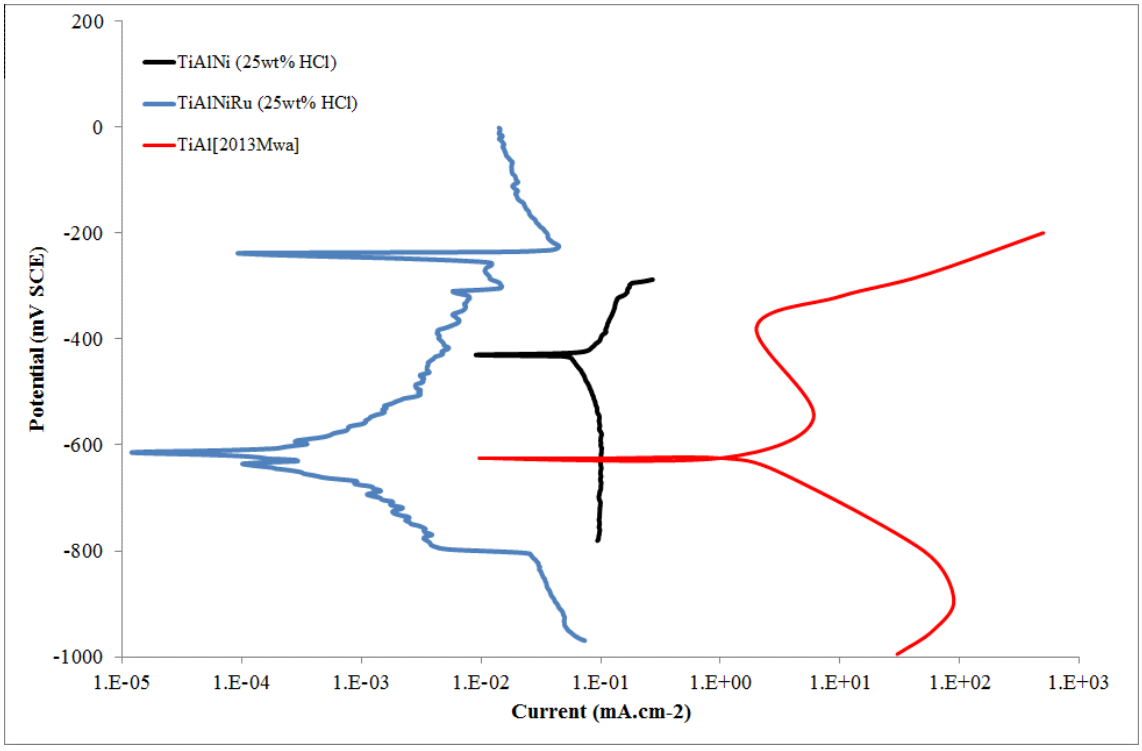

Figure 4.44: Potentiodynamic scans for plain Ti-52.5Al (at.%) [2013Mwa], TAN and TAN+Ru in 25 wt% HCl.

CHAPTER 5: DISCUSSION

5.1 Microstructure and morphology

Mixing pure elemental powders of titanium, aluminium, nickel and ruthenium resulted in the targeted alloy compositions for Ti-52.5Al-10.0Ni (TAN) and Ti-52.5Al-10.0Ni-0.2Ru (TAN+Ru) in at.%, with nickel and ruthenium in the two binary phases. The as-cast microstructures was composed of primary γ-TiAl dendrites and a γ-TiAl + Ti_2NiAl_3 (τ_3) eutectic. This is not in agreement with the isothermal section at 1000°C of the Ti-Al-Ni system (Figure 5.1 [2007Sch]), which shows a three-phase field of TiAl, $TiAl_2$ and Ti_2NiAl_3 (τ_3) phases at 1000°C, although the alloy composition is near to the two-phase region between TiAl and Ti_2NiAl_3 (τ_3).

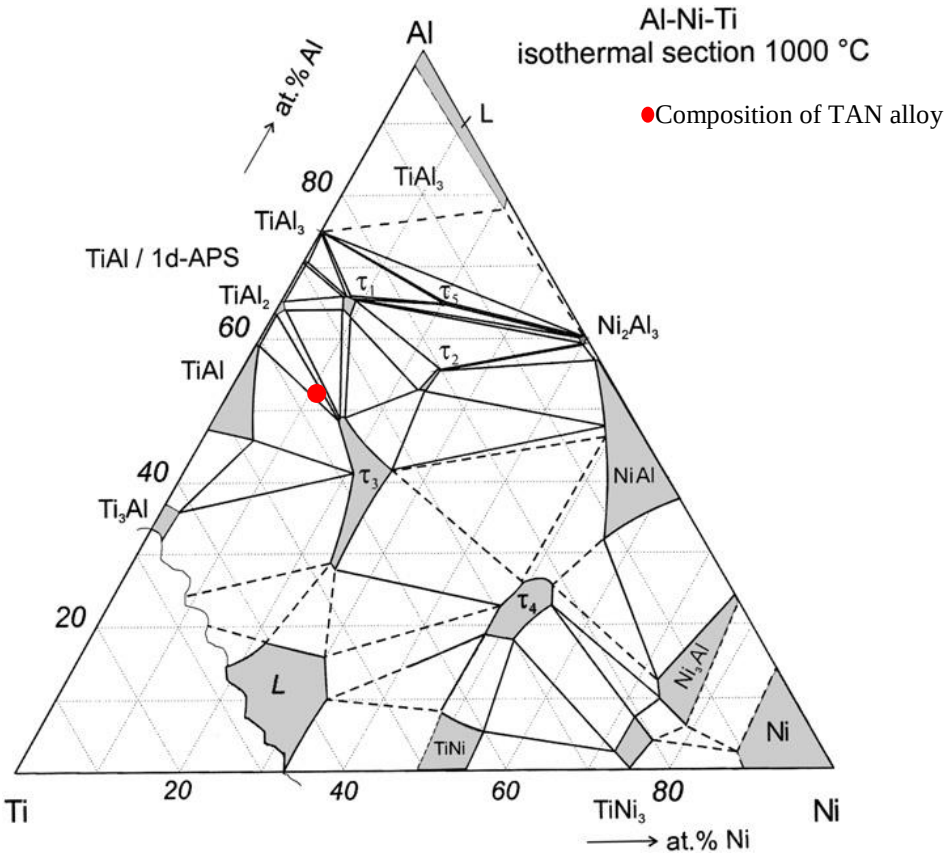

Figure 5.1: Isothermal section of Ti-Al-Ni at 1000°C [2007Sch], showing the composition of the TAN alloy.

However, the γ-TiAl is wider at the solidification temperatures in the Ti-Al binary phase diagram (Figure 2.10 [2008Wit]), so this would be expected in the ternary as well. Thus, it is likely that if the alloy composition were plotted on a higher temperature isothermal section than 1000°C, it would probably lie in the γ-TiAl and τ_3 phase field.

The TAN+Ru alloy had a low ruthenium content, and did not form any additional phases to the alloy without ruthenium. This confirms the isothermal section at 950°C of the Ti-Al-Ru system (Figure 5.2 [1989Kha]), even though the alloy composition was on the (dotted) phase boundary between γ-TiAl and the γ-TiAl + τ phase fields. It should be noted that no samples were shown in this region [1989Kha], and so the boundaries were shown as dotted lines.

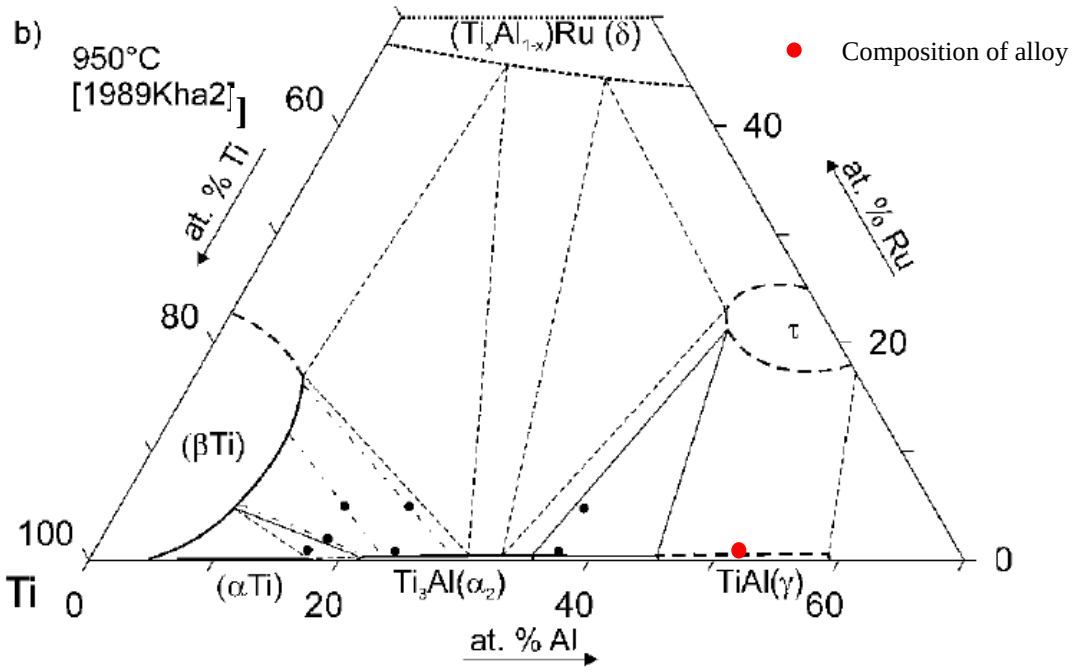

Figure 5.2: Isothermal section of Ti-Al-Ru at 950°C [1989Kha], showing the composition of Ti-52.5Al-0.2Ru (at.%).

5.3 Hardness evaluation

The TAN and TAN+Ru alloys were brittle at room temperature in the as-cast and annealed conditions and after oxidation. They had mechanical defects, such as cracks, in their microstructures which propagated in the eutectic, and pores. Also, the alloys would break during experiments (such as metallographic preparation, hardness tests and

after oxidation tests) at room temperature. This is consistent with plain γ-TiAl alloys having little or no ductility at room temperature (Figure 5.3 [1989Kim]). The ductility of γ-TiAl is influenced by the lattice tetragonality (*c/a*) (Figure 2.12 [1989Kim]). An increase in Al content increased tetragonality and decreased ductility (room temperature elongation)[1989Kim],as shown in Figure 5.3.

The hardness of as-cast, duplex (α_2 + γ) Ti-47.5Al (at.%) alloy was 281 ± 23 HV_{10} [2012Mwa]. This was in agreement with what was found by Kim [1989Kim] that as-cast, duplex Ti-47.5Al (at.%) alloy had a hardness of ~280 HV (Figure 5.3). The alloys produced in this work had much higher hardness values of 579 ± 15 HV_{10} for as-cast TAN and 561 ± 17 HV_{10} for as-cast TAN+Ru. Thus, the higher Al content (52.5 at.%) and possibly alloying with nickel and ruthenium significantly increased the room temperature hardness of TiAl alloys.

According to Kim [1989Kim], the hardness of as-cast γ-TiAl was ~200 HV (Figures 5.3 and 5.4). Oxidation of the γ-TiAl alloy at 1000°C significantly decreased the hardness to ~100 HV. In this work the as-cast TAN and TAN+Ru alloys had a much higher hardness, and oxidation caused a decrease in hardness in both alloys. After the most aggressive oxidation treatment, cyclic oxidation for 120 hours, the hardness of TAN and TAN+Ru (at.%) dropped to 369 ± 12 HV_{10} and 376 ± 15 HV_{10} respectively.

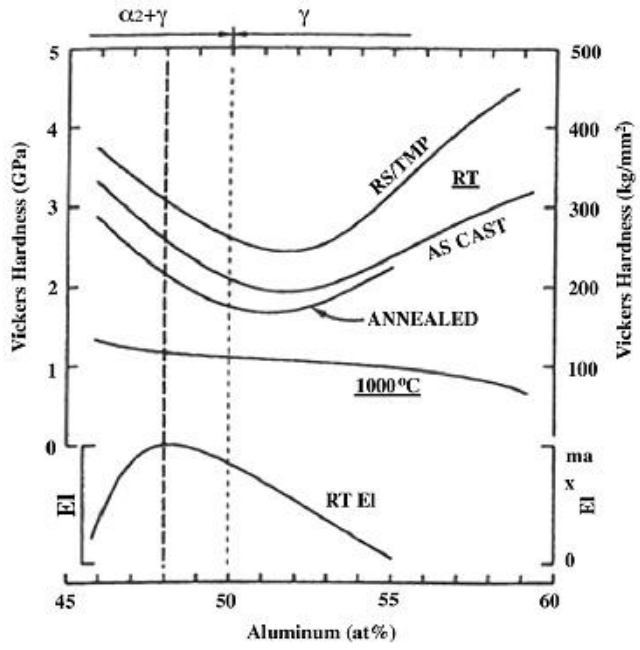

Figure 5.3: Elongation (EL) and Vickers hardness of Ti-Al dual phase (α_2 + γ) and single phase (γ) alloys at room temperature (RT) and 1000°C [1989Kim].

Heat treatment generally decreased the hardness of the alloys (Figure 5.4). The TAN and TAN+Ru alloys had a much higher hardness than the plain Ti-52.5Al (at.%) [1989Kim] and duplex Ti-47.5Al (at.%) [2012Mwa].

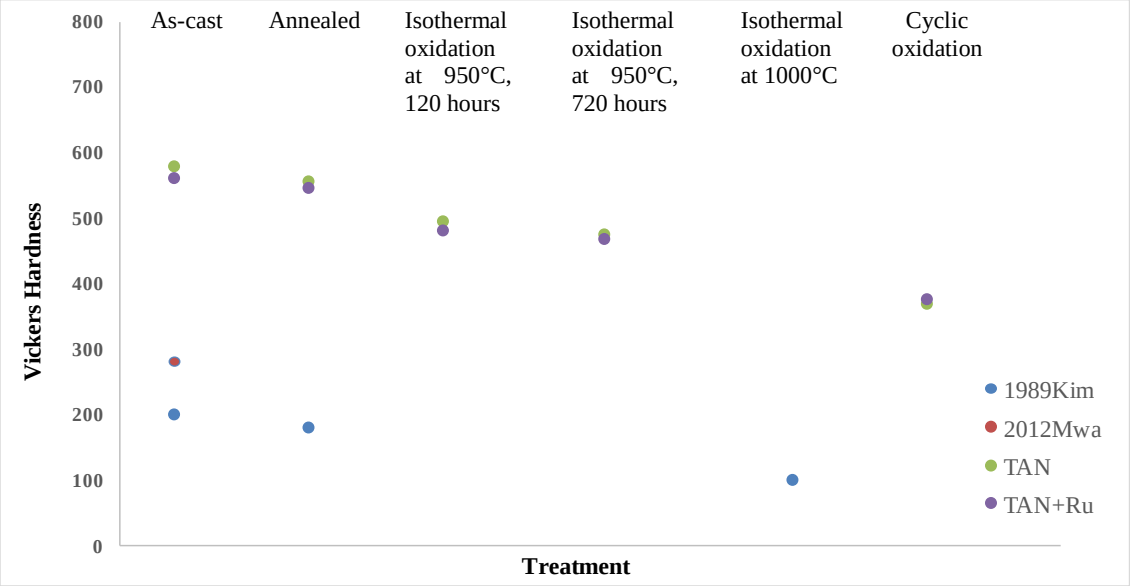

Figure 5.4: Effect of heat treatment on the hardness of alloys Ti-47.5Al (at.%) [2012Mwa], plain Ti-52.5Al (at.%) [1989Kim], TAN and TAN+Ru.

Like most titanium aluminides, the alloys were quite brittle at room temperature with cracks propagating in the eutectic. Annealing the alloys at 1050°C for 120 hours slightly coarsened the eutectic, and dendrites were still present. The annealed alloys had extensive cracks and pores.

Isothermal oxidation in air at 950°C decreased the hardness of both alloys. Oxidation for 120 hours and 720 hours decreased the hardness of the TAN alloy by 15% and 18% respectively. Oxidation for 120 hours and 720 hours decreased the hardness of the TAN+Ru alloy by 14% and 16% respectively. Therefore, a longer exposure time was slightly more detrimental to the hardness of both alloys. Cyclic oxidation, a more aggressive oxidation mechanism, which best simulates service conditions, was even more detrimental to the hardness of the alloys, causing a 36% decrease in the hardness of the TAN alloy and a 32% decrease in the hardness of the TAN+Ru alloy.

The microstructures of both alloys had a substrate of γ-TiAl a eutectic of γ-TiAl + Ti_2NiAl_3 (τ_3) and TiO_2 and Al_2O_3 scales on the surfaces. The TiO_2 scale formed on the

eutectic and the Al_2O_3 scale formed on the γ-TiAl dendrites. Severe cracks propagated in the eutectic. The scale also had extensive cracks and pores and had delaminated in some areas, especially at longer oxidation times. The scale protected the alloys at shorter oxidation times, although at longer exposure times and under cyclic oxidation, the cracks appeared to act as sites of oxidation.

After oxidation, the TAN+Ru alloy had a lower hardness than the TAN alloys, except under cyclic oxidation. The TAN+Ru alloy formed an intermittent sub-surface zone with a composition similar to that of τ_4 phase in the isothermal Al-Ni-Ti phase diagram (Figure 5.1 [2007Sch]), which could explain why the hardness of TAN+Ru was slightly higher than that of TAN. This was not found on any other samples.

5.3 Oxidation behaviour at 950°C

Both alloys readily oxidised when exposed to air and had a significantly lower mass gain (less than 2%) compared to that of a plain, duplex Ti-47.5Al (at.%) alloy, which showed a mass gain of 36.1% [2012Mwa]. The higher aluminium content and the effect of nickel and ruthenium could be the reasons for the improved oxidation resistance. The heat treated alloys had a slightly higher mass gain than the as-cast alloys, which may be from slight oxidation caused by trace amounts of oxygen in the argon atmosphere.

The TAN and TAN+Ru alloys showed good oxidation resistance in air at 950°C. They formed TiO_2 and Al_2O_3 scales which sufficiently protected the underlying substrate, even after 120 hours of exposure to hot air. For TiO_2, this is not in agreement with the isothermal section of Ti-Al-O (Figure 5.5), which shows that Al_2O_3 more stable and in equilibrium with most phases, although the section (Figure 5.5) was for a low oxygen partial pressure (~3.98×10^{-37}). The experiments were done at much higher oxygen partial pressure, and also there was nickel in the alloy, both of which would change the conditions.

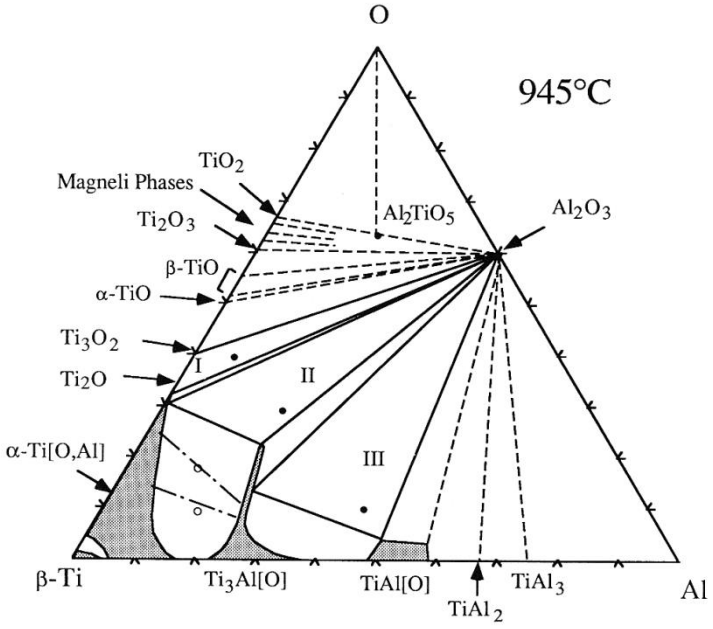

Figure 5.5: Isothermal section at 945°C of Ti-Al-O system at ~3.98 x 10^{-37} oxygen partial pressure [1995Kel].

Also, the DSC curves of the alloys displayed phase transformations between 550°C and 750°C [1993Mei, 1996Bra] (Figure 4.10), which were attributed to the formation of the oxide scales TiO_2 and Al_2O_3 respectively. After 720 hours exposure, oxidation resistance of the alloys decreased. Longer exposure times degraded the oxide scales and on cooling, the scale exfoliated from the substrate.

Ideally, the alloys should form a stable, continuous and protective Al_2O_3 scale on the surface, especially under cyclic oxidation conditions. The scale formed on these alloys was unstable; it started peeling off in some areas and was non-continuous. It consisted of TiO_2 and Al_2O_3, where TiO_2 covered the eutectic and Al_2O_3 covered the dendrites, because the dendrites had a higher Al content (55.6 ± 0.8 at.%) than the eutectic (49.9 ± 0.5 at.%). Therefore, the TAN and TAN+Ru alloys behaved in the same manner as pure γ-TiAl alloys (>52 at.% Al) which form a non-continuous, intermixed TiO_2/Al_2O_3 scale in air [1993Mei, 1996Bra, 1996Tan, 2011App]. As the thermodynamic stability of TiO_2 and Al_2O_3 is similar (Figure 2.22 [2011App]), it is difficult to form Al_2O_3 without forming TiO_2. The presence of TiO_2 in the scale is detrimental, because the diffusion of oxygen is much faster through TiO_2 than through Al_2O_3 [1996Bra, 1996Tan].

The aluminium content in the TAN and TAN+Ru alloys was not high enough for the alloys to form a stable and continuous Al_2O_3 scale. The cracks in the scale and microstructure acted as diffusion paths for oxygen, leading to internal oxidation of the alloys. However, the alloys showed very little internal oxidation, even under cyclic conditions.

Cyclic oxidation of the TAN alloy in hot salt for 120 hours was more aggressive than isothermal oxidation. After 120 hours exposure, the alloy exhibited break-away oxidation where the oxide layer was degraded and had exfoliated. This resulted in extensive metal loss. The alloy also exhibited internal oxidation. The thermal cycling of the alloy from room temperature to 950°C caused the more aggressive conditions in cyclic oxidation. The thermal cycling went through the scale nucleation temperature range of 550°C - 750°C [1993Mei, 1996Bra] and the thermal expansion mismatch between the scale (~5.1 x 10^{-6}/K) [1996Aue] and substrate (~11.8 x 10^{-6}/K) [2011App] generated more stresses in the alloy and resulted in scale degradation and exfoliation.

The TAN+Ru alloy showed better oxidation resistance than TAN, especially in a hot salt environment. The scale on the TAN+Ru alloy was more adherent to the substrate than the scale on the TAN alloy. The presence of ruthenium possibly improved the oxidation resistance of the TAN+Ru alloy. Also, the TAN+Ru alloy formed an intermittent sub-surface zone (Table 4.11) with a composition similar to that of τ_4 phase in the isothermal Al-Ni-Ti phase diagram (Figure 5.1 [2007Sch]). The sub-surface layer may have acted as a barrier between the substrate and oxide scale. The presence of this layer could have retarded the oxidation rate in the TAN+Ru alloy. Figure 5.6 illustrates a possible oxidation mechanism for the TAN+Ru alloy.

Initially a thin and outward-growing TiO_2 scale formed on the surface of the alloy. As oxidation time increased, an inward growing Al_2O_3/TiO_2 scale formed underneath the TiO_2 scale. A nickel-rich sub-surface zone then formed between the intermixed Al_2O_3/TiO_2 scale and substrate. As oxidation time increased, the sub-surface zone degraded, the oxide layer exfoliated and break-away oxidation occurred.

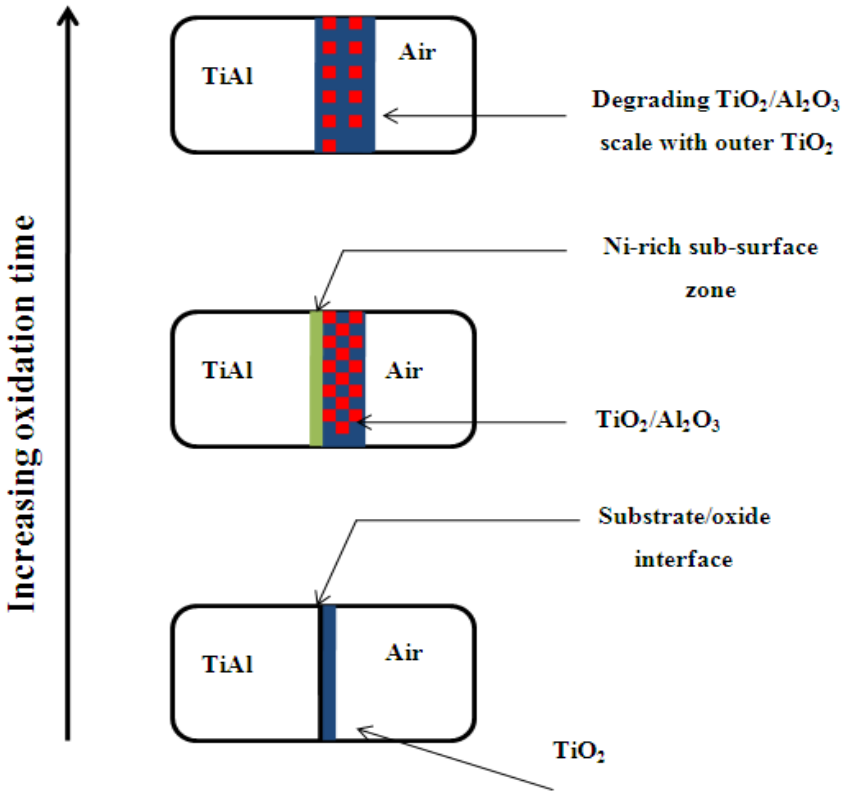

Figure 5.6: Proposed mechanism of oxidation for TAN+Ru in air.

The TAN+Ru alloy had good oxidation kinetics in hot salt and air. In the first ~25 hours of exposure (Figure 4.29), it displayed stage A oxidation kinetics characterised by a low mass increase (Figure 2.23 [2011App]) and the growth of a protective oxide Al_2O_3. At exposure times >25 hours (Figure 4.29), stage B oxidation, where the protective Al_2O_3 scale broke down and a mixed TiO_2 + Al_2O_3 scale formed. The TAN+Ru alloy had parabolic oxidation kinetics under cyclic oxidation conditions, further indicating the good oxidation resistance of the alloy.

The TAN alloy had good oxidation resistance with similar oxidation kinetics to the TAN+Ru alloy in air at 950°C (Figure 4.29). However, in hot salt, the TAN alloy had linear oxidation kinetics and formed non-protective oxides. The alloy had stage C oxidation kinetics, characterised by break-away oxidation where the Al_2O_3 scale breaks down and the non-protective TiO_2 scale forms [2011App].

5.5 Corrosion behaviour in HCl

In dilute 5 wt% HCl (Figure 4.43) and concentrated 25 wt% HCl (Figure 4.44), the addition of nickel to Ti-52.5Al (at.%) improved the corrosion resistance of the alloy by increasing the corrosion potential to more noble values and decreasing the corrosion current density. However, the improvement in corrosion resistance was not by cathodic modification since the corrosion potential of TAN was below the passive region (-296 mV (SCE) to -48 mV (SCE) [2013Mwa] of plain γ-TiAl.

The addition of ruthenium shifted the cathodic process to the active region of TAN (Figures 4.43 and 4.44) and resulted in alloy dissolution. The passivation potential of TAN was not sufficiently negative to allow the ruthenium to change the corrosion potential to a value within its passive range. Therefore, the addition of ruthenium did not cathodically modify the TAN alloy. The ruthenium concentration was possibly too low to cathodically modify the TAN alloy because an addition of 1 at.% ruthenium to Ti-47.5Al (at.%) has been shown to produce a corrosion resistant alloy [2013Mwa].

In both alloys, HCl mainly corroded the τ_3 phase and hence also the eutectic. This exposed the γ-TiAl dendrites, and some fell out (Figure 4.33 and 4.36). The severe cracks in the eutectic possibly acted as paths for corrosion. As most of the ruthenium was present in the eutectic, it did not provide corrosion protection there.

The presence of ruthenium in alloy TAN+Ru was beneficial in promoting a more adherent scale. Even though the TAN+Ru was exposed to higher potentials in the corrosion tests, its scale had better adherence to the substrate than the scale on the TAN alloy, which had disappeared. The presence of voids at the scale/substrate interface affects oxide scale spallation [1974Nas]. Large numbers of voids can act as stress concentration sites and cause the oxide scale to exfoliate from the substrate [1974Nas]. Ruthenium possibly retarded the formation of voids at the scale/substrate interface, and thus improved the oxide scale adherence.

In 25 wt% HCl, the passive region of plain γ-TiAl [2013Mwa] and TAN was non-existent, indicating that it would be hard to cathodically modify the alloys. The acid mainly corroded the τ_3 phase, thus attacking the eutectic and leaving the γ-TiAl dendrites exposed, and some fell out (Figures 4.38). As time progressed, the γ-TiAl dendrites were also corroded, resulting in alloy dissolution.

The electrochemical scans of TAN+Ru were fairly unstable in 5 wt% HCl. This behavior of the Ru-containing alloy was attributed to the non-continuous and unstable oxide layer which was exfoliating.

Thus, there was no synergistic effect of nickel and ruthenium for the Ti-52.5Al (at.%) alloy. In 5 wt% HCl, the addition of ruthenium did not improve the corrosion resistance of the alloy and in 25 wt% HCl, the corrosion potential was less noble. The results may have been better had more ruthenium been added, as in Mwamba et al. [2013Mwa], but then the alloys would also become more costly.

CHAPTER 6: CONCLUSIONS

1. Both γ-TiAl alloys TAN and TAN+Ru formed a two-phase microstructure consisting of γ-TiAl dendrites in a eutectic of γ-TiAl + Ti_2NiAl_3(τ_3). The alloys were brittle at room temperature and had extensive cracks in their microstructure which propagated in the eutectic.

2. The alloys formed TiO_2 and Al_2O_3 scales on their surfaces, when exposed to typical conditions found in aerospace engines. The scale layer was protective, yet unstable, even at short exposure times (120 hours) and was more adherent in the TAN+Ru alloy than the TAN alloy. At longer exposure times (720 hours) and under cyclic conditions, the scale exfoliated, leaving the alloys exposed to oxidation.

3. The addition of nickel and ruthenium to the alloy Ti-52.5Al (at.%) increased the hardness of the alloy. High temperature oxidation of TAN and TAN+Ru reduced the hardness of the alloys.

4. The higher aluminium content, and the presence of nickel and ruthenium improved the oxidation resistance of the alloys. The TAN and TAN+Ru alloys has a mass gain of less than 2% compared to the Ti-47.5Al (at.%) alloy, which showed a mass gain of 36.1% [2012Mwa]. Even at longer isothermal exposure times, the TAN and TAN+Ru alloys had a better oxidation resistance than the Ti-47.5Al (at.%) alloy.

5. In the reducing 5% and 25 wt% HCl environments, both the TAN and TAN+Ru alloys formed Al_2O_3 and Ti_3NiAl_2O non-continuous scales. The alumina scale formed on the γ-TiAl dendrites, while Ti_3NiAl_2O was associated with the γ-TiAl + Ti_2NiAl_3 eutectic. The scales were unstable and partially exfoliated, thus compromising the long-term protection of the alloys.

6. Both the TAN and TAN+Ru alloys had a much lower critical current density (i_{crit}) at 5% and 25 wt% HCl than the Ti-47.%Al (at.%) alloys indicating that they would be more easily passivated. The TAN alloy had a slightly higher i_{corr} at 25 wt% than at 5 wt% indicating that the alloy would be less corrosion resistant at a lower pH environments. The TAN+Ru alloy had a much lower i_{corr} at 25 wt% than at 5 wt%

indicating that the alloy would be more corrosion resistant at lower pH environments.

7. Adding nickel to the Ti-52.5Al (at.%) alloy improved corrosion resistance in a reducing environment (5 wt% and 25 wt% HCl), but not by cathodic modification. Adding ruthenium to the TAN alloy did not improve corrosion resistance in a reducing environment. Thus, for the low-Ru additions of 0.2 at.%, there was no synergistic effect of nickel and ruthenium on Ti-52.5Al (at.%).

8. In general, the addition of nickel to the Ti-52.5Al (at.%) improved the oxidation and corrosion behavior of the alloy, but the alloys were too brittle to be considered for aerospace and automobile applications.

CHAPTER 7: RECOMMENDATIONS

1. A different manufacturing method (such as mechanical alloying, investment casting or powder metallurgy) should be used for these Ni and Ni+Ru TiAl alloys, to determine if cracks and pores can be minimised.

2. Thermo-mechanical treatments could be used to produce a range of microstructures similar to those of dual phase ($\alpha + \gamma$)-TiAl alloys. The aim should be to produce a homogeneous microstructure with a finer grain size [2012Kot].

3. The heat treatment used was inadequate since the alloys had mechanical defects such as cracks in the microstructure. A better annealing/homogenisation treatment should be designed for the alloys *e.g.* the alloys should possibly be heat treated in the range ~1200- 1250°C for 24 -72 hours to form a finer, equiaxed and more stable microstructure.

4. The ductility of the alloys could be improved by optimising the alloy composition. Elements such as Cr, Mn and V could be added to improve the room temperature ductility. These three elements are abundantly available in South Africa, so it would be beneficial to the economy to find additional, value-adding, downstream use for these elements.

5. The heat treated alloys had a higher mass gain than the as-cast alloys which could be from their slight oxidation during heat treatment in an argon atmosphere. The heat treated alloys have a curious hump between 550°C - 750°C, which could be the formation of an oxide film. More investigation is required on what occurs at this temperature range.

REFERENCES

[1911Mon] Monnartz, P. (1911) Iron-chromium Alloys with Special Consideration of Resistance to Acids, Metallurgie (Halle), **8**(7), 161 - 176.

[1948Tom] Tomashov, N.D., Sinelschtschikova, G.P. and Vedineeva, M.A. (1948) Ber. Akad. D. Wissenschaft (Moscow 1962) Bd. I, **105**, 1125 - 1133.

[1951Hal] Hall, E.O. (1951) The Deformation of Ageing of Mild Steel: Discussion of Results, Proc. Phys. Soc., London, **64**, 747 - 753.

[1959Ste] Stern, M. and Wissenberg, H. (1959) The Influence of Noble Metal Alloy Additions on the Electrochemical and Corrosion Behaviour of Titanium, J. of the Electrochem.Soc., **106**(9), 759 - 764.

[1961Gre] Greene, N.D., Bishop, C.R. and Stern, M. (1961). J. Electrochem Soc., **108**, 836 - 841.

[1962Kub] Kubaschawski, O. and Hopkins, B.E. (1962) Oxidation of Metals and Alloys, Butterworths, 2nd Ed., London.

[1965Hau] Hauffe, K. (1965) Oxidation of Metals, Plenum Press, New York, USA.

[1970Woo] Wood, G.C. (1970) High Temperature Oxidation of Metals, Oxidation of Metals, **2**(1), 11 - 57.

[1971Den] Denaro, A.R. (1971) Elementary Electrochemistry, Butterworths and Co. Publishers, 2nd Edition, London.

[1971Uhl] Uhlig, H.H. (1971) Corrosion and Corrosion Control: An Introduction to Corrosion Science and Engineering, John Wiley and Sons Inc., 2nd Edition, New Jersey, USA.

[1973Wes] West, J.M. (1973) Basic Electrochemistry, Van Nostrand – Reinhold Co., London and New York.

[1974Gig] Giggins, C.S., Kear, B.H., Pettit, F.S. and Tien, J.K. (1974) Factors Affecting Adhesion of Oxide Scales on Alloys, Met. Transactions, **5**(7), 1685 - 1688.

[1974Law] Lawless, K.R. (1974) Oxidation of Metals, Progress in Physics, **39**, 231 - 316.

[1974Nas] Kumar, A.,Nasrallah, M. And Douglas, D.L. (1974) The Effect of Yttrium and Thorium on Oxidation Behaviour of Ni-Cr-Al alloys, NASA Contractor Report, Nasa CR-2422, 36 - 41.

[1975LIP] Lipsitt, H.A., Schectman, D. and Schafrik, R.E. (1975) The Deformation and Fracture of TiAl at Elevated Temperatures, Metallurgical and Materials Transactions, **6**, 1991 - 1996.

[1976Cho] Choudhury, N.S., Graham, H.C. and Hinze, J.W. (1976) Properties of High Temperature Alloys with Emphasis on Environmental Effects, J. of Electrochem. Soc., **48**(3), 668 - 680.

[1977Str] Streicher, M.A. (1977) Alloying Stainless Steels with the Platinum Metals, Platinum Metals Review, **21**(2), 51 - 55.

[1979Sed] Sedricks, A.J. (1979) Corrosion of Stainless Steel. John Wiley and Sons. Inc., New York, USA.

[1982Shr] Shreir, L.L. (1982) Electrochemical Principles of Corrosion: A Guide for Engineers, Great Britain Dept. of Industry, National Corrosion Service, London.

[1983Bir] Birks, N. And Meier, G.H. (1983) Introduction to High Temperature Oxidation of Metals, Edward Arnold, London.

[1983Kof] Kofstad, P. (1983) Non-stoichiometry, Diffusion and Electrical Conductivity in Binary Metal Oxides, R. Kriger Publishing Co., Florida, USA.

[1983Lum] Lumsden, J.B., Wilde, B.E. and Stocker, P.J. (1983) Effect of Palladium Additions to AISI 4130 Steel on its Sulfide Cracking Susceptibility, Scr. Metall., **17**, 971 - 974.

[1985She] Shetty, D.K., Wright, D., Mincer, P.N. and Clauer, A.H. (1985) Indentation Fracture of WC-Co Cermets, J. of Mat. Sci., **20**, 1873 - 1882.

[1985Lip] Lipsitt, H.A. (1985) Titanium Aluminides - An Overview Proceedings on High Temperature Ordered Intermetallic Alloys, Materials Research Society Symposium, **39**, 351 - 364.

[1986Fon] Fontana, M.G. (1986) Corrosion Engineering, McGraw-Hill International, 3rd Ed., Singapore.

[1986Hug] Hug, G., Loiseau, A. and Lasalmonie, A. (1986) Nature and Dissociation of the Dislocations in TiAl Deformed at Room Temperature, Philos. Mag, **54**(1), 47 - 65.

[1986Mur] Murray, J.L. (1986) Binary Alloy Phase Diagrams, ASM, Metals Park, Ohio, USA, 173 - 181.

[1987Kwa] Kawabata, T. and Izumi, O. (1987) Dislocation Structures in TiAl Single Crystals Deformed at 77K, Scr. Metall., **21**, 433 - 434.

[1988Sub] Subrahmanyam, J. (1988) Cyclic Oxidation of Aluminized TiAl Alloy, Materials Science, **23**, 1906 - 1910.

[1989Kas] Kasahara, K., Hashimoto, K., Doi, H. and Tsujimoto, T. (1989) Oxidation Behaviour of TiAl at High Temperatures, J. Japan Inst. Metals, **53**(1), 58 - 62.

[1989Kha] Khataee, H.M., Flower, H.M., and West, D.R.F. (1989) Constitution of Ti-Al-Ru System. Mater. Sci. Techno., **5**(7), 632 - 643.

[1989Kim] Kim, Y.W. (1989) Intermetallic Alloys Based on Gamma Titanium Aluminide, JOM, **41**(7), 24 - 30.

[1989McC] McCullough C., Valencial, J.J., Levi, C.G. and Mehrabian, R. (1989) Phase Equilibria and Solidification of Ti-Al alloys, Acta Metall., **37**(5), 1321 - 1336.

[1989Nis] Nishiyama, T., Toyama, K. and Yoshimitsu, T. (1989) Development of Titanium Aluminide Turbocharger Rotors, SAE Transactions, **18**, 17 - 21.

[1989Uma] Umakoshi, Y., Yamaguchi, M., Sakagami, T. and Yamane, T. (1989) Oxidation Resistance of Intermetallic Compounds, J. Mater. Sci., **24**, 1599 - 1603.

[1990Pot] Potgieter, J.H., Heyns, A.M. and Skinner, W. (1990) Cathodic Modification as a means of Improving the Corrosion Resistance of Alloys. Journal of App. Electrochem., **20**, 711 - 715.

[1990Yam] Yamaguchi, M. and Umakoshi, Y. (1990) The Deformation Behavior of Intermetallic Super lattice Compounds, Progress in Mat. Sci., **34**, 1 - 148.

[1991Kim1] Kim, Y.W. and Dimiduk, D. (1991) Progress in the Understanding of Gamma Titanium Aluminides, JOM, 40 - 47.

[1991Kim2] Kim, Y.W. (1991) Microstructural Evolution and Mechanical Properties of a Forged Gamma Titanium Alloy, Acta Met. Materialia, **40**(6), 1121 - 1133.

[1992Bec] Becker, S., Rahmel, A., Schorr, M. and Schutze, M. (1992) Mechanism of Isothermal Oxidation of TiAl Alloys, Oxid. Met., **38**, 425 - 464.

[1992Chi] Chin, S.C.E. and Biederman, R.R. (1992) The Ti-Al Phase Diagram – A Review of the Near Ti-50 at.% Al Phase Field, US Army Materials Technology Laboratory, Report number MTL TR 92-47, 1 - 13.

[1992Fro] Froes, F.H., Suryanarayana, C. and Eliezer, D. (1992) Properties and Applications of Titanium Aluminides, Journal of Materials Sci., **27**, 5113 - 5140.

[1992Jon] Jones, D.E. (1992) Principles and Prevention of Corrosion, Macmillan Publishing Co., New York.

[1992Kat] Kattner, U.R., Lin, J.C. and Chang, Y.A. (1992) Thermodynamic Assessment and Calculation of the Ti-Al System, Met. Trans., **23**(8), 2081 - 2090.

[1992Liu] Liu, C.T. and Kim, Y.W. (1992) Single Crystal-based Microstructure Design of Metal Matrix Composites, Scripta Mater., **27**, 599 - 671.

[1992Mei] Meier, G.H. and Pettit, F.S., (1992), Oxidation of $MoSi_2$ and Comparison with other Silicide Materials, Mat. Sci. and Eng., **A155**, 165 - 181.

[1993Jha] Jha, S.C. and Forster, J.A. (1993) Producing Titanium Aluminide Foils from Plasma-sprayed Preforms, JOM, **45**(7), 57 - 59.

[1993Mei] Meier, G., Petit, F. and Hu, S. (1993) Oxidation Behaviour of Titanium Aluminides, Journal de Physique, **4**(3), 395 - 402.

[1993Oka] Okamoto, H. (1993) Aluminium-Titanium, Journal of Phase Equilibria, **14**(1), 120 - 121.

[1994Boy] Boyer, R., Welsch, G. and Collins, E.W. (1994) Materials Properties Handbook, ASM International. Ohio, USA.

[1994Has] Hashimoto, K., Kimura, M. and Suyama, R. (1994) Alloy Design of Gamma Titanium Aluminide Intermetallic Compounds, Nippon Steel Technical Report, (62), 98 - 103.

[1994Kim] Kim, Y.W. (1994) Ordered Intermetallic Alloys, JOM, **46**(7), 30 - 39.

[1995Hay] Hayes F.H. (1995) The Al-Ti-V (Aluminium-Titanium-Vanadium) System, Journal of Phase Equilibria, **16**(2), 163 - 176.

[1995Imm] Immarigeon, J.P., Holt, R.T, Koul, A.K., Zhao, L., Wallace, W. and Beddoes, J.C. (1995) Light-Weight Materials for Aircraft Applications, Materials Characterization, **34**, 41 - 67.

[1995Kel] Kelkar, G.P. and Carim, A.H. (1995) Phase Equilibria in the Ti-Al-O System at 945°C and Analysis of Ti/Al_2O_3 Reactions, J. Am. Ceramic Soc., **78**(3), 572 - 573.

[1995Kim] Kim, Y.W. (1995) Gamma Titanium Aluminides: Their Status and Future, Journal of Metals, **47**(7), 39 - 41.

[1995Lam] Lamesle, P. and Steinmestz, P. (1995) Growth Mechanisms and Hot Corrosion Resistance of Palladium Modified Aluminide Coatings on Superalloys, Mater. Manufacturing Process, **10**(5), 1053 - 1075.

[1995Rah] Rahmel, A., Quadakkers, W.J. and Schutze, M. (1995) Fundamentals of TiAl Oxidation – A Critical Review, Mater. Corr., **46**, 271 - 285.

[1995Sau] Sauthoff, G. (1995), Intermetallics, Weinheim, NewYork, USA.

[1996Aue] Auerkari, P. (1996) Mechanical and Physical Properties of Engineering Alumina Ceramics, Tech. Res. Centre of Finland (VTT), 8 - 11.

[1996Bey] Beye, R., Verwerft, M., DeHosson, J.T.M. and Gronsky, R. (1996) Oxidation Sub-scale of Gamma Titanium Aluminide, Acta.Mater., **44**(10), 4225 - 4231.

[1996Bra] Brady, M.P., Brindley, W.J., Smialek, J.L. and Locci I.E. (1996) The Oxidation and Protection of Gamma Titanium Aluminides, Journal of Metals, **48**, 46 - 50.

[1996Mer] Mercer, C. and Soboyejo, W.O. (1996) Hall-Petch Relationships in Gamma Titanium Alumnides, Scripta Materialia, **35**(1), 17 - 22.

[1996Saf] Saffarian, H.M., Gan, Q., Hadkar, R. and Warren, G.W. (1996) Corrosion Behaviour of Binary Titanium Aluminide Intermetallics, Corrosion, **52**(8), 626 - 633.

[1996Hin] Hinds, G. (1996) The Electrochemistry of Corrosion, Corrosion Doctors Publications, **12**(1), 4 - 5.

[1996Sch] Schutz, R.W. (1996) Ruthenium Enhanced Titanium Alloys, Platinum Metals Review, **40**(2), 54 - 61.

[1996Tan] Shigeji, T. and Shibata, T. (1996) Influence of Additional Elements on the Oxidation Behaviour of TiAl, Intermetallics, **4**, 85 - 93.

[1996Yan] Yang, L. and McLellan, R.B. (1996) Effect of Palladium on Hydrogen Embrittlement of B-doped Ni_3Al, J. Mater. Res., **11**(4), 862 - 864.

[1997Che] Cheng, T. and McLean, M. (1997) Characterization of TiAl Intermetallic Rods Produced from Elemental Powders by Hot Extrusion Reaction Synthesis, J. Mat. Sci., **32**, 6255 - 6261.

[1997Kel] Keller, M.M., Jones, P.E., Porter, W.J. and Eylon, D. (1997) The Development of a Low Cost TiAl Automotive Valve, JOM, **49**, 42 - 44.

[1997Nic] Nicholls, J.R., Leggett, J. and Andrews, P. (1997) Hot Salt Corrosion of Titanium Aluminides, Mat. & Corr., **48**, 56 - 64.

[1997Sob] Soboyejo, W.O., Ye, F. and Srivatsan, T.S. (1997) The Fatigue and Fracture Behaviour of a Gamma-Titanium Aluminide Intermetallic, Eng. Fracture Mechanics, **56**, 379 - 395.

[1997Yam] Yamaguchi, M. and Inui, H. I. (1997) High Temperature Structure Intermetallics, Acta Mater., **48**, 307 - 322.

[1998App] Appel, F. and Wagner, R. (1998) Microstructure and Deformation of Two-phase Gamma TiAl, Mat. Sci. & Eng., **22**(5), 187 - 268.

[1998Bra] Brass, A.M. and Chene, J. (1998) Hydrogen Absorption in $\alpha_2 + \gamma$ Titanium Aluminides during Mechanical Grinding, Scripta Mater., **39**(11), 1569 - 1575.

[1998Dim] Dimiduk, D., Martin, P. and Kim, Y.W. (1998) Microstructure Development in Gamma TiAl Alloy Mill Products by Thermo-mechanical Processing, Mat. Sci. & Eng., **A243**, 66 - 76.

[1998Ton] Tonneau, A., Hennaff, G., Mabru, G. and Petit, J. (1998) Environmentally-assisted Fatigue Crack Propagation in Aluminides at Room Temperature, Scripta Mater., **39**(11), 1503 - 1508.

[1999Voi] Voice, W. (1999) The Future of Gamma-Titanium Aluminides by Rolls-Royce, Aircraft Eng. & Aerospace Tech., **71**, 337 - 340.

[2000App] Appel, F. (2000) Recent Progress in the Development of Gamma TiAl Alloys, Advanced Engineering Materials, **2**(11), 699 - 720.

[2000Cha] Chandley, D. (2000) Use of Gamma Titanium Aluminide for Automotive Engine Valves, Met. Sci. Tech., **18**(1), 8 - 11.

[2000Van] Van der Lingen, E., and Sandenbergh, R.F. (2000) The Cathodic Modification Behaviour of Ruthenium Additions to Titanium in Hydrochloric Acid, Corrosion Science, **43**(1), 577 - 590.

[2000Yam] Yamaguchi, M., Inui, H. and Ito, K. (2000) High Temperature Structual Intermetallics, Acta. Mater., **48**(1), 307 - 322.

[2002Cho] Choi, C., Kim, H.J., Lee, Y.T. and Kim, Y. (2002) Effects of Microstructural Parameters on the Fatigure Crack Growth of Fully Lamellar Gamma-TiAl alloys, Mat. Sci. and Eng., **A329 - 331**, 545 - 556.

[2003Ber] Bertin, J.J. and Cummings, R.M. (2003) Fifty Years of Hypersonics, Progress in Aero. Sci., 39, 511 - 536.

[2003Das] Das, G., Bartolotta, P.A., Kestler, H. and Clemens,H. (2003) Gamma Titanium Aluminides, TMS, Warrandale, PA, USA.

[2003Dim] Dimiduk, D., Martin, P.L. and Dutton, R. (2003) Gamma Titanium Aluminides, TMS, Warrandale, PA, USA.

[2003Chr] Chraponski, J., Szkliniarz, W., Koscielna, W. and Serek, B. (2003) Microstructure and Chemical Composition of PhasesinTi-48Al-2Cr–2NbIntermetallic Alloy, Mat. Chem. and Physics, **81**, 438 - 442.

[2003Nas] NASA Tech Briefs (2003) PM Gamma Titanium Aluminide and Fabrication Techniques, LEW-17173, NASA Glenn Research Centre Cleveland, Ohio, USA.

[2003Sun] Sun, Z. and Hitoshi, H. (2003) Fabrication of TiAl Alloys by MA-PDS Process and the Mechanical Properties, Intermetallics, **11**, 825 - 835.

[2004Bir] Bird, K. and Wallace, T.A. (2004) Development of Protective Coatings for High Temperature Metallic Materials, J. Spacecraft & Rockets, **41**, 213 - 220.

[2004Lut] Lütjering, G. and Albrecht, J. (2004) Ti-2003 Science and Technology, Wiley-VCH, Weinheim, Germany.

[2004McE] McEwan, J.J. (2004) Corrosion Control in Southern Africa, Corrosion Institute of Southern Africa, Johannesburg, South Africa.

[2004Sob] Soboyejo, W.O.,Shen, W.,Lou, J.,Mercer,C.,Sinha, V. and Soboyejo, A.B.O. (2004) Probabilistic Framework for the Modelling of Fatigue in

Cast Lamellar Gamma-based Titanium Aluminides, Mechanics of Materials, **36**, 177 - 197.

[2005Voi] Voice, W., Henderson, M., Shelton, E. and Wu, X. (2005) Gamma Titanium Aluminide TNB, Intermetallics, **13**(9), 959 - 964.

[2006Bat] Batalu, D., Cosmoleata, G. and Aloman, A. (2006) Critical Analysis of the Ti-Al Phase Diagrams, U.P.B. Sci. Bull., **68**(4), 77 - 90.

[2006Del] Delgado-Alvarado, C. and Sundaram, P.A. (2006) Corrosion Evaluation of Ti-48Al-2Cr-2Nb (at.%) in Ringer's Solution, Acta Biomaterialia, **2**, 701 - 708.

[2006Sch] Schuster, J.C. and Palm, M. (2006) Re-assessment of the Binary Ti-Al Phase Diagram, J. Phase Equil. and Diff., **27**(3), 255– 277.

[2006Sha] Sha, W. (2006) The Evolution of Microstructure during the Processing of Gamma Ti-Al Alloys, JOM, **58**, 64 - 66.

[2007Del] Delgado-Alvarado, C. and Sundaram, P.A. (2007) A Study of the Corrosion Behaviour in 3.5 wt% NaCl Solution and Seawater, Corrosion Science, **49**, 3732 - 3741.

[2007Lut] Lutjering, G. and Williams, J. (2007) Engineering Materials and Processes, Springer, Berlin, Germany.

[2007Sch] Schuster, J.C., Pau, Z., Liu, S., Weitzer, F. And Du, Y. (2007) Constitution of the Ternary System Al-Ni-Ti. Intermetallics, **15**, 1257 - 1267.

[2008Mot] Motsie, R. (2008) An Overview of South Africa's Titanium Mineral Concentrate Industry, Department of Minerals and Energy, 9 - 15.

[2008Riv] Rivera-Denizard, O., Diffoot-Carlo, N., Navas, V. and Sundaram, P.A. (2008) Biocompatibility Studies of Human Foetal Osteoblast Cells Cultured on Gamma Titanium Aluminide, J. Mater. Sci. Mater. Med., **19**(1), 153 - 158.

[2008Wit] Witusiewicz, V.T., Bondar, A.A., Hecht, U., Rex, S. and Velikanova, T. (2008) The Al-B-Nb-Ti system. III. Thermodynamic Re-evaluation of the Constituent Binary System Al–Ti, J. of Alloys & Compounds, **465**(1), 64 - 77.

[2008Zho] Zhou, L., Lin, J., Chen, G. and Wang, Y. (2008) Early Oxidation Behaviour of TiAl and Ti-45Al-8Nb Alloys, TMS, 275 - 288.

[2009Che] Chen, Y.Y., Yua, H.B., Zhang, D.L. and Chaia, L.H. (2009) Effect of Spark Plasma Sintering Temperature on Microstructure and Mechanical Properties of an Ultrafine-grained TiAl Intermetallic, Mat. Sci. & Eng., **A525**, 166 - 173.

[2009Has] Hasegawa, M. and Fukotomi, H. (2009) Lamellar Orientation Control in TiAl Base Alloys by a Two-step Compression Process at High Temperature, Mat. Sci. & Eng., **508**, 106 - 113.

[2009Ham] Jafarian, H., Saebnoori, E., Sabour-Rouhaghdam, A., Shahrabi, T. and Nili-Ahmadabadi, M. (2009) Electrochemical Corrosion of Oxidized Gamma Titanium Aluminide in Ringer's Solution, Iranian J. of Pharm. Sci. **5**(1), 51 - 54.

[2009Ika] Ikaneng, M., (2009), Overview of Nickel Industry in South Africa, Department of Minerals and Energy, 1 - 8.

[2009Sar] Sarkar S., Datta S., Das S. and Basu D. (2009) Oxidation Protection of Gamma-titanium Aluminide using Glass–ceramic Coatings, Surface & Coatings Tech., **203**, 1797 - 1805.

[2010Cha] Chaudhari, G.P. and Acoff, V.L., (2010), Titanium Aluminide Sheets Made Using Roll Bonding and Reaction Annealing, Intermetallics, **18**, 472 - 478.

[2011Ano] Anon. (2011) A Beneficiation Strategy for the Minerals Industry in South Africa, Department of Minerals and Energy, 17 - 18.

[2011App] Appel, F., Paul, J.D.H., and Oehring, M. (2011) Gamma Titanium Aluminide Alloys, Wiley-VCH, Weinheim, Germany.

[2012Kot] Kothari, K., Radhakrishnan, R. and Wereley, N.M. (2012) Advances in Gamma Titanium Aluminides and their Manufacturing Techniques, Progress in Aerospace Science, **55**(1), 1 - 16.

[2012Mwa] Mwamba, I.A., Cornish ,L.A. and van der Lingen, E. (2012) Oxidation Property Evolution of Gamma-TiAl Alloy with Addition of Precious Metals, South African Institute of Mining and Metallurgy Journal, **7A**, 517 - 526.

[2013Ano] Anon. (2013) Council for Scientific and Industrial Research Annual Report, 1 - 8.

[2013Mwa] Mwamba, I.A., Cornish, L.A. and van der Lingen, E. (2013) A Comparative Assessment of Ti-47.5 at.% Al Cathodically Modified by Precious Metal Addition, South African Institute of Mining and Metallurgy Journal, **113**, 97 - 103.

[2014Gea] GE Aviation, The GEnx Commercial Aircraft Engine, downloaded from www.geaviation.com on (October 2014).

[2014Sci] Sciencelab.com Chemicals, downloaded from www.sciencelab.com on (April 2014).

[2015Pix] Jet Engines, downloaded from www.pixgood.com on (August 2015).

APPENDIX

Conference papers from this work:

1. H.C. Mantyi, L.A. Cornish, L.H. Chown and I.A. Mwamba, Characterisation of Gamma-TiAl Alloys with Additions of Nickel and Ruthenium, Light Metals Conference, AMI, pp. 294-301, Pilanesberg, 15th – 17th October 2014. Advanced Materials Research, 1019 (2014) 294-301.

2. H.C. Mantyi, L.A. Cornish, L.H. Chown and I.A. Mwamba, High Temperature Oxidation of γ-TiAl Alloy Ti-52.5Al-10Ni-0.2Ru (at.%), 52nd Microscopy Society of Southern Africa Conference Proceedings, Volume 44, p. 67, Stellenbosch, 2nd – 5th December 2014.

3. H.C. Mantyi, L.A. Cornish, L.H. Chown and I.A. Mwamba, The Effect of Nickel and Ruthenium on the Corrosion Behavior of Gamma Titanium Aluminide Ti-52.5Al (at.%), Nuclear Materials Development Network Conference, AMI, SAIMM Symposium Series S87, pp. 103-111, NMMU, Port Elizabeth, 28th – 30th October 2015.

Advanced Materials Research Vol 1019 (2014) pp 294-301
© (2014) Trans Tech Publications, Switzerland
doi:10.4028/www.scientific.net/AMR.1019.294

Submitted: 2014-05-06
Revised: 2014-07-04
Accepted: 2014-07-05
Online: 2014-10-20

Investigating the High Temperature Oxidation Behavior of TiAl-based alloys with Nickel and Ruthenium Additions

MANTYI H.C. [1,2,a *], CORNISH L.A. [1,2,b], CHOWN L.H. [1,2,c] and MWAMBA I.A. [2,3,d]

[1]School of Chemical and Metallurgical Engineering, University of the Witwatersrand, Johannesburg

[2]DST/NRF Centre of Excellence in Strong Materials, hosted by the University of the Witwatersrand

[3]Advanced Materials Division, Randburg

[a]Hadio.Tsotetsi@students.wits.ac.za, [b]Lesley.Cornish@wits.ac.za, [c]Lesley.Chown@wits.ac.za, [d]AlainM@mintek.co.za

Keywords: Titanium aluminide, gamma-TiAl, microstructure, high temperature oxidation

Abstract. The Ti-52.5Al-10.0Ni (at.%) alloy formed dendrites of γ-TiAl (55.6 at.% Al) surrounded by a eutectic of γ-TiAl + Al_3NiTi_2 (τ_3) phases. The Ti-52.5Al-10.0Ni-0.2Ru (at.%) alloy formed dendrites of γ-TiAl (53.6 at.% Al) surrounded by a eutectic of γ-TiAl + Al_3NiTi_2 (τ_3). The ruthenium was mostly in solid solution (0.3 at.%) in the Al_3NiTi_2 (τ_3) phase, although traces of it were present in the dendrites (0.1 at.% Ru). When oxidized in air from room temperature to 1050°C, the as-cast Ti-52.5Al-10.0Ni-0.2Ru (at.%) had a mass gain of 0.60% and the as-cast Ti-52.5Al-10.0Ni (at.%) had a mass gain of 0.97%. Isothermal oxidation of both alloys at 1050°C for 120 hours formed mixed metal oxides of TiO_2+Al_2O_3 on the surface.

Introduction

The γ-TiAl phase is an ordered face-centered tetragonal phase with an $L1_0$ structure, whose homogeneity ranges from 50-57 at.% Al (Fig. 1[1]). The good thermo-physical properties of γ-TiAl, especially at elevated temperatures, has attracted much research on TiAl-based alloys. In most engineering applications, γ-TiAl always contains a small amount of the α_2-Ti_3Al phase to optimise thermo-physical properties [2]. The α_2-Ti_3Al phase has a hexagonal DO_{19} structure with a homogeneity range from 20-36 at.% Al. [1-2]. Alloys in the 36-50 at.% Al region have a duplex microstructure consisting of γ-grains and duplex lamellar grains of alternating layers of γ-TiAl and α_2-Ti_3Al [2]. The γ-TiAl alloys have high melting points, low density in the range 3.9-4g.cm^{-3}, high specific strength and elastic moduli, low diffusivity, good oxidation and corrosion resistance, good creep resistance and high burn resistance, i.e. not capable of igniting and burning when subjected to high temperatures [2].

TiAl-based alloys have a strong potential to increase the thrust-to-weight ratio in aircraft engines [3]. They can especially be used to make the engine's low pressure turbine blades and the high pressure compressor blades, which are traditionally made from nickel-based superalloys (NBSAs) whose density is nearly twice that of TiAl-based alloys. NBSAs are already operating at 80% of their melting point and γ-TiAl has a higher melting point (1460°C) [3-9]. TiAl alloys are also being considered to replace 21-2N high temperature steel as they are 50% lighter, have a lower thermal expansion and exhibit high tensile strength at 700-800°C [3-9].

The largest challenge to the widespread use of TiAl-based alloys is their low ductility at ambient temperature, especially γ-TiAl with a high Al content (> 50 at.% Al) [10]. Their rigid bond structure restricts their ability to accommodate plastic deformation, thus reducing their ductility [10]. Other challenges to the use of TiAl based alloys is their high production costs compared to those of steel and NBSAs, and inadequate oxidation resistance at temperatures greater than 750°C [11].

The maximum applicable temperatures for TiAl-based alloys are determined by oxidation resistance and not creep or strength retention [11]. An improvement in oxidation resistance is thus a

All rights reserved. No part of contents of this paper may be reproduced or transmitted in any form or by any means without the written permission of Trans Tech Publications, www.ttp.net. (ID: 197.78.159.146-26/05/15,12:57:58)

key factor in their increased use at high temperatures. Various alloy modifications and coatings are being investigated [12-14] to improve resistance to oxidation.

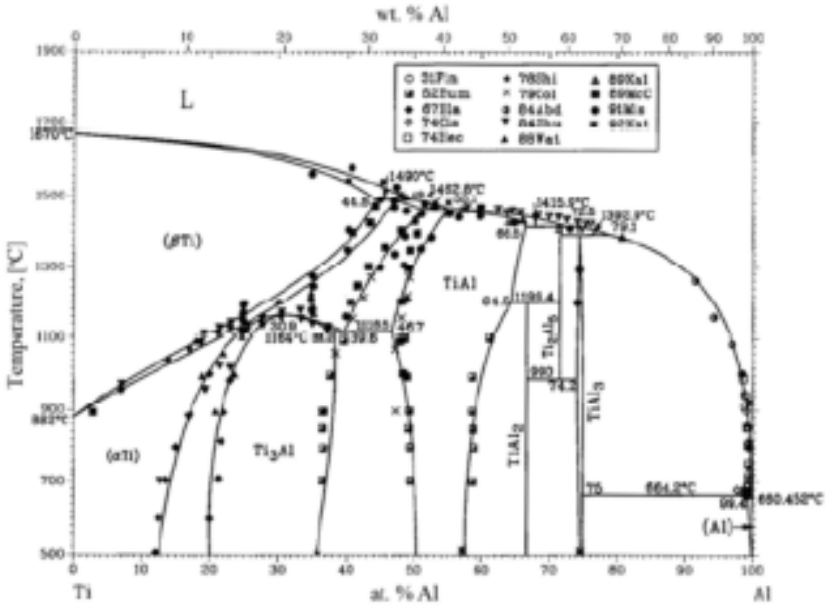

Figure 1: Experimental titanium-aluminium binary phase diagram [1].

TiAl alloys developed so far consist of 46-52 at.% Al [8-11]. At this composition and at temperatures above 720°C, the alloys either have a single γ phase or the duplex ($\gamma+\alpha_2$) structure. These alloys usually contain 1-10 at.% of other alloying elements such as nickel, silicon and chromium to improve oxidation and corrosion resistance [8-11]. In some instances, 1-2 at.% of a third alloying element such as tungsten, niobium, tantalum and manganese is also added to improve ductility, oxidation and corrosion resistance at high temperatures [11].

Despite the high aluminium content of γ-TiAl, these alloys do not exclusively form the protective alumina scale (Al_2O_3) when oxidized in air [11]. Instead, they form the intermixed Al_2O_3+TiO_2 oxides which are less protective than the continuous Al_2O_3 scale, because the TiO_2 has a much higher growth rate than Al_2O_3 [11]. The TiO_2 may also act as a short-circuit transport path, enabling the interstitial dissolution of oxygen and nitrogen particles into the alloy at elevated temperature, which results in embrittlement and degradation of the fatigue life [11].

Additions of precious metals 0.2 at.% of Ag, Au, Ru, Pd and Pt to a Ti-47.5 at.% Al alloy gave significant improvement in oxidation resistance [12]. The alloys formed an external TiO_2 scale, then an Al_2O_3 scale and finally an Al_2O_3+TiO_2 mixed oxide scale nearest the substrate. The precious metals went into solution in γ-TiAl underneath the mixed oxide scale. TiAl alloyed with the relatively low melting point precious metals (Au and Ag) ultimately formed a porous oxide scale with cracks. TiAl alloyed with precious metals of relatively high melting point (Ru and Pt) formed a continuous, non-porous oxide scale without any cracks.

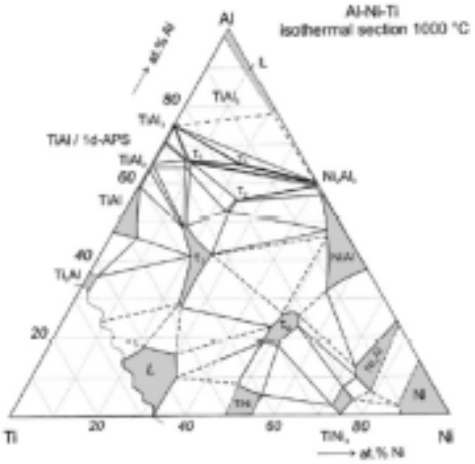

Figure 2: Isothermal section of Ti-Al-Ni at 1000°C [15].

The isothermal section of the Ti-Al-Ni ternary phase diagram (Fig. 2) shows the co-existence of TiAl, $TiAl_2$ and Al_3NiTi_2 (τ_9) phases at 1000°C, with a wide two-phase region between TiAl and Al_3NiTi_2 (τ_9).

In this work, 10.0 at.% Ni and 0.2 at.% Ru were added to a γ-TiAl alloy to improve its high temperature oxidation properties. The alloy was characterized in terms of microstructure, hardness and oxidation behavior.

Experimental procedure

Preparation of TiAl compound. The Ti-52.5 at.% Al alloy was produced by melting powders of high grade Ti, Al, Ni and Ru in a button arc furnace under an argon atmosphere. Two alloys Ti-52.5Al-10.0Ni (at.%) and Ti-52.5Al-10.0Ni-0.2Ru (at.%) were produced. Each alloy was cut into various samples for further test work.

Characterization of alloys. The as-cast samples were prepared metallographically and observed using the Carl Zeiss Sigma field emission scanning electron microscopes (FE-SEM). The composition and phases of the samples were determined using a combination of energy dispersive X-ray spectroscopy (EDX) and X-ray diffraction (XRD). The PANAlytical X'Pert Pro powder diffractometer was used for XRD test work. Phase identification was conducted using X'Pert Highscore plus software.

The samples were annealed at 1050°C for 120 hours in a carbolite tube furnace under argon flow, where they were heated at a rate of 10°C/min and subsequently furnace cooled. After heat treatment, the samples were characterized in terms of microstructure and hardness. The future-tech FV-800 vicker's hardness tester was used for the test work.

Oxidation test work. The oxidation behavior of the alloys was determined by thermogravimetric analysis (TGA) using a NETZSCH STA. The tests were conducted in air and samples were heated from room temperature to 1050°C. The longer term effect of oxidation in air was determined by heating the alloys in a tube furnace for 120 hours at 1050°C.

Results and discussion

Microstructural characterization of alloys. Fig. 3 and 4 show the SEM micrographs for the as-cast alloys; both had dendrites in a eutectic, and their EDX analyses are shown in Tables 1 and 2. Both the alloys had dendrites of γ-TiAl surrounded by a eutectic of TiAl and Al_3NiTi_2 (τ_9). In

XRD, no Ti, Ni and Al peaks were observed, indicating complete alloying. Most of the Ni and Ru were in the Al_3NiTi_2 (τ_3) phase, but there were traces in the dendrites as well.



Figure 3: SEM micrograph of as-cast Ti-52.5Al-10.0Ni (at.%) showing TiAl dendrites (dark) in a TiAl+Al_3NiTi_2(τ_3) eutectic (light).

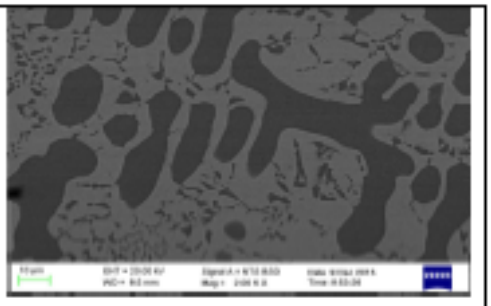

Figure 4: SEM micrograph of as-cast Ti-52.5Al-10.0Ni-0.2Ru (at.%) showing TiAl dendrites (dark) in a TiAl+Al_3NiTi_2(τ_3) eutectic (light).

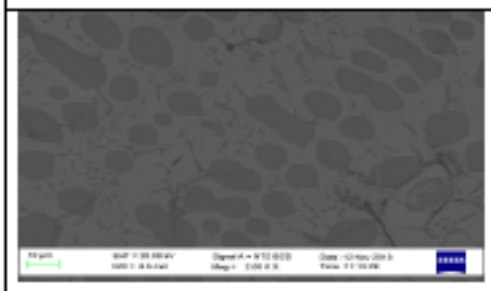

Figure 5: SEM micrograph of annealed Ti-52.5Al-10.0Ni (at.%) showing TiAl dendrites (dark) in a TiAl + Al_3NiTi_2(τ_3) eutectic (light).

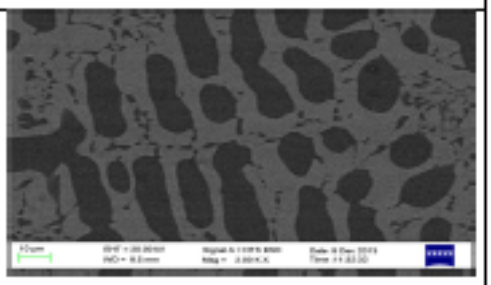

Figure 6: SEM micrograph of annealed Ti-52.5Al-10.0Ni-0.2Ru (at.%) showing TiAl dendrites (dark) in a TiAl + Al_3NiTi_2(τ_3) eutectic (light).

After annealing for 120 hours at 1050°C, the structures were similar with some coarsening of the eutectic (Fig. 5 and 6).

Table 1: EDX for as-cast alloy Ti-52.5Al-10.0Ni (at.%)

Area	Elemental composition (at.%)			Phase
	Ti	Al	Ni	
Overall	37.4 ± 1.1	52.8 ±1.2	9.8 ± 0.5	-
Dendrites	43.9 ± 1.3	55.6 ± 0.8	0.5 ± 0.08	γ-TiAl
Eutectic (light)	37.8 ± 1.1	49.9 ± 0.5	12.3 ± 1.2	Al_3NiTi_2 (τ_3)
Eutectic (overall)	41.2 ± 0.9	52.2 ± 0.8	6.6 ± 1.3	γ-TiAl+Al_3NiTi_2 (τ_3)

Table 2: EDX for as-cast alloy Ti-52.5Al-10.0Ni-0.2Ru (at.%)

Area	Elemental composition (at.%)				Phase
	Ti	Al	Ni	Ru	
Overall	39.7 ± 1.4	50.6 ± 1.3	9.6 ± 1.0	0.1 ± 0.05	-
Dendrites	45.2 ± 1.5	53.6 ± 1.1	1.1 ± 0.2	0.1 ± 0.04	γ-TiAl
Eutectic (light)	36.2 ± 1.8	48.4 ± 0.7	15.1 ± 1.1	0.3 ± 0.06	Al_3NiTi_2 (τ_3)
Eutectic (overall)	42.1 ± 1.1	50.3 ± 0.6	7.6 ± 1.1	0.1 ± 0.05	γ-TiAl+Al_3NiTi_2 (τ_3)

Hardness evaluation. Both the alloys were fairly hard and brittle (Table 3). Annealing caused a slight decrease in hardness. The macro-hardness of a plain as-cast TiAl alloy is 281 HV_{10} [17], therefore the addition of Ni and Ru increased the hardness of the alloy significantly.

Table 3: Vickers hardness (HV_{10}) for Ti-52.5Al-10.0Ni (at.%) and Ti-52.5Al-10.0Ni-0.2Ru (at.%)

Hardness HV_{10}		
Condition	Ti-52.5Al-10.0Ni (at.%)	Ti-52.5Al-10.0Ni-0.2Ru (at.%)
As-cast	579 ± 15	561 ± 17
Annealed (120h,1050°C)	556 ± 15	546 ± 12

Oxidation behavior of alloys. Fig. 7 shows that the Ti-52.5Al-10.0Ni-0.2Ru (at.%) alloy had a lower mass gain than the Ti-52.5Al-10.0Ni (at.%) alloy, in both the as-cast and heat treated conditions. The mass gains of the as-cast TiAlNiRu (0.61 at.%) and heat treated TiAlNiRu (1.07 at.%) showed that the heat treatment process reduced the oxidation resistance of the alloy. The reason could be that the heat treatment might not have been in a pure inert atmosphere and the alloy may have oxidized slightly. When compared to other TiAl based alloys that had additions of precious metals (Ru, Ag, Ir, Pd and Pt), the TiAlNiRu alloy had a good oxidation resistance [17].

The isothermal oxidation of the alloys at 1050°C for 120 hours gave a mixed metal oxide of TiO_2/Al_2O_3 with Ni and Ru in solid solution (Fig. 8 and 9), which were taken from the surfaces of the specimens.

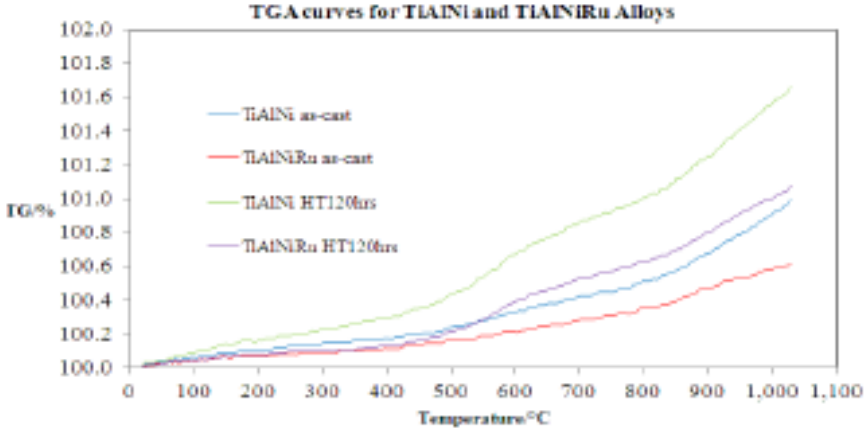

Figure 7: TGA curves of as-cast and heat treated alloys.

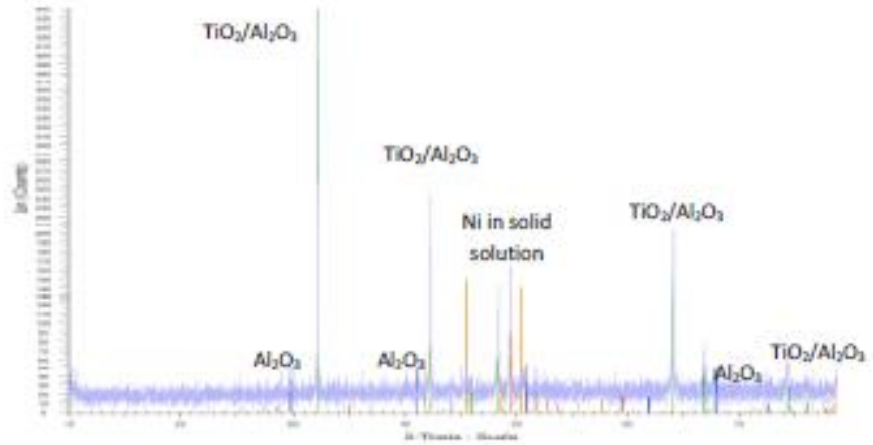

Figure 8: XRD pattern of Ti-52.5Al-10.0Ni (at.%) after oxidation in air for 120 h at 1050°C.

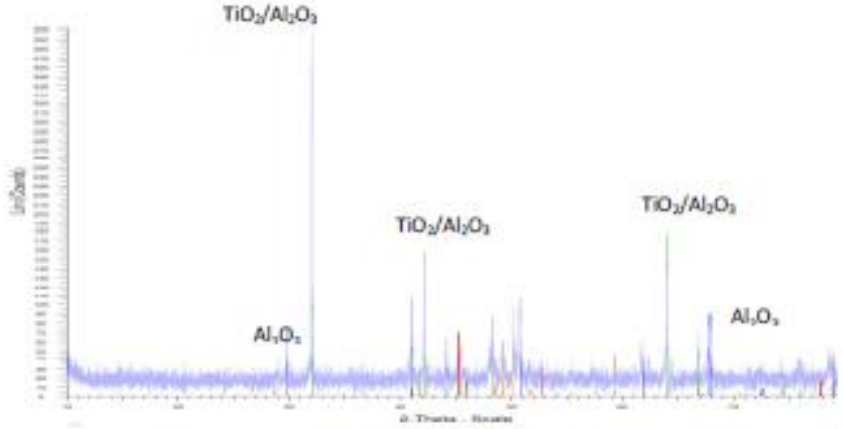

Figure 9: XRD pattern of Ti-52.5Al-10.0Ni-0.2 Ru (at.%) after oxidation in air for 120 h at 1050°C.

A cross section of the oxidized TiAlNiRu alloy showed an intermixed metal oxide scale of TiO_2+Al_2O_3. The oxide scale had trace amounts of nickel (~0.05 at.%) and no ruthenium was detected.

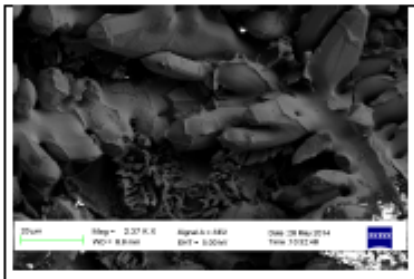

Figure 10: SEM micrograph of oxidized Ti-52.5Al-10.0Ni-0.2Ru (at.%) showing the TiO_2/Al_2O_3 mixed scale on the surface.

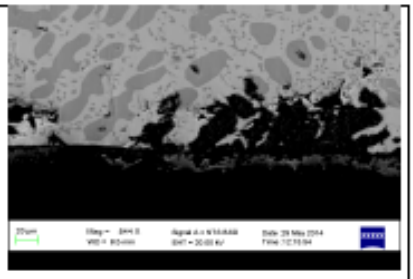

Figure 11: SEM micrograph of a cross section of alloy Ti-52.5Al-10.0Ni-0.2Ru (at.%) showing a discontinued oxide scale.

Conclusions and recommendations

The addition of 10.0 at.% Ni and 0.2 at.% Ru to a Ti-52.5 Al at.% alloy produced an as-cast microstructure of γ-TiAl dendrites surrounded by a eutectic of TiAl and Al_3NiTi_2 (τ_3). Most of the Ni and Ru was in solid solution in the Al_3NiTi_2 (τ_3) phase, although some trace amounts were in the dendrites. The Ti-52.5Al-10.0Ni-0.2Ru (at.%) alloy was fairly brittle at room temperature, making it unsuitable for structural applications. The alloy showed good short term oxidation behavior at elevated temperatures when compared to other TiAl-based alloys. However, the presence of a mixed oxide scale of TiO_2/Al_2O_3 instead of a protective Al_2O_3 scale is a concern. Longer term oxidation tests (30 days) will be conducted to further investigate the oxidation behavior of the alloy.

References

[1] H. Okamoto, Aluminium-titanium, Journal of Phase Equilibria. 14 (1993) 120 - 121.

[2] F. Appel, J.D.H. Paul, M. Oehring, Gamma Titanium Aluminide Alloys, Wiley-VCH, 2011.

[3] F.H. Froes, C. Suryanarayana and D. Eliezer, Properties and applications of titanium aluminides, Journal of Materials Science. 27 (1992) 5113 - 5140.

[4] K. Kothari, R. Radhakrishnan and N.M. Wereley, Advances in gamma titanium aluminides and their manufacturing techniques, Progress in Aerospace Sciences. 55 (2012) 1 - 16.

[5] J.P. Immarigeon, R.T. Holt, A.K. Koul, L. Zhao, W. Wallace and J.C. Beddoes, Light- weight materials for aircraft applications, Materials Characterization. 34 (1995) 41 - 67.

[6] W. Voice, The future of gamma titanium alumnides by rolls-royce, Aircraft Engineering and Aerospace Technology. 71 (1999) 337 - 340.

[7] M.M. Keller, P.E. Jones, W.J. Porter and D. Eylon, The development of a low cost TiAl automotive valve, JOM. 49 (1997) 42 - 44.

[8] T. Nishiyama, K. Toyama and T. Yoshimitsu, Development of titanium aluminide turbocharger rotors, SAE Transactions. 18 (1989) 17 - 21.

[9] D. Chandley, Use of gamma titanium aluminide for automotive engine valves, President Metal Casting Technology. 18 (2000) 8 - 11.

[10] K. Young-Won, Intermetallic alloys based on gamma titanium aluminide. 41 (1989) 24 - 30.

[11] M.P. Brady, W.J. Brindley, J.L. Smialek and I.E. Locci, The oxidation and protection of gamma titanium aluminides, JOM. 48 (1996) 46 - 50.

[12] R.W. Schutz, Ru enhanced Ti alloys, Platinum Metals Review. 40 (1996) 54 - 61.

[13] M. Thomas and M.P. Bacos, Processing and characterisation of TiAl-based alloys, Journal of Aerospace Lab. 3 (2011) 1 - 11.

[14] C. Leyens, R. Braun, M. Frohlich and P.E.H. Hovsepien, Recent progress in the coating protection of gamma titanium aluminides, JOM. 58 (1996) 17 - 21.

[15] J.C. Schuster, Z. Pau, S. Liu, F. Weitzer, Y. Du, Constitution of the ternary system Al-Ni-Ti, Intermetallics. 15 (2007) 1257 – 1267.

[16] A. Khataee, H.M. Flower and D.R.F. West, Constitution of Ti-Al-Ru system, Materials Science Technology. 5 (1989) 632 – 643.

[17] I.A. Mwamba, L.A. Cornish and E. van der Lingen, Oxidation property evolution of gamma-TiAl alloy with addition of precious metals, SAIMM Journal. 7A (2012) 517 - 526.

HIGH TEMPERATURE OXIDATION OF γ-TiAl ALLOY Ti-52.5Al-10Ni-0.2Ru (at.%)

H.C. Mantyi[1,2], L.A. Cornish[1,2], L.H. Chown[1,2] and I.A. Mwamba[2,3]

[1]School of Chemical and Metallurgical Engineering, University of the Witwatersrand, Johannesburg,
[2]DST-NRF Centre of Excellence in Strong Materials, hosted by the University of the Witwatersrand,
[3]Advanced Materials Division, Mintek, Randburg

Titanium alloys are extensively used in aero-engines[1-2] as they have a low density (~4.5g.cm^{-3}), good weldability and corrosion resistance. However, they have limited burn resistance and can cause titanium fires above 800°C, which are typical temperatures in the high pressure compressor section of aero-engines[1-2]. The more burn-resistant but denser (~8g.cm^{-3}) nickel-based superalloys (NBSAs) are thus used to prevent titanium fires[1-2]. Gamma titanium aluminide (γ-TiAl) has the potential to replace NBSAs as they are more burn-resistant than conventional titanium alloys and they are lighter than both NBSAs and those titanium alloys (~3.8g.cm^{-3})[3]. The weight savings through the use of γ-TiAl could result in more efficient aero-engines which use less fuel, are more environmentally friendly and cost less to operate[1-3]. The challenge with γ-TiAl is the limited oxidation resistance at temperatures above 850°C, because they tend to form the TiO_2 oxide instead of a continuous and protective Al_2O_3 oxide[2-5]. This research investigates if nickel and ruthenium could inhibit the formation of TiO_2 and promote the formation of Al_2O_3 in a single-phase gamma titanium aluminide alloy Ti-52.5Al-10Ni-0.2Ru (at.%).

The alloy was made by mixing and melting pure elemental powders of Ti, Al, Ni and Ru in a button arc furnace under an argon atmosphere. The alloy was cut into samples which were metallographically prepared to a 1200 grit finish. The as-cast samples were oxidized in air in a furnace at 950°C for 120 hours and 720 hours. The samples were characterized using scanning electron microscopy (SEM) with energy dispersive X-ray spectroscopy (EDX) and X-ray diffraction (XRD).

The as-cast alloy had dendrites of γ-TiAl (53.6±1.1 at.%Al) surrounded by a γ-TiAl + Al_2NiTi_2 (τ_3) eutectic. The ruthenium was mainly in solid solution (0.3±0.1 at.%) in Al_2NiTi_2 (τ_3), compared to the dendrites (0.1±0.04 at.%) where the error was in the second decimal place. The alloy was brittle at room temperature with a hardness of ~561 HV_{10}.

After oxidation for 120 hours at 950°C, a continuous, intermixed oxide layer of TiO_2 (21.2±0.3 at.% Ti) and Al_2O_3 (24.6±0.1 at.% Al) was formed on the surface (Fig. 1), with trace amounts of Ni and no Ru. The substrate had dendrites of γ-TiAl (55.7±0.1 at.% Al) surrounded by a γ-TiAl + Ni_3Al eutectic. Ruthenium and nickel were in solid solution (0.2±0.1 at.% Ru and 10.6±0.1 at.% Ni) in the eutectic. Small amounts of oxygen were found in the eutectic (2.7±0.2 at.%).

A longer oxidation period of 720 hours at 950°C resulted in intermixed TiO_2+Al_2O_3 oxides with considerably more TiO_2. The yellow-grey oxide was exfoliated from the substrate on cooling.

The amounts of nickel and ruthenium in alloy Ti-52.5Al-10Ni-0.2Ru (at.%) did not inhibit the formation of TiO_2 when the alloy was oxidized in air at 950°C. Compared to NBSAs used in turbines[6], the Ti-52.5Al-10Ni-0.2Ru (at.%) has a good oxidation resistance, although long exposure times resulted in the oxide exfoliating from the substrate. Cyclic oxidation tests should be conducted to determine oxidation kinetics.

References
1. Kothari, K., Radhakrishnan, R. and Wereley, N.M. (2012) Progress in Aero. Sci. 55(1), 1.
2. Appel, F., Paul, J.D.H. and Oehring, M. (2011) Gamma Titanium Aluminide Alloys, Wiley-VCH.
3. Lütjering, G. and Albrecht, J. (2004) Ti-2003 Science and Technology, Wiley-VCH.
4. Choudhury, N.S., Graham, H.C. and Hinze, J.W. (1976) J. Electrochem. Soc. 48(3), 668.
5. Brady, M.P. *et al.* (1996) JOM. 48(1), 46.
6. Gupta, O.P. *et al.* (2012) J. Adv. Sci. Res. &Tech. 2(2), 1.

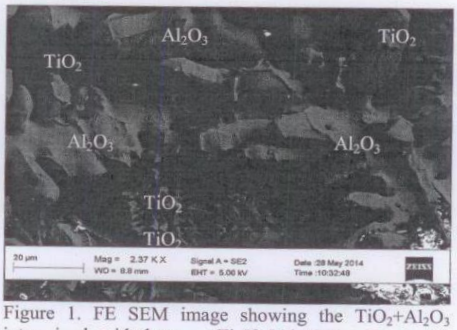

Figure 1. FE SEM image showing the TiO_2+Al_2O_3 intermixed oxide layer on Ti-52.5Al-10Ni-0.2Ru (at.%) alloy after oxidation in air for 120 hours at 950°C.

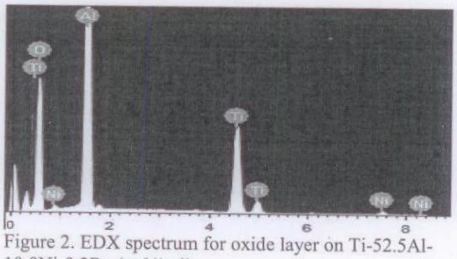

Figure 2. EDX spectrum for oxide layer on Ti-52.5Al-10.0Ni-0.2Ru (at.%) alloy.

Corresponding author: *hadiomantyi@hotmail.com*

The effect of ruthenium on the corrosion behaviour of gamma titanium aluminide Ti-52.5Al-10.0Ni (at.%)

H.C. Mantyi*†, L.A. Cornish*†, L.H. Chown*† and I.A. Mwamba†‡
**School of Chemical and Metallurgical Engineering, University of the Witwatersrand, Johannesburg*
†DST-NRF Centre of Excellence in Strong Materials, University of the Witwatersrand
‡Advanced Materials Division, Mintek, Randburg

Gamma titanium aluminide (γ-TiAl) as-cast alloys Ti-52.5Al-10.0Ni (at.%) and Ti-52.5Al-10.0Ni-0.2Ru (at.%) were evaluated for corrosion resistance in 5 (dilute) and 25 (concentrated) wt% HCl solutions using potentiodynamic scans at room temperature. The alloys were assessed to determine whether the presence of ruthenium would cause Ti-52.5Al-10.0Ni (at.%) to passivate by cathodic modification, and become corrosion resistant in dilute and concentrated HCl.

In the non-oxidising HCl environment, the Ti-52.5Al-10.0Ni (at.%) alloy formed a thin and non-continuous Al_2O_3 oxide scale on the surface of the γ-TiAl dendrites, with Ti_3NiAl_2O found in the γ-TiAl + Ti_2NiAl_3 (τ_3) + NiTi eutectic regions. In concentrated HCl, the Al_2O_3 oxide scale was present on the γ-TiAl dendrites, but to a lesser extent.

The Ti-52.5Al-10.0Ni-0.2Ru (at.%) alloy also formed a thin and non-continuous alumina scale on the surface of γ-TiAl dendrites, with Ti_3NiAl_2O found in the γ-TiAl + Ti_2NiAl_3 (τ_3) + NiTi eutectic regions. The scale on the Ti-52.5Al-10.0Ni-0.2Ru (at.%) alloy had better adherence than that on Ti-52.5Al-10.0Ni (at.%), even in the concentrated HCl environment.

In the dilute HCl environment, the addition of ruthenium to Ti-52.5Al-10.0Ni (at.%) did not change the corrosion potential of the alloy and the corrosion current density decreased only slightly. The Ti-52.5Al-10.0Ni-0.2Ru (at.%) alloy had unstable passivation, falling outside the passive region of Ti-52.5Al-10.0Ni (at.%). Therefore, the addition of ruthenium did not improve the corrosion resistance of Ti-52.5Al-10.0Ni (at.%) by cathodic modification.

In concentrated HCl, the addition of ruthenium significantly reduced the corrosion current density of Ti-52.5Al-10.0Ni (at.%), although the corrosion potential was less noble. Thus, the addition of ruthenium resulted in unstable passivation, which allowed alloy dissolution, and was not beneficial.

Keywords: Titanium aluminide, cathodic modification, corrosion

Introduction

Gamma titanium aluminides (γ-TiAl) are lightweight (~3.8 $g.cm^{-3}$) intermetallic compounds with good corrosion, oxidation and burn resistance at elevated temperatures [1-3]. Most of the research on γ-TiAl has been focused on the high temperature aerospace applications, due to the weight savings which can be achieved [1-3]. Titanium alloys have excellent corrosion resistance in aggressive environments [4-5], and are being used in other industries such as petrochemical processing, offshore oil and gas, marine environments and the fabrication of medical implants.

Titanium and titanium alloys have excellent corrosion resistance in most neutral and oxidizing aqueous environments [4-6]. However, in reducing environments, such as low pH chloride solutions, titanium alloys are susceptible to crevice and pitting corrosion. Thus, palladium-containing titanium alloys are being used in low pH chloride solutions to improve corrosion resistance, although palladium is increasingly being replaced by ruthenium to reduce costs. The Ti-Ru alloys can be used to make lighter and cost effective components for: downhole oil and geothermal sour wells, hot brine plate exchangers, chlor-alkali and chlorate cell anodes and liners.

The concept of alloying metals with noble metals to improve corrosion resistance [7] was probably first discovered by Monnartz in 1911, on finding that the corrosion resistance of stainless steels in certain acids could be improved by winding a platinum wire or alloying with platinum. The presence of platinum in the stainless steel produces a more noble alloy by increasing the electrode potential to a value higher than the passivity potential. In a corrosive environment, the alloy passivates by forming a sparingly soluble, protective and hydrated oxide film on the surface. This technique is known as cathodic modification.

Alloying titanium and stainless steels with small amounts of Pt, Pd, Rh and Ru [5-9] improved the corrosion resistance in low pH reducing solutions, without adversely affecting their good corrosion resistance in oxidizing solutions. Streicher [7] demonstrated that nickel and ruthenium in Fe-28.5Cr-4Mo stainless steel induced passivity in boiling H_2SO_4 and improved pitting and stress corrosion cracking resistance. Thus, it is worthwhile to investigate the synergistic effect of nickel and ruthenium on the corrosion of titanium alloys.

TiAl alloys are susceptible to pitting corrosion and stress corrosion cracking in low pH environments [10-12]. PGMs have been used to enhance corrosion resistance and mechanical properties of steels and nickel aluminides [13-15], and could also have an important effect on titanium aluminides, which was the reason for this investigation. Recently [9], the addition of PGMs to duplex Ti-47.5Al (at.%) improved its corrosion resistance in 5 wt% and 15 wt% HCl by cathodic modification. The additions increased the corrosion potential to the passive region of plain TiAl, indicating the spontaneous passivation of PGM-alloyed TiAl in the low pH solutions. PGMs are thought to accumulate on the surface of TiAl alloys, improving the hydrogen evolution efficiency and inhibiting anodic dissolution [9].

Figure 1 shows the effect of cathodic modification, where line A_0 represents the cathodic polarization curve of a base metal, and line A_1 that of the same metal which has been alloyed and therefore cathodically modified [8]. Therefore, the addition of corrosion-resistant noble metals, such as palladium and ruthenium, to A_0 should produce the cathodically modified alloy A_1, where the corrosion potential is more noble and falls in the passive region of alloy A_0.

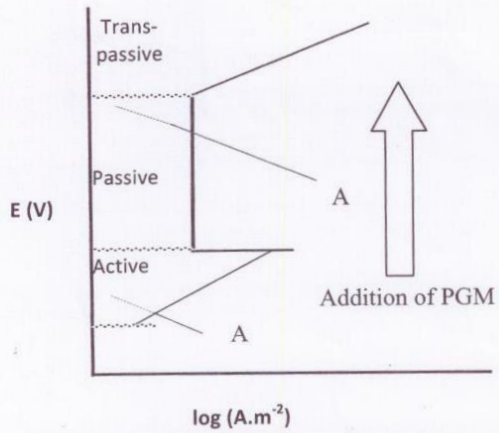

Figure 1 – Schematic diagram of the effect of cathodic modification (after Potgieter et al [8])

In this investigation, the base alloy was Ti-52.5Al-10.0Ni (at.%) and 0.2 at.% ruthenium was the cathodic component being introduced. For Ti-52.5Al-10.0Ni-0.2Ru (at.%) to be corrosion resistant by cathodic modification, the following criteria must be met in the base alloy [8]:

- Ti-52.5Al-10.0Ni (at.%) must have a small critical current density (i_{crit}) that can be exceeded by the current of the hydrogen cathodic reaction on Ti-52.5Al-10.0Ni-0.2Ru (at.%) at the given passivation potential.
- The passivation potential of Ti-52.5Al-10.0Ni (at.%) must be sufficiently negative to allow the ruthenium to change the corrosion potential of Ti-52.5Al-10.0Ni-0.2Ru (at.%) to a value within the passive range of Ti-52.5Al-10.0Ni (at.%).
- The transpassive potential of Ti-52.5Al-10.0Ni (at.%) should be sufficiently positive to allow a wide passive range.

Also, ruthenium should be corrosion resistant in HCl and the new alloy should have a higher exchange current density i_o (and lower overvoltage) for the cathodic process of hydrogen evolution than Ti-52.5Al-10.0Ni (at.%).

Alloys had already been made, and the as-cast Ti-52.5Al-10.0Ni (at.%) and Ti-52.5Al-10.0Ni-0.2Ru (at.%) alloys had γ-TiAl dendrites surrounded by a eutectic of γ-TiAl + Ti_2NiAl_3 (τ_3) [16]. In Ti-52.5Al-10.0Ni (at.%), the composition of γ-TiAl was 55.6 ± 0.8 at.% Al, and most of the nickel (12.3 ± 1.2 at.%) was in the τ_3 phase [16]. Ti-52.5Al-10.0Ni-0.2Ru (at.%) had 53.6 ± 1.1 at.% Al in γ-TiAl, with most of the nickel (15.1 ± 1.1 at.%) and ruthenium (0.3 ± 0.1 at.%) in the τ_3 phase [16]. Both alloys were brittle, with cracks mainly growing alongside the dendrites.

This study investigated whether the addition of ruthenium to Ti-52.5Al-10.0Ni (at.%) could produce a cathodically-modified alloy which would passivate and be corrosion-resistant in hydrochloric acid.

Experimental procedure

Alloy manufacture and microstructure characterisation

The Ti-52.5Al-10.0Ni (at.%) and Ti-52.5Al-10.0Ni-0.2Ru (at.%) γ-TiAl alloys were produced by mixing and melting powders of high grade titanium, aluminium, nickel and ruthenium in a button arc furnace under an argon atmosphere. The as-cast samples were prepared metallographically and observed using a Zeiss Sigma field emission scanning electron microscope (FE-SEM) with energy dispersive X-ray spectroscopy (EDX) to determine the element composition of the samples. A PANAlytical X'Pert Pro powder diffractometer was used for X-ray diffraction (XRD) to confirm the phases present.

Electrochemical tests

The sample surfaces were ground to a 1200 grit SiC paper finish, degreased with methanol, rinsed with distilled water, and dried. The surfaces were prepared just prior to starting the polarization experiments, to limit long-term oxidation. Before conducting the scan, each sample was immersed in the HCl solution to obtain a stable corrosion potential. An ACM AutoTafel potentiostat/galvanostat system with a conventional three-electrode system with a saturated calomelelectrode (SCE) was used. Potentiodynamic scans were done from -1000 mV to +400 mV at a scanning rate of 10 $mV.min^{-1}$. All electrochemical tests were repeated twice for each sample.

Results and discussion

Microstructure characterisation

When exposed to HCl, SEM indicated (Figures 2 and 3) that the Ti-52.5Al-10.0Ni (at.%) alloy formed a thin and non-continuous Al_2O_3 oxide scale on the γ-TiAl dendrites, with Ti_3NiAl_2O found in the γ-TiAl + τ_3 + NiTi eutectic regions. In some areas, the alumina was clearly visible (Figure 2) and in other areas the layer was too thin to be observed in SEM (Figure 3). Alumina and Ti_3NiAl_2O were clearly shown by XRD (Figures 4 and 7).

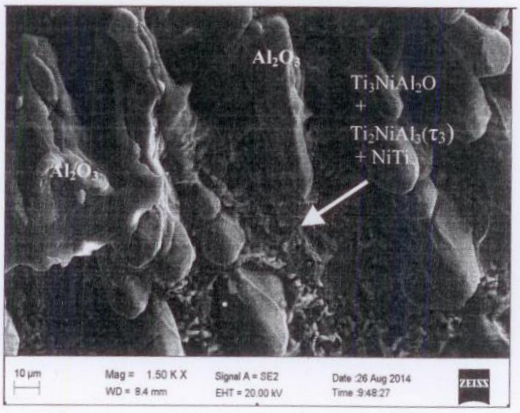

Figure 2 – SEM-SE image of the corroded surface of alloy Ti-52.5Al-10.0Ni (at.%)

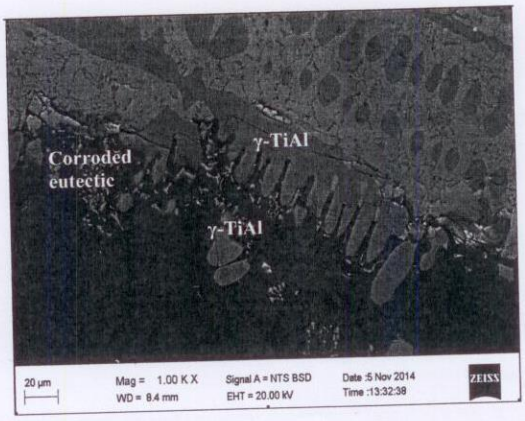

Figure 3 – SEM-BSE image of a cross section of corroded Ti-52.5Al-10.0Ni (at.%) alloy

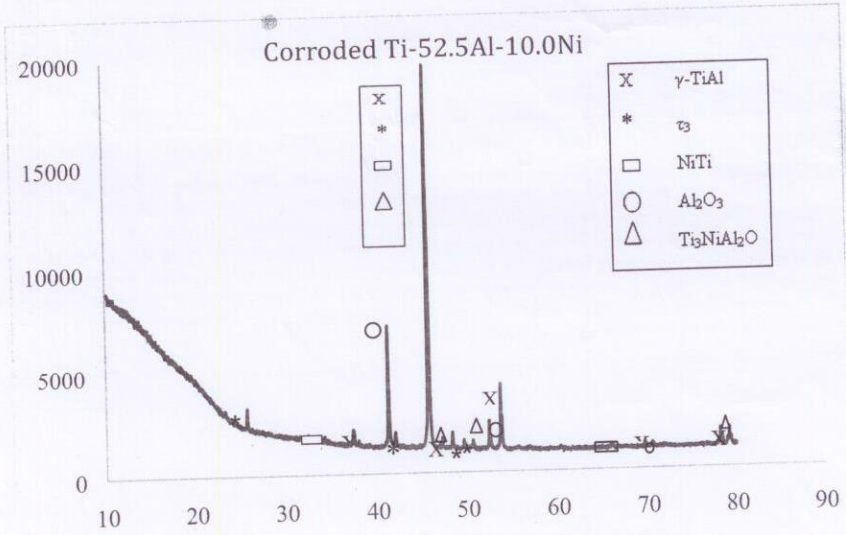

Figure 4 – XRD pattern for Ti-52.5Al-10.0Ni (at.%) surface corroded in 5 wt % HCl

The Ti-52.5Al-10.0Ni-0.2Ru (at.%) alloy also formed a thin and non-continuous Al_2O_3 scale on the γ-TiAl dendrites, with Ti_3NiAl_2O found in the γ-TiAl + τ_3 + NiTi eutectic regions (Figures 5 and 6). Ruthenium was not present in the γ-TiAl dendrites, but was present (0.3 ± 0.1 at.%) in the eutectic region. (However, values under 0.5 at.% are less accurate with EDX.) No ruthenium was found in the scale on the dendrites, although there were trace amounts of nickel (0.5 ± 0.1 at.%). Although the Ti-52.5Al-10.0Ni-0.2Ru (at.%) alloy was exposed to higher potentials in the corrosion tests, its scale (Figure 6) had better adherence to the substrate than the scale on Ti-52.5Al-10.0Ni (at.%) (Figure 3), which had disappeared, demonstrating that the ruthenium was beneficial in promoting a more adherent scale.